



NAVAL POSTGRADUATE SCHOOL

MONTEREY, CALIFORNIA

THESIS

**EXPERIMENTAL VALIDATION OF MODEL UPDATING
AND DAMAGE DETECTION VIA EIGENVALUE
SENSITIVITY METHODS WITH ARTIFICIAL
BOUNDARY CONDITIONS**

by

Matthew D. Bouwense

September 2017

Thesis Advisor:
Second Reader:

Joshua H. Gordis
Young W. Kwon

Approved for public release. Distribution is unlimited.

THIS PAGE INTENTIONALLY LEFT BLANK

REPORT DOCUMENTATION PAGE			Form Approved OMB No. 0704-0188	
Public reporting burden for this collection of information is estimated to average 1 hour per response, including the time for reviewing instruction, searching existing data sources, gathering and maintaining the data needed, and completing and reviewing the collection of information. Send comments regarding this burden estimate or any other aspect of this collection of information, including suggestions for reducing this burden, to Washington headquarters Services, Directorate for Information Operations and Reports, 1215 Jefferson Davis Highway, Suite 1204, Arlington, VA 22202-4302, and to the Office of Management and Budget, Paperwork Reduction Project (0704-0188) Washington, DC 20503.				
1. AGENCY USE ONLY (Leave blank)		2. REPORT DATE September 2017		3. REPORT TYPE AND DATES COVERED Master's thesis
4. TITLE AND SUBTITLE EXPERIMENTAL VALIDATION OF MODEL UPDATING AND DAMAGE DETECTION VIA EIGENVALUE SENSITIVITY METHODS WITH ARTIFICIAL BOUNDARY CONDITIONS			5. FUNDING NUMBERS	
6. AUTHOR(S) Matthew D. Bouwense				
7. PERFORMING ORGANIZATION NAME(S) AND ADDRESS(ES) Naval Postgraduate School Monterey, CA 93943-5000			8. PERFORMING ORGANIZATION REPORT NUMBER	
9. SPONSORING /MONITORING AGENCY NAME(S) AND ADDRESS(ES) N/A			10. SPONSORING / MONITORING AGENCY REPORT NUMBER	
11. SUPPLEMENTARY NOTES The views expressed in this thesis are those of the author and do not reflect the official policy or position of the Department of Defense or the U.S. Government. IRB number N/A.				
12a. DISTRIBUTION / AVAILABILITY STATEMENT Approved for public release. Distribution is unlimited.			12b. DISTRIBUTION CODE	
13. ABSTRACT (maximum 200 words) <p>The use of finite element modeling (FEM) in design has expanded as computers have become more capable. Despite these advancements, the construction of physical prototypes remains an essential aspect of design and testing. FEM limitations include the inability to accurately account for joints, damping, and geometric complexities. Due to the reality gap between a FEM and the prototype, there may be design deficiencies that cannot be identified until the prototype is tested. Using eigenvalue sensitivities, enhanced by artificial boundary conditions (ABC), the gap between simulation and reality can be closed via FEM updating. With an updated FEM, the same eigenvalue sensitivities can be utilized to detect damage in structural systems in use. Damage that produces differences in natural frequencies between the structure and its FEM can be related to the loss in flexural rigidity, as it is usually assumed that mass modeling is correct. This indicator allows adjustment of a FEM to match a prototype or to detect damage in a potentially compromised structure via comparison to an updated FEM. Based on simulation, a combination of multiple pin and spring ABCs is optimal for producing an ideal sensitivity matrix, and thus, ideal damage detection capability. However, in the experimental realm, the synthesis transformation used to apply ABCs to the measured frequency response functions can distort the frequency response function peaks, leading to error. A compromise of a single pin ABC permits both effective model updating and damage detection.</p>				
14. SUBJECT TERMS finite element model, eigenvalue sensitivity, artificial boundary condition, frequency response function, natural frequency, model update, damage detection			15. NUMBER OF PAGES 129	
			16. PRICE CODE	
17. SECURITY CLASSIFICATION OF REPORT Unclassified	18. SECURITY CLASSIFICATION OF THIS PAGE Unclassified	19. SECURITY CLASSIFICATION OF ABSTRACT Unclassified	20. LIMITATION OF ABSTRACT UU	

THIS PAGE INTENTIONALLY LEFT BLANK

Approved for public release. Distribution is unlimited.

**EXPERIMENTAL VALIDATION OF MODEL UPDATING AND DAMAGE
DETECTION VIA EIGENVALUE SENSITIVITY METHODS WITH ARTIFICIAL
BOUNDARY CONDITIONS**

Matthew D. Bouwense
Lieutenant, United States Navy
B.S., United States Naval Academy, 2010

Submitted in partial fulfillment of the
requirements for the degree of

MASTER OF SCIENCE IN MECHANICAL ENGINEERING

from the

**NAVAL POSTGRADUATE SCHOOL
September 2017**

Approved by: Joshua H. Gordis
Thesis Advisor

Young W. Kwon
Second Reader

Garth V. Hobson
Chair, Department of Mechanical and Aerospace Engineering

THIS PAGE INTENTIONALLY LEFT BLANK

ABSTRACT

The use of finite element modeling (FEM) in design has expanded as computers have become more capable. Despite these advancements, the construction of physical prototypes remains an essential aspect of design and testing. FEM limitations include the inability to accurately account for joints, damping, and geometric complexities. Due to the reality gap between a FEM and the prototype, there may be design deficiencies that cannot be identified until the prototype is tested. Using eigenvalue sensitivities, enhanced by artificial boundary conditions (ABC), the gap between simulation and reality can be closed via FEM updating. With an updated FEM, the same eigenvalue sensitivities can be utilized to detect damage in structural systems in use. Damage that produces differences in natural frequencies between the structure and its FEM can be related to the loss in flexural rigidity, as it is usually assumed that mass modeling is correct. This indicator allows adjustment of a FEM to match a prototype or to detect damage in a potentially compromised structure via comparison to an updated FEM. Based on simulation, a combination of multiple pin and spring ABCs is optimal for producing an ideal sensitivity matrix, and thus, ideal damage detection capability. However, in the experimental realm, the synthesis transformation used to apply ABCs to the measured frequency response functions can distort the frequency response function peaks, leading to error. A compromise of a single pin ABC permits both effective model updating and damage detection.

THIS PAGE INTENTIONALLY LEFT BLANK

TABLE OF CONTENTS

I.	INTRODUCTION.....	1
A.	BACKGROUND	1
B.	LITERATURE REVIEW.....	4
C.	SCOPE OF THESIS	6
D.	SOFTWARE NOTES.....	7
II.	THEORY	9
A.	EULER-BERNOULLI BEAM THEORY	9
B.	FINITE ELEMENT MODELING.....	10
C.	EIGENVALUE SENSITIVITY	16
D.	APPLICATION OF ARTIFICIAL BOUNDARY CONDITIONS IN THE FINITE ELEMENT MODEL	18
E.	SELECTION OF ARTIFICIAL BOUNDARY CONDITIONS	19
F.	FREQUENCY RESPONSE FUNCTION ANALYSIS.....	21
III.	EXPERIMENTAL APPROACH.....	23
A.	TEST ARTICLES	23
B.	INSTRUMENTATION.....	24
C.	MODAL TESTING.....	27
IV.	FEM MESHING AND DAMAGE SCENARIO CANDIDACY	31
A.	MESH PATTERNS.....	31
B.	DAMAGE CONDITION SELECTION	34
V.	ABC SELECTION AND COMPOSITE MATRIX ASSEMBLY	39
A.	BASELINE SENSITIVITY MATRIX.....	39
B.	PIN-BASED ABC LIBRARIES.....	40
C.	ALTERNATIVE ABC TYPES	45
D.	CONCLUDING REMARKS	46
VI.	FEM UPDATING	49
A.	COMPLICATIONS REGARDING MODEL UPDATE	51
B.	MODEL UPDATE RESULTS	61
C.	CONCLUDING REMARKS	66
VII.	DAMAGE DETECTION.....	69
A.	DAMAGE DETECTION COMPLICATIONS.....	69

B.	DAMAGE DETECTION RESULTS	72
C.	CONCLUDING REMARKS	74
VIII.	CONCLUSION	77
A.	KEY OUTCOMES	77
B.	RECOMMENDATIONS	78
APPENDIX A. TEST ARTICLE DETAILS		81
APPENDIX B. INSTRUMENTATION DETAILS		85
APPENDIX C. SUPPLEMENTARY TABLES		95
LIST OF REFERENCES		107
INITIAL DISTRIBUTION LIST		109

LIST OF FIGURES

Figure 1.	Discretized Function Approximation. Source: [1].	1
Figure 2.	Sample Stress-Strain Curve. Source: [2].	2
Figure 3.	Example FRF Generated from Experimental Data	4
Figure 4.	Shear and Moment Acting on a Beam Element. Source: [9].	9
Figure 5.	Transverse Displacement of a Uniform Beam Element.	11
Figure 6.	Shape Functions Showing Boundary Conditions.	12
Figure 7.	Candidate Row Vector and Selected Row Subspace.	21
Figure 8.	Rectangular Beam With Fifteen Taps for Accelerometers	23
Figure 9.	Suspended Beam	24
Figure 10.	Mounting Studs with 2.54 cm (1 in) Scale	24
Figure 11.	Accelerometers with 5.08 cm (2 in) Scale	25
Figure 12.	Impact Hammer	26
Figure 13.	Handheld Shaker with Accelerometer Attached at Top	26
Figure 14.	Experimental FRF Comparison. Source: [12].	29
Figure 15.	Simple FEM Nodes (Crosses) and Accelerometers (Circles)	32
Figure 16.	Transition FEM Nodes (Crosses) and Accelerometers	33
Figure 17.	Detail of Transition Mesh Nodes (Crosses)	33
Figure 18.	Cross-Sectional View of Milled Notches (“Damage”)	34
Figure 19.	Isometric View of Milled Notches (“Damage”)	35
Figure 20.	Natural Frequencies as Stiffness Is Reduced at Damage	36
Figure 21.	Change in Natural Frequencies as Stiffness Is Reduced	36
Figure 22.	Baseline [S] MDI and PDI	39
Figure 23.	Simulated Damage Detection Results with Baseline [S].	40

Figure 24.	Single Pin Composite Sensitivity Matrix MDI and PDI	41
Figure 25.	Simulated Damage Results with Single Pin Composite Matrix	42
Figure 26.	Two Pin Composite Sensitivity Matrix MDI and PDI	43
Figure 27.	Simulated Damage Results with Two Pin Composite Matrix	43
Figure 28.	Three Pin Composite S Matrix MDI and PDI	44
Figure 29.	Simulated Damage Results with Three Pin Composite Matrix	44
Figure 30.	Single Pin, Spring, Point Mass Composite Matrix MDI and PDI	46
Figure 31.	Simulated Damage Results with Single Pin, Spring, Point	46
Figure 32.	Experimentally Obtained FRFs from Each Modal Test.....	51
Figure 33.	FRF Distortion with 0.02 Hz Resolution and Two Pin ABCs.....	52
Figure 34.	FRF Distortion with 0.02 Hz Resolution and Two Pin ABCs.....	53
Figure 35.	Synthesized FRF with One Pin at 0.3125 Hz Resolution.....	54
Figure 36.	Synthesized FRF with Two Pins at 0.3125 Hz Resolution.....	54
Figure 37.	Synthesized FRF with Two Pins at 0.08 Hz Resolution.....	55
Figure 38.	Example of Disregarded Flexural Rigidity Adjustments.	56
Figure 39.	Model Update with Single Pin ABC at 0.3125 Hz Resolution.	57
Figure 40.	Distortion of an FRF Peak at Mode 2.	58
Figure 41.	Example of Shifting Mode Frequencies.....	59
Figure 42.	Clean Peak at Mode 1 at 10.625 Hz.....	60
Figure 43.	Deviation of FEM Natural Frequencies.....	61
Figure 44.	FEM Case A Flexural Rigidity Updates Over Three Iterations.....	63
Figure 45.	FEM Case B Flexural Rigidity Updates Over Three Iterations.....	63
Figure 46.	FEM Case C Flexural Rigidity Updates Over Three Iterations	64
Figure 47.	FEM Case D Flexural Rigidity Updates Over Three Iterations	64
Figure 48.	FEM Case E Flexural Rigidity Updates Over Three Iterations.....	65

Figure 49.	FEM Case F Flexural Rigidity Updates Over Three Iterations	65
Figure 50.	Reduction of Eigenvalue Percent Differences between FEMs	66
Figure 51.	Case C Damage Detection Results.....	70
Figure 52.	Case E Damage Detection Results.	70
Figure 53.	Detail of FRF Peak Distortion with Two Pin ABC Configuration	71
Figure 54.	Case A Damage Detection Results with Clear Damage.....	72
Figure 55.	Case B Damage Detection Results with Clear Damage.....	73
Figure 56.	Case D Damage Detection Results with Clear Damage.....	73
Figure 57.	Case F Damage Detection Results with Clear Damage	74
Figure 58.	A Potential Future Test Article; an Available Frame	79
Figure 59.	Test Beam Inspection Report	81
Figure 60.	Drawing of “Intact” Test Article	82
Figure 61.	Drawing of “Damaged” Test Article.....	83
Figure 62.	Force Hammer with Calibration Certificate	85
Figure 63.	Accelerometer SN# 10226 with Calibration Sheet.....	86
Figure 64.	Accelerometer SN# 10847 with Calibration Sheet.....	86
Figure 65.	Accelerometer SN# 10866 with Calibration Sheet.....	87
Figure 66.	Accelerometer SN# 10877 with Calibration Sheet.....	87
Figure 67.	Accelerometer SN# 10860 with Calibration Sheet.....	88
Figure 68.	Accelerometer SN# 10868 with Calibration Sheet.....	88
Figure 69.	Accelerometer SN# 10851 with Calibration Sheet.....	89
Figure 70.	Accelerometer SN# 11798 with Calibration Sheet.....	89
Figure 71.	Accelerometer SN# 10874 with Calibration Sheet.....	90
Figure 72.	Accelerometer SN# 10867 with Calibration Sheet.....	90
Figure 73.	Accelerometer SN# 10858 with Calibration Sheet.....	91

Figure 74.	Accelerometer SN# 10856 with Calibration Sheet.....	91
Figure 75.	Accelerometer SN# 10857 with Calibration Sheet.....	92
Figure 76.	Accelerometer SN# 10854 with Calibration Sheet.....	92
Figure 77.	Accelerometer SN# 10859 with Calibration Sheet.....	93
Figure 78.	PCB Shaker Specifications Sheet. Source: [16]	94

LIST OF TABLES

Table 1.	Test Beam Properties.....	23
Table 2.	Accelerometer and Mount Properties	25
Table 3.	FEM Natural Frequency Error (Compared to Theoretical Values)	33
Table 4.	Natural Frequency Differences for Damage at Element 5	37
Table 5.	Composite Sensitivity Matrix Comparison	47
Table 6.	Updated FEM Case Comparison.....	62
Table 7.	Damage Detection Performance Comparison	75
Table 8.	FEM-Generated Natural Frequency Comparison	95
Table 9.	Natural Frequency Shift for Various Damage Scenarios	96
Table 10.	Orthogonal Projection Sensitivity Library Selections	99
Table 11.	Initial FEM-Experimental Eigenvalue Percent Differences	103
Table 12.	Updated FEM Comparison.....	104
Table 13.	Averages of Eigenvalue Absolute Percent Differences	105

THIS PAGE INTENTIONALLY LEFT BLANK

LIST OF ACRONYMS AND ABBREVIATIONS

Abbreviations

ABC	artificial boundary condition
CSET	connection set
DOF	degree of freedom
FEM	finite element method, finite element model
FRF	frequency response function
ISSET	internal set
MDI	mode dependency index
MFA	maximum false alarm
OCS	omitted coordinate system
PBC	perturbed boundary condition
PDE	partial differential equation
PDI	parameter dependency index
RME	relative magnitude error

Symbols

[]	matrix
{ }	vector

THIS PAGE INTENTIONALLY LEFT BLANK

ACKNOWLEDGMENTS

First of all, I would like to thank my thesis advisor and professor, Dr. Joshua Gordis. His instruction, guidance, and previous work are what made this research possible.

I would like to recognize our visiting academic, Dr. Jae-Cheol Shin. His unique approaches and methods allowed for the exploration of additional concepts.

Additionally, I wish to acknowledge Dr. Young Kwon. His eager support as a reader was critical to refining this work.

I would also like to thank my wife, Mai, for her unwavering support and patience over the course of this academic venture.

Finally, I wish to express my gratitude to my parents, Russ and Cindy, whose selfless encouragement has been never ending.

THIS PAGE INTENTIONALLY LEFT BLANK

I. INTRODUCTION

A. BACKGROUND

The research presented here centers on the usage of the finite element method (FEM). Engineers have always faced problems dependent on time and space throughout the design process. These calculations require the use of partial differential equations (PDEs), which may be unsolvable via analytic means. Enter the FEM. As described by computer modeling company, COMSOL, this alternative approach involves discretizing the PDE to create an approximation that can be solved using numerical methods [1]. Approximations can be generated through the linear combination of base functions and the application of boundary conditions. Figure 1 illustrates this process. FEM can be applied to a variety of scenarios, such as convection-diffusion problems, Navier-Stokes equations, and structural dynamics [1].

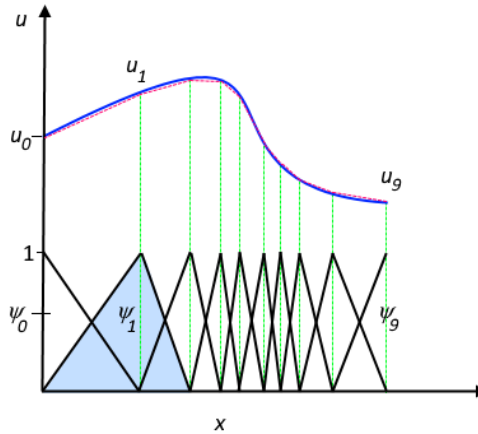


Figure 1. Discretized Function Approximation. Source: [1]. The initial function (blue) is seen alongside its approximation (red dashes), which is a linear combination of basis functions (black).

As structural dynamics is the subject of concern for this thesis, it is important to specify that the linear theory of elasticity is utilized. This permits the linear association between stress and strain. It is, therefore, essential that any

testing does not result in exceeding the proportional limit of the test sample's stress-strain curve. Figure 2 illustrates the linear stress-strain relationship below this limit. Obviously, any plastic deformation is unacceptable. With these criteria in mind, Euler-Bernoulli beam theory may be properly applied.

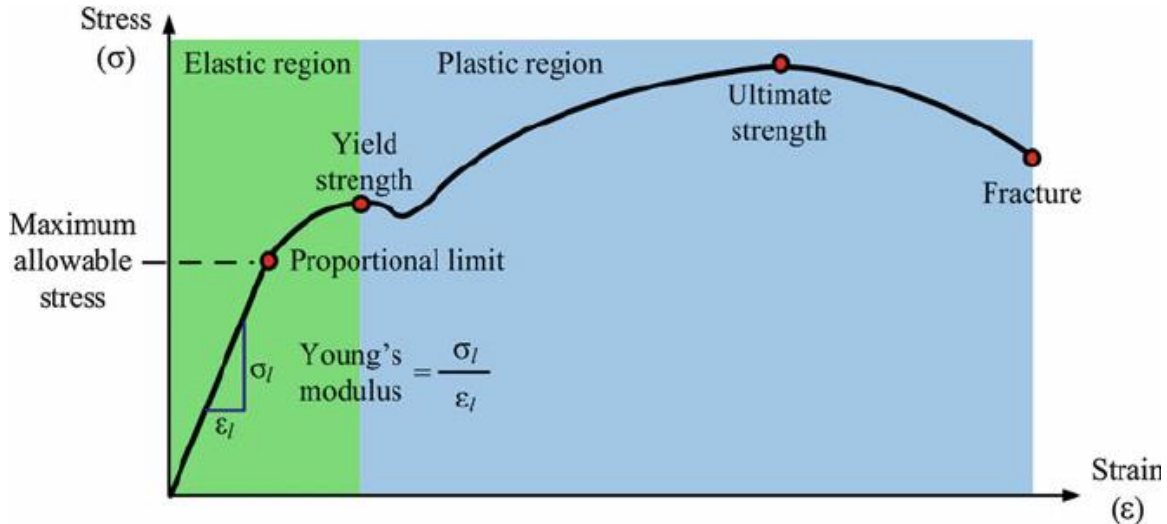


Figure 2. Sample Stress-Strain Curve. Source: [2]. Note the linear stress-strain relationship preceding the proportional limit.

With the aid of Euler-Bernoulli beam theory, the beam bending problem is simplified. According to O. A. Bauchau and J. I. Craig, this theory is based on three fundamental assumptions [3]. First, the beam cross section remains undeformed in its own plane. Second, the cross section of a beam remains plane after deformation. Third, the cross section remains normal to the deformed neutral axis [3]. This allows for relative ease in calculating the response of a beam when subjected to various loads.

With Euler-Bernoulli beam theory at one's disposal, a FEM can be generated that adheres to its principles, thus permitting the simulation of load application and resultant responses. To expedite computation time, Euler-Bernoulli beam theory is applied using simple one-dimensional line model to represent the beam in question. Due to the beam's uncomplicated geometry, the

use of such a basic FEM is acceptable. An additional consideration is the level of discretization in the simulated beam. As seen in Figure 1, the function is divided into discrete components, each of which is approximated using a linear combination of basis functions. Likewise, the beam FEM can be discretized into a certain number of elements. A high element count can provide approximations that are more accurate. However, as the number of elements increases, so does the computation time. This processing time is a major limiting factor of FEM complexity. As with function u in Figure 1, the size of the elements can be varied, so relatively uniform geometry is covered by larger elements, while sharper changes in geometry are accounted for with smaller elements.

While increasing the element count can improve the accuracy of the FEM, it does not entirely eliminate inconsistencies between a simulated item and its physical counterpart. There remain unique complexities in the real world that are not initially accounted for by FEM. For example, structural joints and damping are phenomena that cannot be accurately calculated without experimental input and will, therefore, be lacking in a first iteration FEM. Additionally, physical irregularities such as deviations from material homogeneity, variations in production, etc., may exist. These differences between simulation and reality can be revealed by generating and comparing frequency response functions (FRF) for the FEM and its physical associate.

Of particular interest is the frequency at which function peaks exist. The peaks of an FRF generated from simulated data correspond to natural frequencies. FRFs obtained via experimental testing can also identify natural frequencies, once damping is accounted for. By comparing these two functions, a matrix of frequency differences can be assembled. This, in turn, can be applied to eigenvalue sensitivities to determine the structural discrepancy. Figure 3 exhibits a typical FRF.

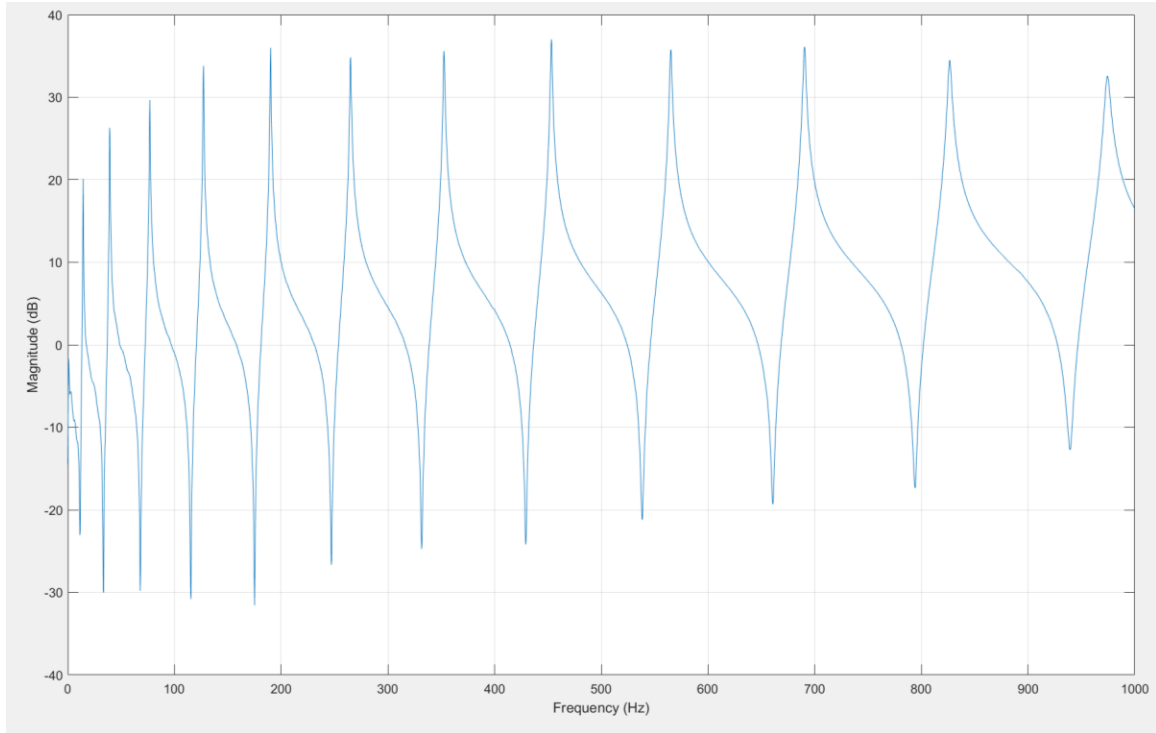


Figure 3. Example FRF Generated from Experimental Data

B. LITERATURE REVIEW

The concept of using artificial boundary conditions for model updating and damage detection has been explored by J. H. Gordis since the 1990s. His article “Artificial Boundary Conditions for Model Updating and Damage Detection” in *Mechanical Systems and Signal Processing* describes the approach [4]. This published work states that FEM improvement is required to establish an acceptable level of confidence in the FEM’s ability to predict structure response. According to Gordis, “This inaccuracy of the FE model is reduced (the model is ‘improved’) by the adjustment of selected physical and material parameters which define the model. These parameters can include dimensional properties of structural elements, moduli of elasticity, and densities, for example” [4]. An inherent complication with this approach is the fact that modal tests yield a number of modal parameters that is usually less than the number of parameters

that define the FEM. This produces an underdetermined problem, as there is not enough usable data to reliably adjust (update) the FEM [4].

In Reference [4], Gordis notes the work of S. Li, S. Shelley, and D. Brown, who introduced a method of expanding the measured modal parameter database through the use of perturbed boundary conditions (PBCs). This approach requires physical modifications to the test structure. This can include the addition of mass at selected points. With every different modification, an additional modal test must be conducted [4]. While this method does provide the requisite data, it is relatively time consuming and costly due to the implementation of multiple structure modifications and the performance of numerous modal tests.

Gordis presents an alternative solution. Through the use of artificial boundary conditions (ABCs) vice PBCs, physical modifications can be avoided. Imposing boundary conditions, such as the mass additions, can be easily done in the simulated realm. Though these ABCs produce multiple FEMs, corresponding measured mode frequencies can be obtained from a single modal test. Additionally, more complex modifications, such as the application of pins, can be applied, thus creating an even larger database of modal parameters [4]. As stated in a subsequent article by J. H. Gordis and K. Papagiannakis, for each pin-based ABC, an omitted coordinate system (OCS) is defined. This system corresponds to a structure with additional restraints placed at some combination of locations [5].

Gordis reveals that without the application of boundary conditions, the parameter database remains limited, and the eigenvalue sensitivity matrix (assembled from the parameter database) risks containing data sets that are linearly dependent (or near-linearly dependent) to one another [4]. This linear dependence results in a poorly conditioned matrix. In other words, it is a matrix that is rank deficient. The unfortunate result is a rank deficient matrix that can fail to produce the required adjustments for model updating or detect damage in every element.

Even with a large database of modal parameters generated from both baseline FEMs and those with ABCs applied, a well-conditioned sensitivity matrix is not guaranteed. An ideal combination of parameters must be selected for sensitivity matrix assembly. Gordis and Papagiannakis offer an approach to sensitivity matrix construction using QR decomposition with column pivoting [5]. In their approach, all pin-based ABC location combinations are applied to a simple beam FEM. Errors were intentionally introduced to the FEM, and each parameter set was utilized in an attempt to localize these errors. In each scenario, relative magnitude error (RME) and maximum false alarm (MFA) were calculated. When these criteria reached near-zero values, the sensitivity row set was saved. The specific columns selected for this ideal set are identified by utilizing the permutation matrix of the QR decomposition [5].

J. Shin and J. H. Gordis offer a simplified, alternative approach to parameter selection called orthogonal projection. This method is focused on addressing the condition number of the sensitivity matrix. The condition number as a direct indication of the level of linear dependence between data sets within the matrix. The lower the condition number, the less linear dependence exists. With linear dependence minimized, model update and damage detection accuracy is maximized [6]. This method can be universally applied to any ABC type, location, or quantity without modification. Due to its simplicity and ease of implementation, this approach is preferred for use in this thesis.

C. SCOPE OF THESIS

This thesis delves into the variety of ABCs that can be used to populate a candidate matrix for data set selection and eigenvalue sensitivity optimization. Different types, numbers, and locations of ABCs are explored in an effort to provide a substantial library of parameter and modal options.

Additionally, different styles of FEMs are compared with regard to accuracy and computation time. The structure that is modeled is a rectangular cross-section free-free beam. Since force application and resultant translation is

uniaxial, a simple two-DOF per node FEM is utilized. However, different element sizes and numbers can be tried. These various models are used to identify a candidate “damaged condition” for the test beam.

Finally, experimental validation of the eigenvalue sensitivity concept is investigated. Associated complications with working in physical realm will be discussed along with devised solutions. Recommendations for achieving the best results are presented.

D. SOFTWARE NOTES

FEM construction, model updating, and simulated damage detection is performed using MATLAB 2017a software [7]. Beam impact testing and data collection is conducted with Pulse Reflex software by Brüel & Kjær [8].

THIS PAGE INTENTIONALLY LEFT BLANK

II. THEORY

A. EULER-BERNOULLI BEAM THEORY

Since all FEMs constructed for this thesis follow Euler-Bernoulli beam theory, it is important that the associated equations are discussed. This begins with considering the forces and moments acting on a beam. W. T. Thomson and M. D. Dahleh state that the sum of forces in the y -direction is [9]:

$$dV - p(x)dx = 0 \quad (1)$$

where V is the shear force and $p(x)$ is the loading per unit length of the beam. The sum of moments about any point is [9]:

$$dM - Vdx - \frac{1}{2} p(x)(dx)^2 = 0 \quad (2)$$

where M is the bending moment [9]. Figure 4 illustrates these variables.

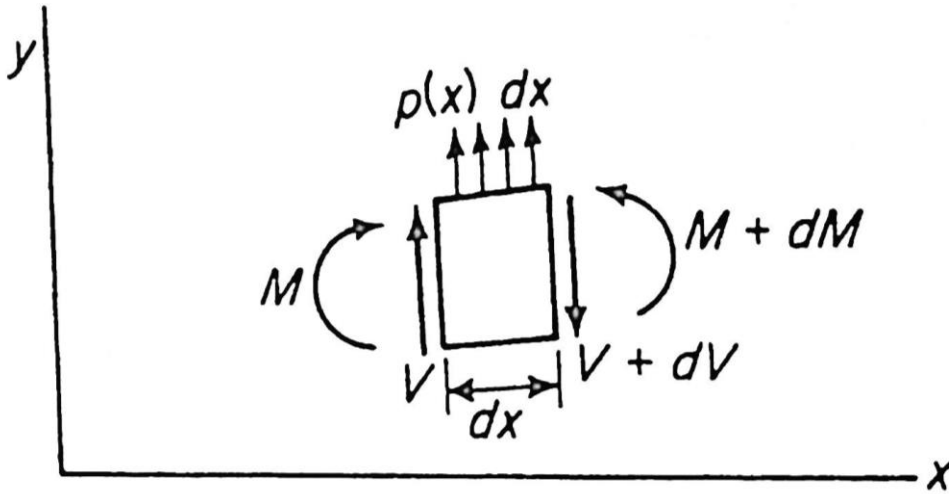


Figure 4. Shear and Moment Acting on a Beam Element. Source: [9].

These equations provide the following relationships [9]:

$$\frac{dV}{dx} = p(x) \quad (3)$$

$$\frac{dM}{dx} = V \quad (4)$$

Based on these relationships, the following equation is obtained [9]:

$$\frac{d^2M}{dx^2} = \frac{dV}{dx} p(x) \quad (5)$$

The bending moment, M , is related to the flexure equation [9]:

$$M = EI \frac{d^2y}{dx^2} \quad (6)$$

Substituting M in Equation (5) produces [9]:

$$\frac{d^2}{dx^2} \left(EI \frac{d^2y}{dx^2} \right) = p(x) \quad (7)$$

According to William Thomson and Marie Dahleh's *Theory of Vibration with Applications*, "beam vibrating about its static equilibrium position under its own weight, the load per unit length is equal to the inertia load due to its mass and acceleration. Because the inertia force is in the same direction as $p(x)$...we have, by assuming harmonic motion" [9]:

$$\frac{d^2}{dx^2} \left(EI \frac{d^2y}{dx^2} \right) - \rho \omega^2 y = 0 \quad (8)$$

where E is the modulus of elasticity, I is the second moment of inertia, ρ is mass density, and ω is the natural frequency [9].

B. FINITE ELEMENT MODELING

With the principles of Euler-Bernoulli beam theory specified, the FEM can be constructed accordingly. For a simple, one-dimensional model, each node features two degrees of freedom (DOF), one translational, the other rotational.

According to R. R. Craig, Jr., for a uniform beam element, transverse displacement is defined as [10]:

$$V(x,t) = \sum_{i=1}^4 \psi_i(t) v_i(t) \quad (9)$$

where V is the transverse displacement at a particular point along the length of the beam element(x) at a particular moment in time (t). v is the transverse and angular displacements at each end of the beam element, as seen in Figure 5 [10].

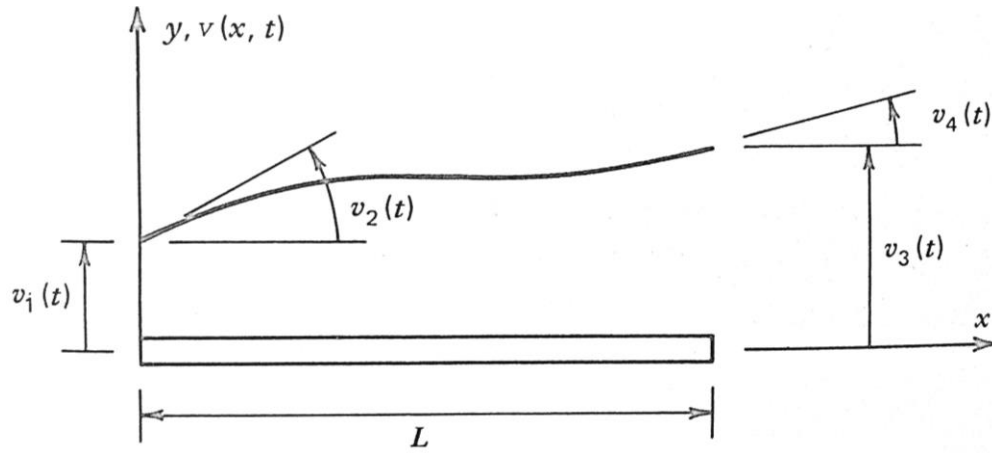


Figure 5. Transverse Displacement of a Uniform Beam Element.
Source: [10].

ψ is the shape functions (i.e., basis functions) that are linearly combined to replicate the transverse displacement function. These shape functions must adhere to the following boundary conditions [10]:

$$\begin{aligned} \psi_1(0) &= 1, & \psi_1'(0) &= \psi_1(L) = \psi_1'(L) = 0 \\ \psi_2'(0) &= 1, & \psi_2(0) &= \psi_2(L) = \psi_2'(L) = 0 \\ \psi_3(L) &= 1, & \psi_3(0) &= \psi_3'(0) = \psi_3'(L) = 0 \\ \psi_4'(L) &= 1, & \psi_4(0) &= \psi_4'(0) = \psi_4(L) = 0 \end{aligned} \quad (10)$$

Figure 6 illustrates these shape functions along an element with length L and their respective boundary conditions.

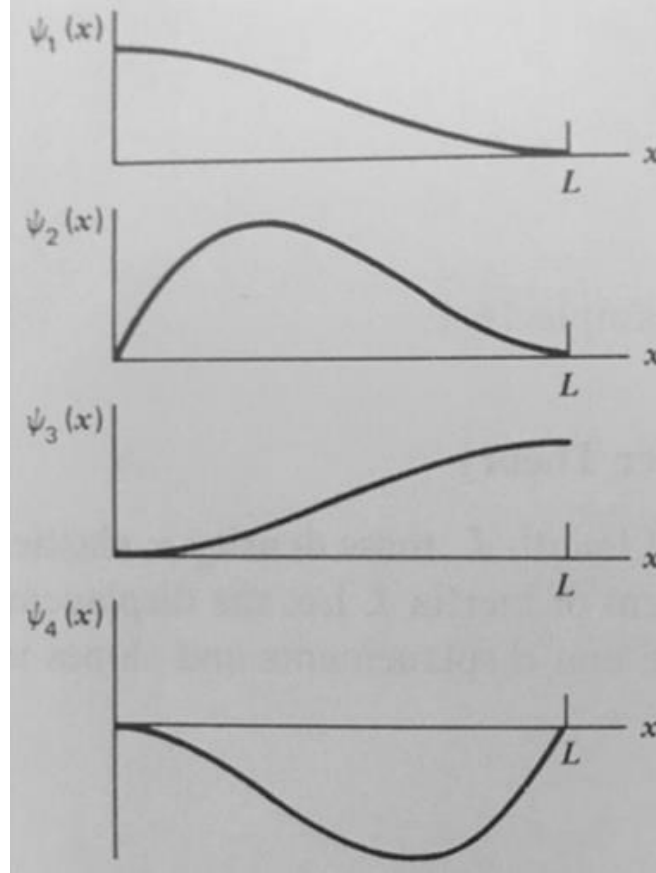


Figure 6. Shape Functions Showing Boundary Conditions.
Source: [10].

The general solution to Equation (9) is a cubic polynomial [10]:

$$V(x) = c_1 + c_2 \left(\frac{x}{L} \right) + c_3 \left(\frac{x}{L} \right)^2 + c_4 \left(\frac{x}{L} \right)^3 \quad (11)$$

Substituting the boundary conditions into Equation (11) produces the four shape functions [10]:

$$\begin{aligned}
\psi_1 &= 1 - 3\left(\frac{x}{L}\right)^2 + 2\left(\frac{x}{L}\right)^3 \\
\psi_2 &= x - 2L\left(\frac{x}{L}\right)^2 + L\left(\frac{x}{L}\right)^3 \\
\psi_3 &= 3\left(\frac{x}{L}\right)^2 - 2\left(\frac{x}{L}\right)^3 \\
\psi_4 &= -L\left(\frac{x}{L}\right)^2 + L\left(\frac{x}{L}\right)^3
\end{aligned} \tag{12}$$

Using the principles of Bernoulli-Euler beams along with these shape functions, stiffness and mass coefficients can be calculated [10]:

$$k_{ij} = \int_0^L EI \psi_i'' \psi_j'' dx \tag{13}$$

$$m_{ij} = \int_0^L \rho A \psi_i \psi_j dx \tag{14}$$

By substituting the shape functions from Equation (12) into Equations (13) and (14), the element stiffness and mass matrices can be obtained [10]:

$$K_{elem} = \left(\frac{EI}{L^3} \right) \begin{bmatrix} 12 & 6L & -12 & 6L \\ & 4L^2 & -6L & 2L^2 \\ & & 12 & -6L \\ \text{symm.} & & & 4L^2 \end{bmatrix} \tag{15}$$

$$M_{elem} = \left(\frac{\rho AL}{420} \right) \begin{bmatrix} 156 & 22L & 54 & -13L \\ & 4L^2 & 13L & -3L^2 \\ & & 156 & -22L \\ \text{symm.} & & & 4L^2 \end{bmatrix} \tag{16}$$

It is important to note that these matrices only account for a single element in a model composing of N elements, $N+1$ nodes, and $2*(N+1)$ total DOF. All elements must be adjoined to assemble the model in its entirety and to account for the fact that interior elements have common nodes (and their respective DOF) with adjacent elements. This is done by overlapping element stiffness and mass matrices at DOFs in common as shown on the following page:

$$K_{global} = \begin{bmatrix} K_{1,1}^1 & K_{1,2}^1 & K_{1,3}^1 & K_{1,4}^1 & 0 & 0 & 0 & 0 & 0 & 0 \\ K_{2,1}^1 & K_{2,2}^1 & K_{2,3}^1 & K_{2,4}^1 & 0 & 0 & 0 & 0 & 0 & 0 \\ K_{3,1}^1 & K_{3,2}^1 & K_{3,3}^1 + K_{1,1}^2 & K_{3,4}^1 + K_{1,2}^2 & K_{1,3}^2 & K_{1,4}^2 & 0 & 0 & 0 & 0 \\ K_{4,1}^1 & K_{4,2}^1 & K_{4,3}^1 + K_{2,1}^2 & K_{4,4}^1 + K_{2,2}^2 & K_{2,3}^2 & K_{2,4}^2 & 0 & 0 & 0 & 0 \\ 0 & 0 & K_{3,1}^2 & K_{3,2}^2 & K_{3,3}^2 + K_{1,1}^3 & K_{3,4}^2 + K_{1,2}^3 & 0 & 0 & 0 & 0 \\ 0 & 0 & K_{4,1}^2 & K_{4,2}^2 & K_{4,3}^2 + K_{2,1}^3 & K_{4,4}^2 + K_{2,2}^3 & 0 & 0 & 0 & 0 \\ 0 & 0 & 0 & 0 & 0 & 0 & \ddots & 0 & 0 & 0 \\ 0 & 0 & 0 & 0 & 0 & 0 & 0 & K_{3,3}^{2N+1} + K_{1,1}^{2(N+1)} & K_{3,4}^{2N+1} + K_{1,2}^{2(N+1)} & K_{1,3}^{2(N+1)} & K_{1,4}^{2(N+1)} \\ 0 & 0 & 0 & 0 & 0 & 0 & 0 & K_{4,3}^{2N+1} + K_{2,1}^{2(N+1)} & K_{4,4}^{2N+1} + K_{2,2}^{2(N+1)} & K_{2,3}^{2(N+1)} & K_{2,4}^{2(N+1)} \\ 0 & 0 & 0 & 0 & 0 & 0 & 0 & K_{3,1}^{2(N+1)} & K_{3,2}^{2(N+1)} & K_{3,3}^{2(N+1)} & K_{3,4}^{2(N+1)} \\ 0 & 0 & 0 & 0 & 0 & 0 & 0 & K_{4,1}^{2(N+1)} & K_{4,2}^{2(N+1)} & K_{4,3}^{2(N+1)} & K_{4,4}^{2(N+1)} \end{bmatrix} \quad (17)$$

$$M_{global} = \begin{bmatrix} M_{1,1}^1 & M_{1,2}^1 & M_{1,3}^1 & M_{1,4}^1 & 0 & 0 & 0 & 0 & 0 & 0 \\ M_{2,1}^1 & M_{2,2}^1 & M_{2,3}^1 & M_{2,4}^1 & 0 & 0 & 0 & 0 & 0 & 0 \\ M_{3,1}^1 & M_{3,2}^1 & M_{3,3}^1 + M_{1,1}^2 & M_{3,4}^1 + M_{1,2}^2 & M_{1,3}^2 & M_{1,4}^2 & 0 & 0 & 0 & 0 \\ M_{4,1}^1 & M_{4,2}^1 & M_{4,3}^1 + M_{2,1}^2 & M_{4,4}^1 + M_{2,2}^2 & M_{2,3}^2 & M_{2,4}^2 & 0 & 0 & 0 & 0 \\ 0 & 0 & M_{3,1}^2 & M_{3,2}^2 & M_{3,3}^2 + M_{1,1}^3 & M_{3,4}^2 + M_{1,2}^3 & 0 & 0 & 0 & 0 \\ 0 & 0 & M_{4,1}^2 & M_{4,2}^2 & M_{4,3}^2 + M_{2,1}^3 & M_{4,4}^2 + M_{2,2}^3 & 0 & 0 & 0 & 0 \\ 0 & 0 & 0 & 0 & 0 & 0 & \ddots & 0 & 0 & 0 \\ 0 & 0 & 0 & 0 & 0 & 0 & 0 & M_{3,3}^{2N+1} + M_{1,1}^{2(N+1)} & M_{3,4}^{2N+1} + M_{1,2}^{2(N+1)} & M_{1,3}^{2(N+1)} & M_{1,4}^{2(N+1)} \\ 0 & 0 & 0 & 0 & 0 & 0 & 0 & M_{4,3}^{2N+1} + M_{2,1}^{2(N+1)} & M_{4,4}^{2N+1} + M_{2,2}^{2(N+1)} & M_{2,3}^{2(N+1)} & M_{2,4}^{2(N+1)} \\ 0 & 0 & 0 & 0 & 0 & 0 & 0 & M_{3,1}^{2(N+1)} & M_{3,2}^{2(N+1)} & M_{3,3}^{2(N+1)} & M_{3,4}^{2(N+1)} \\ 0 & 0 & 0 & 0 & 0 & 0 & 0 & M_{4,1}^{2(N+1)} & M_{4,2}^{2(N+1)} & M_{4,3}^{2(N+1)} & M_{4,4}^{2(N+1)} \end{bmatrix} \quad (18)$$

With stiffness and mass matrices accounting for the entire FEM (i.e., global matrices), the equation of motion can be applied as presented by W. T. Thomson and M.D. Dahleh [9]:

$$[M]\{\ddot{x}\} + [C]\{\dot{x}\} + [K]\{x\} = \{f(t)\} \quad (19)$$

where $[M]$ is the global (system) mass matrix, $[C]$ is the global damping matrix, and $[K]$ is the global stiffness matrix. The u vectors, from left to right, are transverse acceleration, transverse velocity, and transverse position. Vector f contains the external forces and moments. This equation of motion is generally a set of M coupled equations. Fortunately, through the use of modal transformation, these equations can be decoupled by premultiplying Equation (19) by the modal matrix P (the modal matrix is determined by the solution of the homogeneous undamped equation). Letting $\{x\} = [P]\{y\}$, the following equation is obtained [9]:

$$[P]^T [M] [P] \{\ddot{y}\} + [P]^T [C] [P] \{\dot{y}\} + [P]^T [K] [P] \{y\} = [P]^T \{f(t)\} \quad (20)$$

The mass and stiffness terms of Equation (20) produce diagonal matrices. However, the damping term is generally not diagonal. In order to make this term diagonal, proportional damping must be assumed. These actions permit the uncoupling of Equation (19), with its i th equation taking the following form [9]:

$$\ddot{y}_i + 2\xi_i \omega_i \dot{y}_i + \omega_i^2 y_i = \Gamma_i f_i(t) \quad (21)$$

where ξ is the damping ratio, defined by R. R. Craig, Jr., is [10]:

$$\xi = \frac{c}{c_{cr}} \quad (22)$$

where c is the damping coefficient (obtained experimentally) and c_{cr} is the critical damping coefficient [10]:

$$c_{cr} = 2m\omega_i = \frac{2k}{\omega_i} = 2\sqrt{km} \quad (23)$$

ω_i is natural frequency, which is defined as [10]:

$$\omega_i = \sqrt{\frac{k}{m}} \quad (24)$$

and Γ_i is the mode participation factor, which is defined by Thomson and Dahleh as [9]:

$$\Gamma_i = \frac{\sum_j \phi_i(x_j)[P](x_j)}{\sum_j m_j \phi_i^2(x_j)} \quad (25)$$

Note the lack of an element and global damping matrix in the previous calculations. The experimental rig supporting the free-free beam in question results in insignificant damping. Therefore, $[C]$ can be omitted from Equation (19) and will not be considered when simulating dynamic response. Additionally, the beam will not be subjected to external loading. Therefore, Equation (19) can be reduced to:

$$[M]\{\ddot{x}\} + [K]\{x\} = 0 \quad (26)$$

However, it is important to note that experimental data analysis involves using an algorithm that calculates damping ratio based on FRF shape. The relationship between damped and undamped natural frequency is:

$$\omega_d = \omega_n \sqrt{1 - \xi^2} \quad (27)$$

where ω_d is the damped natural frequency, ω_n is the undamped natural frequency, and ξ is the damping ratio.

C. EIGENVALUE SENSITIVITY

In order to allow for model updating and damage detection, a relationship between differences in natural frequencies and differences in physical parameters must be defined. According to J. H. Gordis, the sensitivity is a rate of

change of some eigenvalue, λ , of mode i , with respect to the change of some physical parameter, p as shown here [11]:

$$S_{ij} = \frac{\partial \lambda_i}{\partial p_j} \quad (28)$$

Therefore, changes in an eigenvalue can be predicted given a change in a physical parameter [11]:

$$\lambda_i^* = \lambda_i + (S_{ij} * \Delta p_j) \quad (29)$$

where λ_i^* is the altered eigenvalue that is the result of a parameter modification, Δp_j . By constructing a sensitivity matrix $[S]$ of S_{ij} elements, each row representing a mode and each column representing a parameter, the following equation can be formed [11]:

$$\{\Delta \lambda\} = [S] \{\Delta p\} \quad (30)$$

Equation (30) is what allows for model updating by comparing simulated and experimental obtained natural frequencies. It is also what provides indication of damage in the form of Δp , which is generated from a variance in natural frequencies from an updated model and a damaged physical beam [11].

To generate the sensitivity matrix, one must calculate each element, S_{ij} . To do so, the eigensystem must first be defined [11]:

$$[K - \lambda_i M] \{\phi^{(i)}\} = \{0\} \quad (31)$$

where $\phi^{(i)}$ is the eigenvector for mode i . Both $[K]$ and $[M]$ are functions of certain physical parameters. In this work, the perturbation (Δp) will be defined only as changes in flexural rigidity (E^*I). Therefore, only $[K]$ will be affected by these perturbations. Taking the derivative of Equation (31) yields [11]:

$$\left[\frac{\partial K}{\partial p_j} - \lambda_i \frac{\partial M}{\partial p_j} - \frac{\partial \lambda_i}{\partial p_j} M \right] \{\phi^{(i)}\} + \{\phi^{(i)}\}^T [K - \lambda_i M] \left\{ \frac{\partial \phi^{(i)}}{\partial p_j} \right\} = 0 \quad (32)$$

Pre-multiplying by $\{\phi^{(i)}\}^T$ and transposing Equation (32) produces [11]:

$$\{\phi^{(i)}\}^T \left[\frac{\partial K}{\partial p_j} - \lambda_i \frac{\partial M}{\partial p_j} - \frac{\partial \lambda_i}{\partial p_j} M \right] + \left\{ \frac{\partial \phi^{(i)}}{\partial p_j} \right\}^T [K - \lambda_i M] \{\phi^{(i)}\} = 0 \quad (33)$$

Invoking Equation (29) and assuming mass-normalized shapes, $\{\phi^{(i)}\}^T [M] \{\phi^{(i)}\} = 1$, the equation can be manipulated to yield [11]:

$$S_{ij} = \frac{\partial \lambda_i}{\partial p_j} = \{\phi^{(i)}\}^T \left[\frac{\partial K}{\partial p_j} - \lambda_i \frac{\partial M}{\partial p_j} \right] \{\phi^{(i)}\} = 0 \quad (34)$$

It is essential to note that these derivatives are calculated by using a forward difference approximation based on the linear terms of the Taylor series [11]. Therefore, if $\partial \lambda_i$ from Equation (28) exceeds the linearity of the eigenvalue sensitivity, the equation will not be usable.

D. APPLICATION OF ARTIFICIAL BOUNDARY CONDITIONS IN THE FINITE ELEMENT MODEL

Due to linear dependence between the rows of the eigenvalue sensitivity matrix, the rank of the matrix is less than the number of parameters. This can lead to a failure to detect damage in certain elements. In order to bolster the capability of the sensitivity matrix, ABCs are applied to allow the construction of a full-rank sensitivity matrix. However, a full rank sensitivity matrix is only a minimum standard of acceptability. J. Shin and J. H. Gordis state that effective model updating and accurate damage detection is also dependent on the matrix's condition number [6]. This number can be driven toward unity (perfect linear independence) with the judicious use of ABCs. The types of ABCs examined here include artificial pins, point masses, and springs.

Pins eliminate translation while preserving rotation at their location. Therefore, an artificial pin will eliminate the translational DOF at the FEM element node at which it is applied. This effect is represented in the FEM by eliminating the row and column associated with the pinned DOF in the global mass and

stiffness matrices. For springs to ground, the diagonal stiffness matrix element associated with the modified DOF is increased by the spring constant. Point masses are applied in a similar fashion, except it is the diagonal mass matrix element that is adjusted. Like the pins, springs and point masses only affect the translational DOFs; rotational DOFs remain unaltered. Multiple ABCs can be applied at various nodes. A key consideration is that the ABC locations on the FEM must correspond to the accelerometers placed on the physical structure. This way, the same ABC configuration can be applied to the measured data.

Each ABC configuration provides its own sensitivity matrix. These matrices can be stacked into one all-encompassing sensitivity library matrix as shown here:

$$[S]_{library} = \begin{bmatrix} [S^{(0)}] \\ [S^{(1)}] \\ [S^{(2)}] \\ \vdots \\ [S^{(n)}] \end{bmatrix} \quad (35)$$

E. SELECTION OF ARTIFICIAL BOUNDARY CONDITIONS

J. Shin and J. H. Gordis state that with an eigenvalue sensitivity matrix library established, individual rows from this matrix must be selected to form a square matrix that can be applied in Equation (30) [6]:

$$\begin{Bmatrix} \{\Delta\lambda_{r_0}^{(0)}\} \\ \{\Delta\lambda_{r_1}^{(1)}\} \\ \{\Delta\lambda_{r_2}^{(2)}\} \\ \vdots \\ \{\Delta\lambda_{r_n}^{(n)}\} \end{Bmatrix} = \begin{bmatrix} [S_{r_0}^{(0)}] \\ [S_{r_1}^{(1)}] \\ [S_{r_2}^{(2)}] \\ \vdots \\ [S_{r_n}^{(n)}] \end{bmatrix} \{\Delta p\} \quad (36)$$

These matrices are referred to as “composites” as results in Equation (36) being rewritten as [6]:

$$\{\Delta\Lambda\} = [\bar{S}] \{\Delta p\} \quad (37)$$

where $\Delta\Lambda$ is the composite vector of eigenvalue differences, and \bar{S} is the composite sensitivity matrix [6]. Each row from the eigenvalue sensitivity matrix library is a candidate for populating the composite sensitivity matrix. These individual rows are identified as $S_{i,j}^L$ where L is the total number of rows in the library, i is the row index and j is the ABC configuration. Normalized rows are defined as [6]:

$$\tilde{S}_{i,j}^L = S_{i,j}^L / \|S_{i,j}^L\| \quad (38)$$

The main objective in populating the composite sensitivity matrix is to append rows from the candidate library that maximize the angle between these candidates and the subspace spanned by previously selected rows, $R(\bar{S}^T)$. During the composite matrix assembly, the set of rows selected thus far is \bar{S} and the candidate row is $\tilde{S}_{i,j}^L$. The angle between $\tilde{S}_{i,j}^L$ and \bar{S} is produced by [6]:

$$\cos \theta_{i,j} = \frac{\{\tilde{S}_{i,j}^L\}^T [P] \{\tilde{S}_{i,j}^L\}}{\|\tilde{S}_{i,j}^L\| \bullet \| [P] \{\tilde{S}_{i,j}^L\} \|} \quad (39)$$

where $[P]$ is the projector defined as [6]:

$$P = \bar{S} (\bar{S}^T \bar{S})^{-1} \bar{S}^T \quad (40)$$

Figure 7 illustrates the vector of a candidate row projecting onto the subspace spanned by rows already selected.

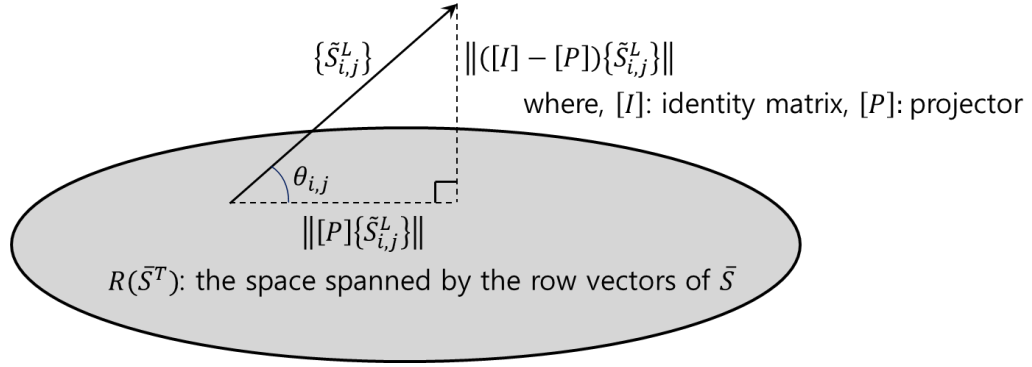


Figure 7. Candidate Row Vector and Selected Row Subspace.
Source [6].

In addition to the condition number, the mode dependency index (MDI) and the parameter dependency index (PDI) also serve as indicators of linear dependency. Specifically, MDI and PDI reflect the linear independency between any two rows or two columns in the sensitivity matrix, respectively. MDI and PDI are defined as [6]:

$$MDI_{i,j} = \frac{\left| [R_{(i)}] [R_{(j)}]^T \right|}{\sqrt{[R_{(i)}] [R_{(i)}]^T [R_{(j)}] [R_{(j)}]^T}} \quad (41)$$

$$PDI_{i,j} = \frac{\left| [C_{(i)}] [C_{(j)}]^T \right|}{\sqrt{[C_{(i)}] [C_{(i)}]^T [C_{(j)}] [C_{(j)}]^T}} \quad (42)$$

where R is one of the two rows of the composite sensitivity matrix being examined for linear dependence, and C is one of the two columns [6].

F. FREQUENCY RESPONSE FUNCTION ANALYSIS

With the composite eigenvalue sensitivity matrix and eigenvalue difference vector populated, the associated ABC configurations must now be applied to experimental data. Modal testing of a physical beam does not yield global mass

and stiffness matrices, such as the ones generated by the FEM. Therefore, a different approach is required to apply the selected ABC configurations to the test data.

According to J. H. Gordis, the FRF matrix, $[H]$, is generated by the modal test. Ignoring damping, each FRF matrix is defined as [4]:

$$H_{ij}(\Omega) = \sum_{r=1}^p \frac{\phi_i^r \phi_j^r}{\omega_r^2 - \Omega^2} \quad (43)$$

where is ϕ_i^r a mass normalized mode shape, ω_r is the r th natural frequency, and Ω is the forcing frequency. These FRFs are then assigned to different coordinate sets. The first set, the connection set (CSET), contains FRFs that belong to a modified DOF. For example, the placement of an artificial pin will result in the translational DOF of the pinned node being assigned to the CSET. The remaining DOFs (not altered by ABCs) are assigned to the internal set (ISET). The partitioned FRF matrices take the following form [4]:

$$H = \begin{bmatrix} H_{ii} & H_{ic} \\ H_{ci} & H_{cc} \end{bmatrix} \quad (44)$$

The new FRF can be generated by applying the partitions to the following formula [4]:

$$H^* = H_{ii} - H_{ic} H_{cc}^{-1} H_{ci} \quad (45)$$

This modified FRF matrix, H^* , is recalculated for every frequency in the desired bandwidth. Taking the average of its diagonals will yield an FRF that all of the modes within the test bandwidth. Plotting this function will reveal amplitude peaks that correspond to the test article's natural frequencies. These frequencies can then be compared to the FEM natural frequencies, thus producing the composite vector of eigenvalue differences. This permits the use of Equation (37) to solve for any parameter change required for model updating or for detecting damage [4].

III. EXPERIMENTAL APPROACH

A. TEST ARTICLES

The test articles utilized for modal testing are extruded aluminum rectangular beams. Upon receipt, these beams were drilled and tapped to accommodate accelerometer mounting screws. The first beam was not altered any further to be used as an “intact” structure. The second was reserved for further alterations to act as damage. Table 1 lists the beam properties and Appendix A features the inspection report.

Table 1. Test Beam Properties

Material	Al 6061-T6511
Mass, kg (lbm)	2.449 (5.4)
Length, cm (in)	182.88 (72)
Width, cm (in)	5.09 (2.004)
Thickness, cm (in)	0.9627 (0.379)
Tap Diameter, cm (in)	0.4064 (0.16)
Distance from Beam Edge to Tap, cm (in)	1.27 (0.5)
Distance Between Taps, cm (in)	12.8778 (5.07)

Due to the focus on ABCs, the beam was suspended in a free-free condition. This was accomplished by utilizing two elastic cords attached to an overhead, each about 270 cm (106.3 in) in length. The resultant pendulum frequency is 0.54 Hz, far less than any natural frequency and, therefore, does not interfere with the modal testing. Figure 8 shows one of the rectangular beams and Figure 9 shows the test rig with the suspended, free-free test article.



Figure 8. Rectangular Beam With Fifteen Taps for Accelerometers



Figure 9. Suspended Beam

B. INSTRUMENTATION

Each of the fifteen taps allows for the attachment of two accelerometer 10–32 mounting studs (shown in Figure 10). One is used for attaching the accelerometer, while the other is used as an impact point for the force hammer.

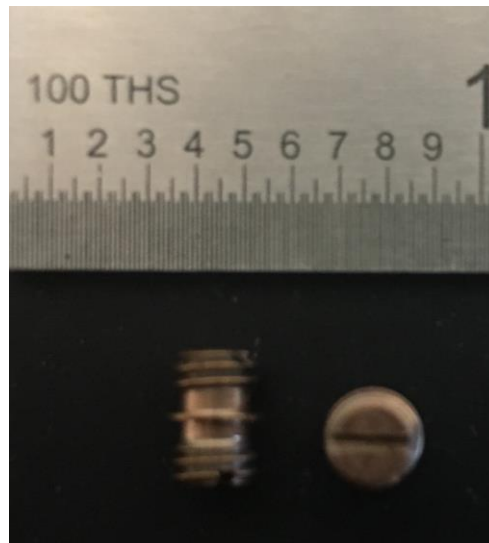


Figure 10. Mounting Studs with 2.54 cm (1 in) Scale

The accelerometers are PCB Piezotronics ICP Model 336C04 (shown in Figure 11). Table 2 contains the dimensions of the accelerometer and its mount.

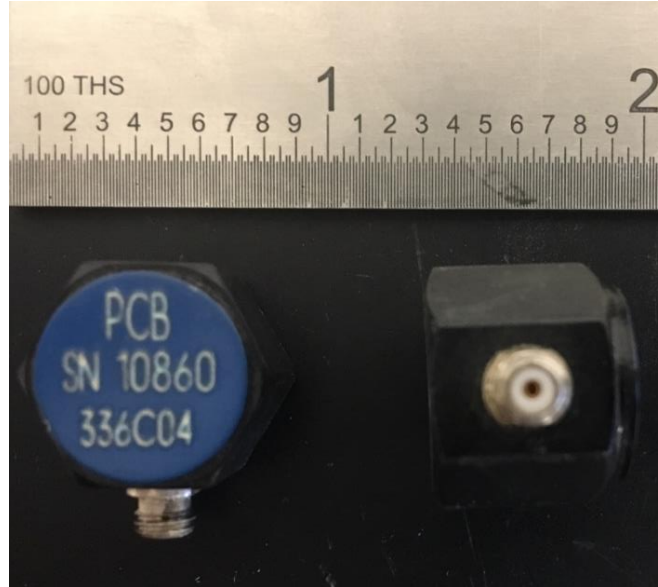


Figure 11. Accelerometers with 5.08 cm (2 in) Scale

Table 2. Accelerometer and Mount Properties

Accelerometer Mass, g (oz)	5.07 (0.179)
Accelerometer Diameter, cm (in)	1.575 (0.62)
Accelerometer Height, cm (in)	1.397 (0.55)
Mounting Screw Mass, g (oz)	0.72 (0.0254)
Mounting Screw Diameter, cm (in)	0.4191 (0.165)
Mounting Screw Height, cm (in)	0.7061 (0.278)

The impact hammer is a PCB Piezotronics Model 086B03 (shown in Figure 12). Before conducting the modal test, each accelerometer's calibration was verified using a PCB Piezotronics Model 194C06 handheld shaker (shown in Figure 13) in conjunction with the Pulse Reflex Software. Appendix B features the calibration and specification sheets for each of these instruments.



Figure 12. Impact Hammer



Figure 13. Handheld Shaker with Accelerometer Attached at Top

C. MODAL TESTING

Modal testing can be conducted in multiple fashions, each with their own unique method of providing beam excitation: step sine, random burst, single impact, and random impact.

The step sine approach utilizes a shaker and force transducer (load cell) attached to a mounting screw. The shaker must be suspended from a stand to maintain the rig's free-free condition. An additional consideration is the length and stiffness of the attachment rod ("stinger"). A stinger that is too long or lacks the adequate stiffness will result in energy dissipation and skew results. Beam excitation is conducted at a specified frequency interval across the entirety of the desired bandwidth. The Pulse Reflex software pauses at each frequency to ensure that all transients have dissipated and that beam response is caused solely by excitation at the dwell frequency. The higher the frequency resolution, the longer the process takes to cover a specified bandwidth. Due to the minimum desired frequency resolution of 0.3125 Hz and the 1000 Hz bandwidth, the step sine approach is extremely time consuming.

The burst random technique also employs a shaker and accompanying force transducer. As the name suggests, the shaker generates a random time signal that contains all frequencies within the bandwidth of interest to produce the beam's dynamic response. Compared to step sine, this method is significantly quicker to complete.

The single impact method uses a force hammer to impact each node where an accelerometer is mounted. The node is struck once with the hammer and the response is recorded for a period of time. The higher the desired frequency resolution, the longer the recording time required. To ensure consistent results, these single impacts are repeated several times and the resulting frequency response functions are averaged at each node.

Random impact also utilizes the impact hammer. Instead of using a single hammer strike, numerous hammer impacts are applied over a period of time. The

times at which data is collected by the Pulse Reflex software are randomized in order to ensure there are no artificialities produced from inadvertent periodicity in hammer impacts.

Out of the four methods, the single and random impact modal tests were deemed most useful for the purposes of this research. The shaker-based techniques required additional setup due to the more complex rig. Additionally, due to the beam's low mass, the attached shaker added an unacceptably high mass percentage to the test article, which could potentially corrupt results. As can be seen in Figure 14, the shaker-based approaches also generated additional noise at lower frequencies. The hammer methods, on the other hand, require less setup, and produce a cleaner FRF at lower frequencies. In addition, there is no risk of mass loading of the test article by the shaker. It is important to note that the single impact method, while effective at the initially utilized 0.3125 Hz frequency resolution, required a twelve second recording time for a resolution of 0.08 Hz. Due to this long recording time, random impact was utilized for resolutions of 0.08 Hz and higher.

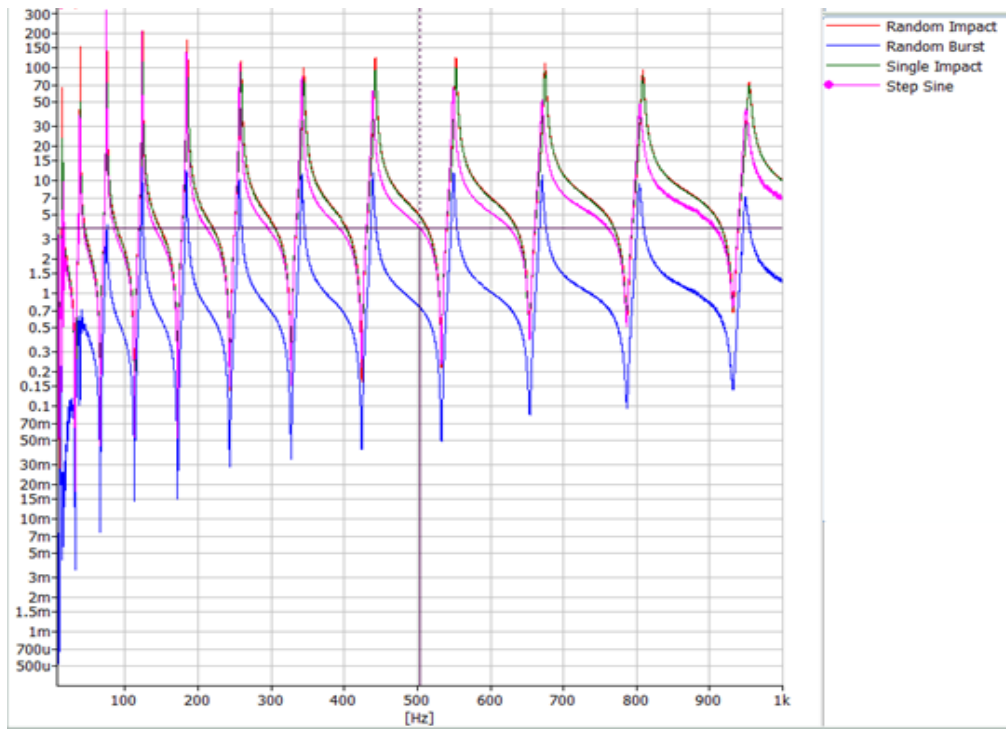


Figure 14. Experimental FRF Comparison. Source: [12].

THIS PAGE INTENTIONALLY LEFT BLANK

IV. FEM MESHING AND DAMAGE SCENARIO CANDIDACY

The first issue that needs to be addressed is the specifications of the “damaged” beam. The installed beam damage must produce a discernable difference in peak frequencies in as many modes as possible in order to provide Equation (37) with a usable eigenvalue difference vector. In order to find a suitable “damage” condition, numerous FEM models representing various candidate conditions must be developed.

A. MESH PATTERNS

Although the basic geometry of the beam FEM remains constant, several different meshing patterns may be utilized. The base requirement is that a single element account for the physical alteration made to represent damage. This way, the impact on the system’s stiffness is accurately accounted for. However, this leaves the rest of the beam open to various options in element size, number, and arrangement. To assess the viability of these various mesh arrangements, the beam’s theoretical natural frequencies are calculated. W.D. Pilkey’s *Formulas for Stress, Strain, and Structural Matrices* provides a table of various beam conditions and their associated formulae for calculating natural frequencies for all modes [13].

In order to replicate these values as precisely as possible, a high-fidelity FEM was generated using 360 elements, each covering 0.508 cm (0.2 in) of the beam’s length. As can be seen in Table 3, the high-fidelity FEM natural frequencies have minute differences when compared to their theoretical counterparts. Therefore, this mesh pattern is capable of producing an accurate FEM. However, this high-fidelity arrangement is limited with regard to implementing various damage conditions. With a constant element size, beam alterations to represent damage must ideally be the same length as the element. An alteration that is smaller or larger than 0.508 cm (0.2 in) would require resizing every element to match its dimension. Additionally, the high number of

elements results in longer computation times. While the element count (360 elements in a very simple FEM) in and of itself is not concerning, one must understand that the model is used to simulate numerous damaged conditions. Regenerating the FEM for each condition certainly has the potential to make the process time-consuming.

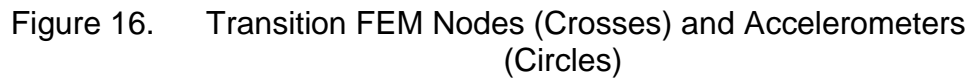
As in alternative, a simple FEM using the minimum number of elements was also produced. Two elements were used to represent the two sections spanning between the edge of the beam and an accelerometer mount. Thirteen additional elements covered the unaltered beam sections in between the accelerometer locations. A sixteenth element of variable size was positioned in between two accelerometer locations to cover the alteration (“damage”). The remaining seventeenth and eighteenth element covered the remaining space between the accelerometers not affected by the alteration. Figure 15 shows the arrangement of nodes with the accelerometer locations.



Figure 15. Simple FEM Nodes (Crosses) and Accelerometers (Circles)

Obviously, the minimum number of elements is advantageous with regard to computation time. However, as seen in Table 3, there are detectable differences between the natural frequencies calculated from the simple FEM and the corresponding theoretical values.

A third option was produced using a transition mesh. This FEM is similar to the simple model, in that the beam alteration is covered by a variable sized element. However, in this case, the elements surrounding the damage element gradually increase in size, while still maintaining nodes at accelerometer locations. Figures 16 and 17 show the overall mesh and the transition in detail.



This model offers flexibility in alteration sizing and a compromise between element count and computation time. As per Table 3, the difference between the transition mesh FEM natural frequency and the theoretical values is superior to that of the simple model (Appendix C provides a more detailed table regarding FEM comparison). Due to these advantages, the transition mesh FEM was utilized in assessing damage condition candidates.

Table 3. FEM Natural Frequency Error
(Compared to Theoretical Values)

Mode	High Fidelity FEM (% absolute error)	Simple FEM (% absolute error)	Transition FEM (% absolute error)
1	0.0001	0.0008	0.0007
2	0.0000	0.0054	0.0044
3	0.0000	0.0201	0.0173
4	0.0000	0.0597	0.0489
5	0.0000	0.1283	0.1005
6	0.0000	0.2178	0.2076
7	0.0000	0.3821	0.3504
8	0.0000	0.6817	0.5064
9	0.0000	0.9993	0.7962
10	0.0000	1.2631	1.0278
11	0.0000	1.7552	1.3744
12	0.0000	2.4256	2.2570
1 through 12	0.0001	7.9392	6.6918

B. DAMAGE CONDITION SELECTION

With a flexible FEM with reasonable accuracy and computation time available, various damage conditions can be assessed. Since the primary objective of this research is experimental validation, a relatively simple scenario featuring a single damaged location is utilized.

The preferred beam alteration to represent damage is two milled notches across the width of the beam. The simple geometry of these notches permits accurate simulation by the FEM damage element. The reduced thickness of the beam covered by this element reduces the second moment of inertia, and, therefore, lowers the element stiffness. Having a notch on either side of the beam permits similar beam flexure in either direction, thus eliminating non-linearities in the dynamic response. Figures 18 and 19 show the milled notches used to represent damage in the test beam. It is also important to note that the notch geometry must preclude the possibility of the notch sides coming in contact with each other as the beam bends. Such an occurrence could introduce nonlinear gap closing in the beam's dynamic response.



Figure 18. Cross-Sectional View of Milled Notches (“Damage”)

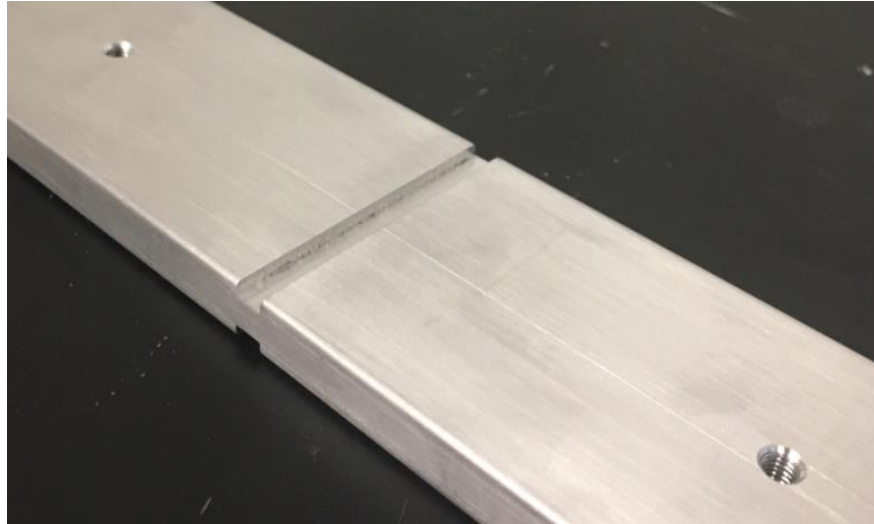


Figure 19. Isometric View of Milled Notches (“Damage”)

With the acceptance of basic geometry of the “damage,” various locations and notch dimensions have to be assessed. As previously stated, the objective is to select a damage scenario that results in discernable natural frequency changes across as many modes as possible (Figures 20 and 21 show the effect of stiffness reduction on natural frequencies). Such a condition would provide the most useful data via the eigenvalue difference vector in Equation (37).

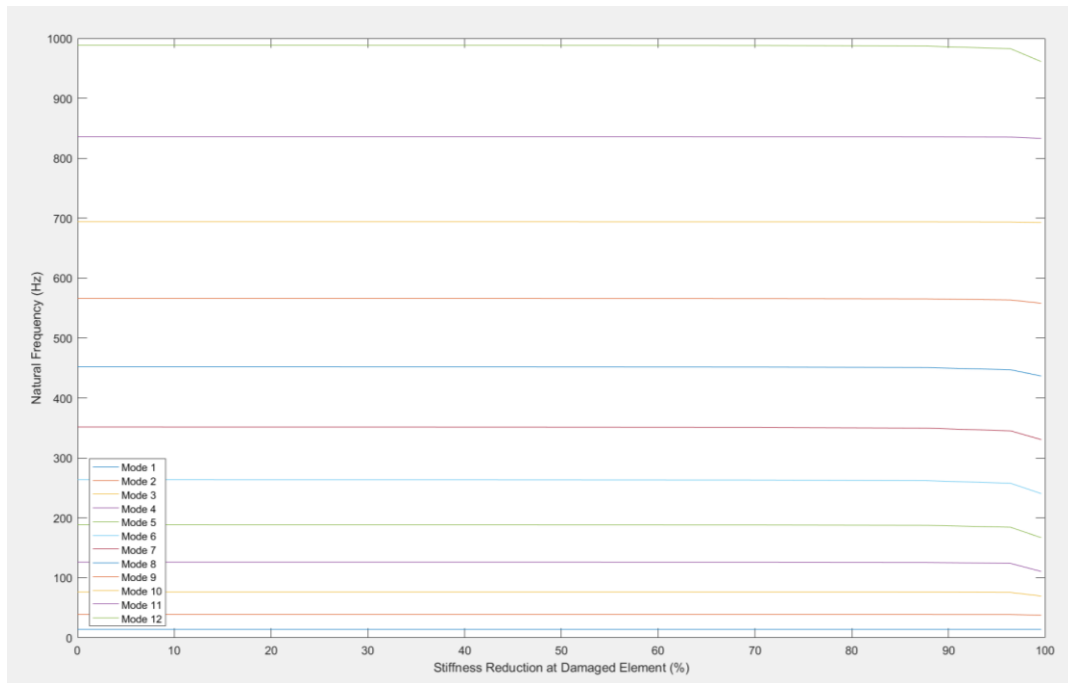


Figure 20. Natural Frequencies as Stiffness Is Reduced at Damage Location

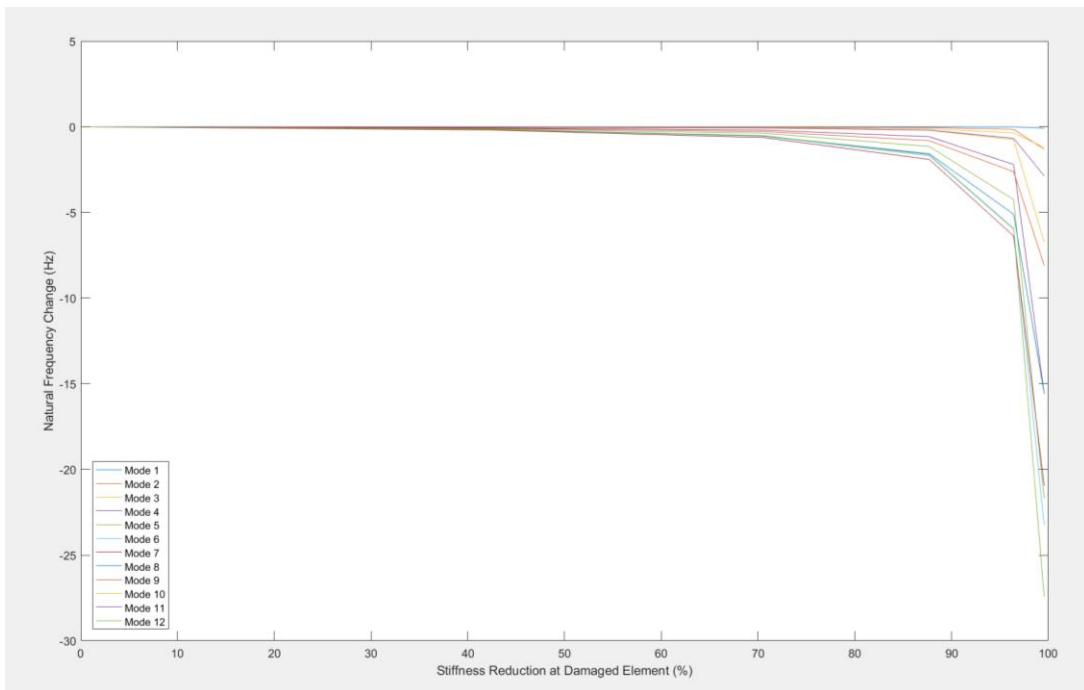


Figure 21. Change in Natural Frequencies as Stiffness Is Reduced

A variety of notch widths, depths, and locations were simulated. Specifically, twelve potential elements, five notch widths, and five notch depths were evaluated for a total of 300 different damage scenarios. Each resultant change in natural frequency within the first twelve modes was graded based on their detectability. An ideal frequency delta is detectable by instrumentation with a frequency resolution of 0.625 Hz. An acceptable delta is detectable with a resolution of 0.3125 Hz. Table 4 shows the resultant shift in natural frequencies due to the installation of damage of various dimensions at a particular element. Based on these criteria, notches placed at interior element 5 (between accelerometers 5 and 6) with a width of 0.476 cm (0.1875 in) and a depth of 0.238 cm (0.09375 in). This alteration creates frequency differences in ten modes that are detectable with 0.625 Hz resolution.

Table 4. Natural Frequency Differences for Damage at Element 5

Damage Width (cm)	0.47625				
Damage Depth (cm)	0.15875	0.3175	0.47625	0.635	0.79375
Mode 1	0.017929	0.060279	0.181296	0.667838	4.056329
Mode 2	0.06472	0.226432	0.686749	2.339248	8.509918
Mode 3	0.016528	0.057506	0.172764	0.573156	1.94215
Mode 4	0.066833	0.240258	0.74249	2.561609	9.170284
Mode 5	0.269053	0.95183	2.844721	8.823834	22.80683
Mode 6	0.069577	0.244716	0.721788	2.164174	5.379531
Mode 7	0.152492	0.539591	1.625137	5.197318	14.52639
Mode 8	0.65211	2.277295	6.615923	18.82277	39.89659
Mode 9	0.200309	0.693144	1.970191	5.332921	10.86344
Mode 10	0.237565	0.832377	2.44729	7.264367	17.1688
Mode 11	1.147385	3.962996	11.21054	29.60283	55.45561
Mode 12	0.359958	1.22922	3.38744	8.496358	15.57912

THIS PAGE INTENTIONALLY LEFT BLANK

V. ABC SELECTION AND COMPOSITE MATRIX ASSEMBLY

With a viable damage scenario chosen, potential composite sensitivity matrices must be constructed and evaluated before proceeding with the experimental portion of the research. As previously stated, many ABC configurations (with varying ABC types, locations, and characteristics) are applied to create a sensitivity row library. Orthogonal projection is then employed to evaluate each row and make selections that minimize matrix linear dependence. The composite sensitivity matrix is then utilized in a simulated damage detection scenario to gauge its performance. Simulation conditions, featuring damage of varying magnitude and at multiple locations, is used for each composite sensitivity matrix in order to provide a consistent assessment.

A. BASELINE SENSITIVITY MATRIX

To act as a control for sensitivity library comparison, the baseline (no ABCs) sensitivity matrix of fourteen rows and fourteen columns provides the first set of sensitivity data to be assessed via the orthogonal projection method. The MDI and PDI for the matrix is shown in Figure 22.

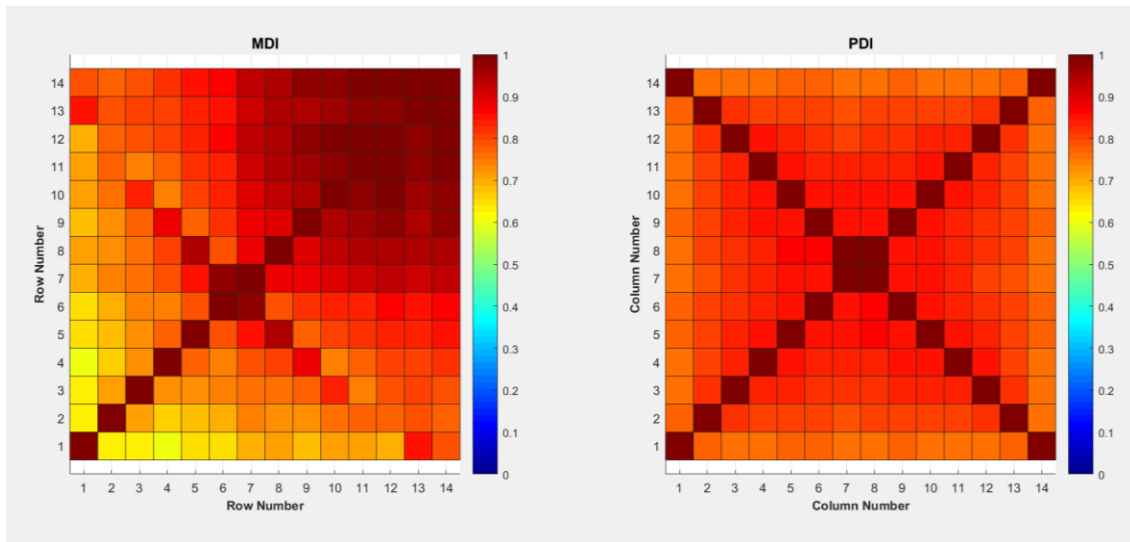


Figure 22. Baseline [S] MDI and PDI

When subjected to the damage detection simulation, the “detected” damage results are completely inaccurate when compared to the “true” damage locations and magnitudes (see Figure 23). All quantitative results are summarized in Table 5.

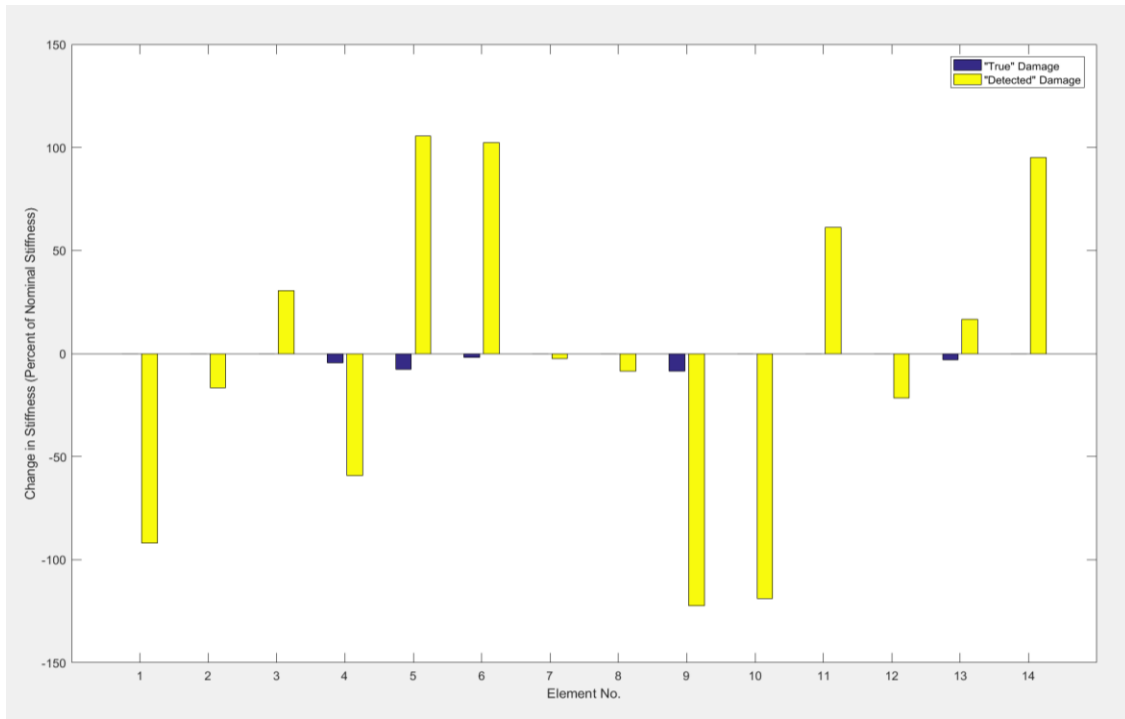


Figure 23. Simulated Damage Detection Results with Baseline [S]

B. PIN-BASED ABC LIBRARIES

Pin-based ABCs are simple to apply from a coding perspective and are relatively quick to assess, as they do not have adjustable characteristics (unlike a spring, which can have varying stiffness). The first ABC-augmented library to be evaluated consists of matrices produced from the baseline configuration (no ABCs applied) and single pin scenarios. For each scenario, one pin is applied at a translational DOF associated with an accelerometer location on the test article. In total, this amounts to sixteen ABC configurations (one baseline and fifteen single pin configurations for each accelerometer location). By arranging these

matrices in accordance with Equation (35), a sensitivity library of 224 rows and fourteen columns is formed. From the library, orthogonal projection only selected rows created by single pin configurations. The selected rows from this expanded library resulted in a sharp drop in composite matrix linear dependence, as indicated in Figure 24. This, in turn, provided remarkably improved damage detection results, as per Figure 25.

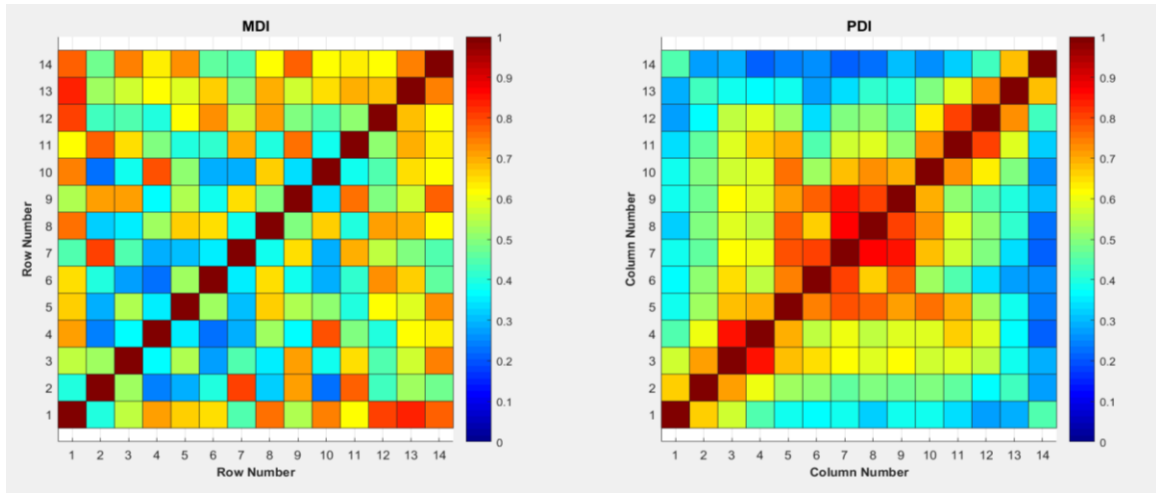


Figure 24. Single Pin Composite Sensitivity Matrix MDI and PDI

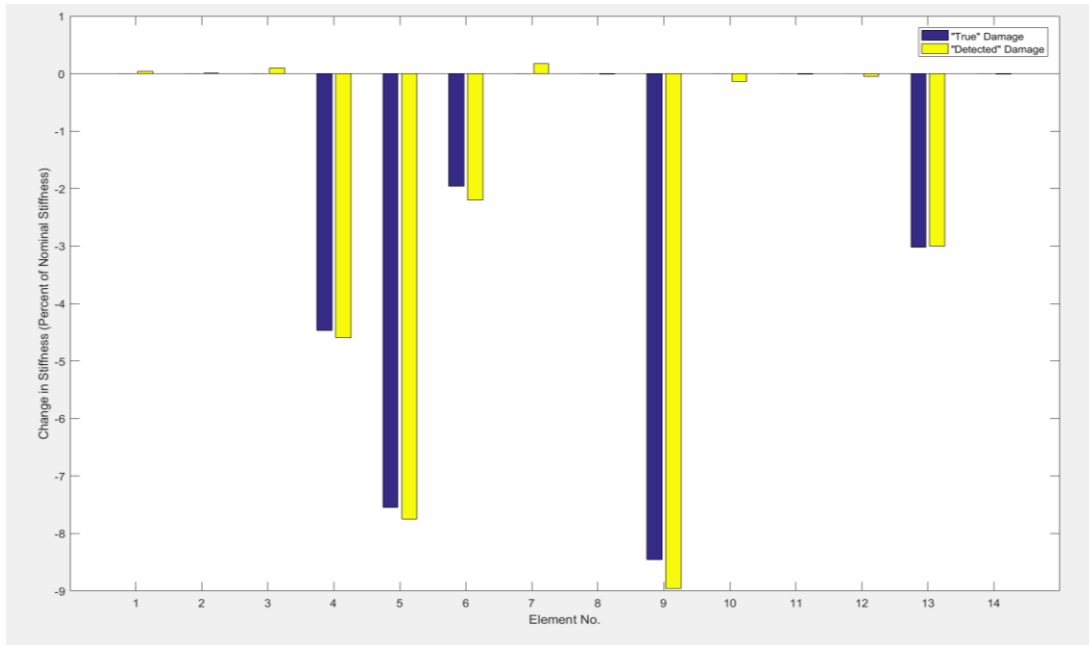


Figure 25. Simulated Damage Results with Single Pin Composite Matrix

The current sensitivity library featuring the baseline matrix and all single pin scenarios can be further expanded by adding rows generated from two pin configurations. The number of available sensitivity rows grows extensively to a count of 1694. It is noteworthy that orthogonal projection only selected rows from two pin ABC configurations. The greater number of candidate rows allows for a further decrease the matrix's linear dependence even further, as evidenced by the associated MDI and PDI (see Figure 26). Once again, simulated damage detection results are promising (see Figure 27).

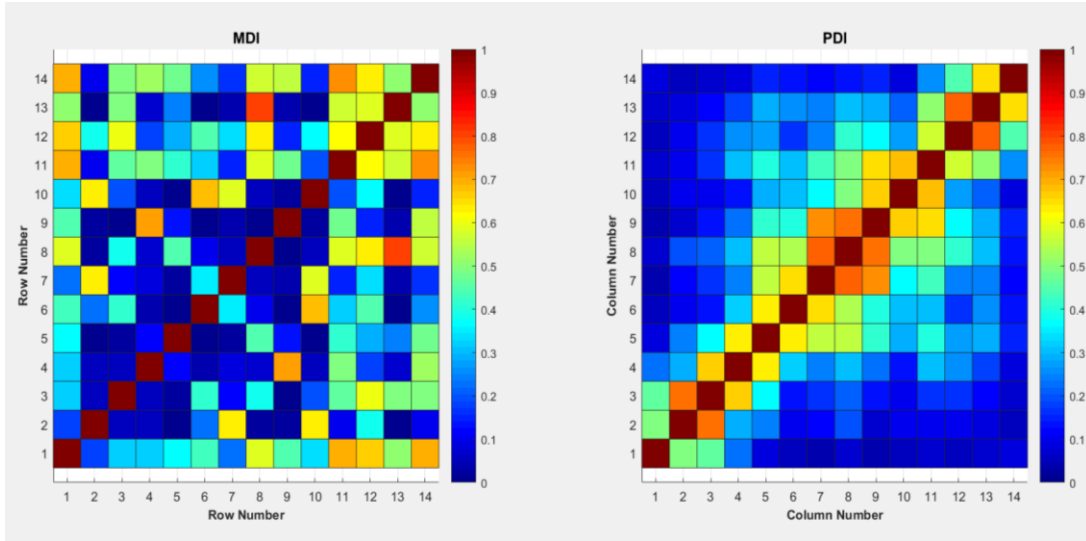


Figure 26. Two Pin Composite Sensitivity Matrix MDI and PDI

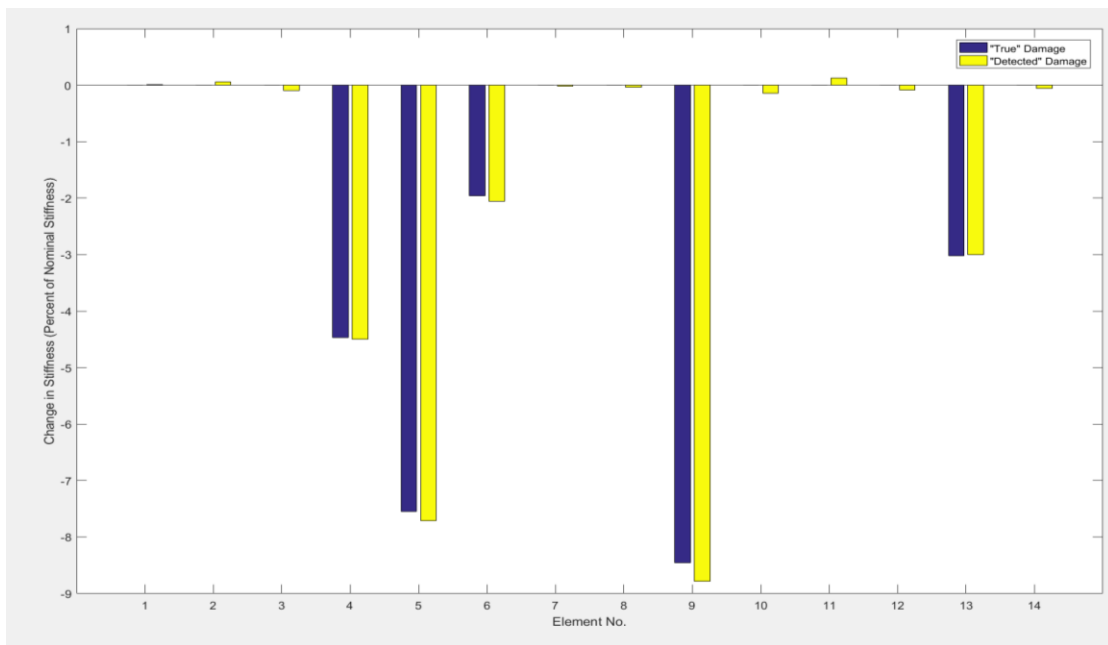


Figure 27. Simulated Damage Results with Two Pin Composite Matrix

Adding sensitivity rows generated from three pin ABC configurations exponentially grows the size of the sensitivity library to 8064 rows. In a manner, similar to the previous cases, orthogonal projected selected rows from configurations with the highest pin count. Linear dependency is further reduced,

but the improvement is not as significant compared to previous additions. MDI and PDI barely show the reduction in linear dependency (Figure 28) and the damage simulation exhibits minutely improved results (Figure 29). All quantitative results associated with pin-based ABCs are found in Table 5.

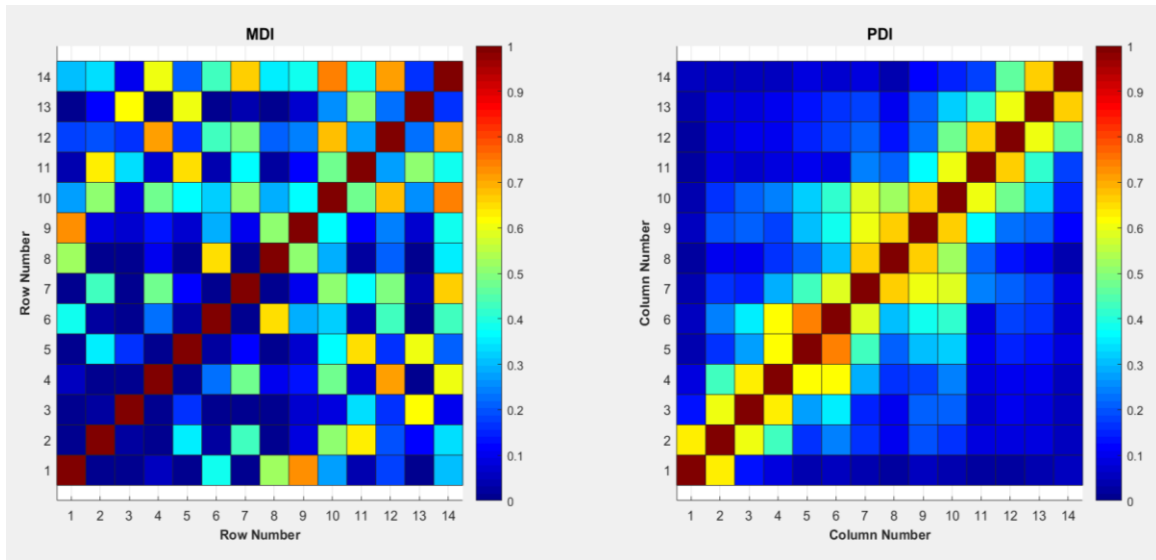


Figure 28. Three Pin Composite S Matrix MDI and PDI

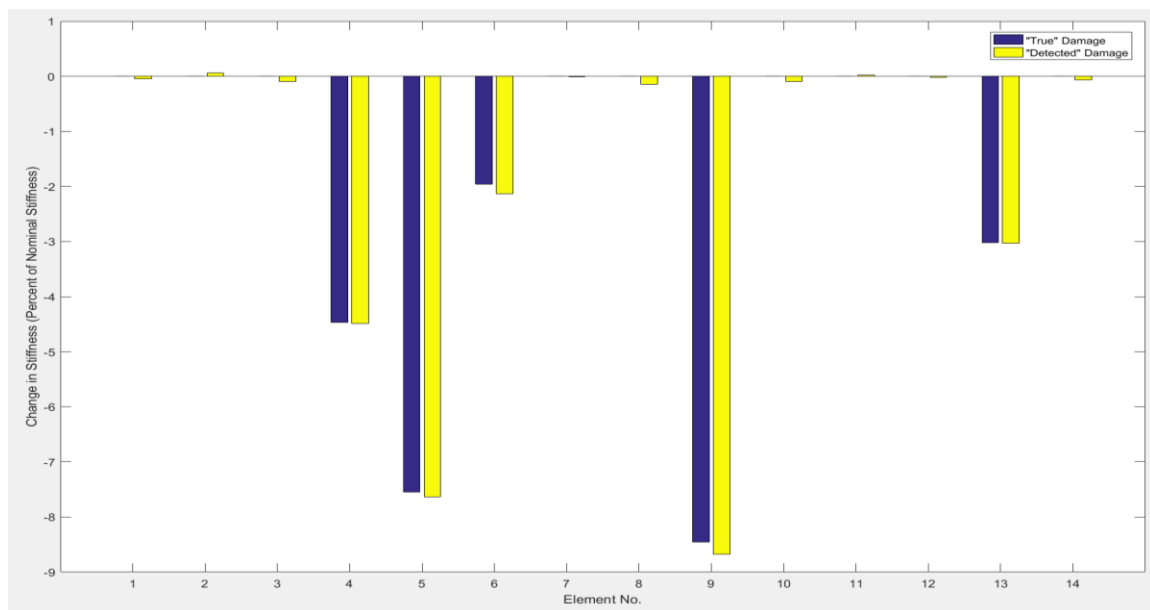


Figure 29. Simulated Damage Results with Three Pin Composite Matrix

C. ALTERNATIVE ABC TYPES

As previously alluded, there are additional ABCs besides pins. R.J.C. Konze conducted research on the use of springs and point masses as ABCs. Based on conclusion and recommendations from “Synthetic modification in the frequency domain for finite element model update and damage detection,” a single spring with stiffness ranging from 175.13 N/mm (1000 lb/in) to 1751.3 N/mm (10000 lb/in) generates the most useful sensitivity rows for a free-free beam. For point masses, the recommended values range from 0.45359 kg (1 lbm) to 1.8143 kg (4 lbm) [12].

A separate sensitivity library was created with row inputs from the baseline sensitivity matrix, single pin ABCs, single spring ABCs, and single point mass ABCs. As with the previous cases, each ABC was applied to each node corresponding to the fifteen accelerometer locations. The library size reached 3164 rows. Interestingly, of the fourteen composite sensitivity matrix rows, orthogonal projection selected twelve rows from spring-based ABCs, two from pin-based ABCs, and none from point mass-based ABCs. Compared to the composite matrix constructed from a single pin ABCs, alone, the spring-pin composite exhibited lower linear dependency (see Figure 30). This composite sensitivity matrix also produced satisfactory simulated damage detection results (see Figure 31). Quantitative results are summarized in Table 5.

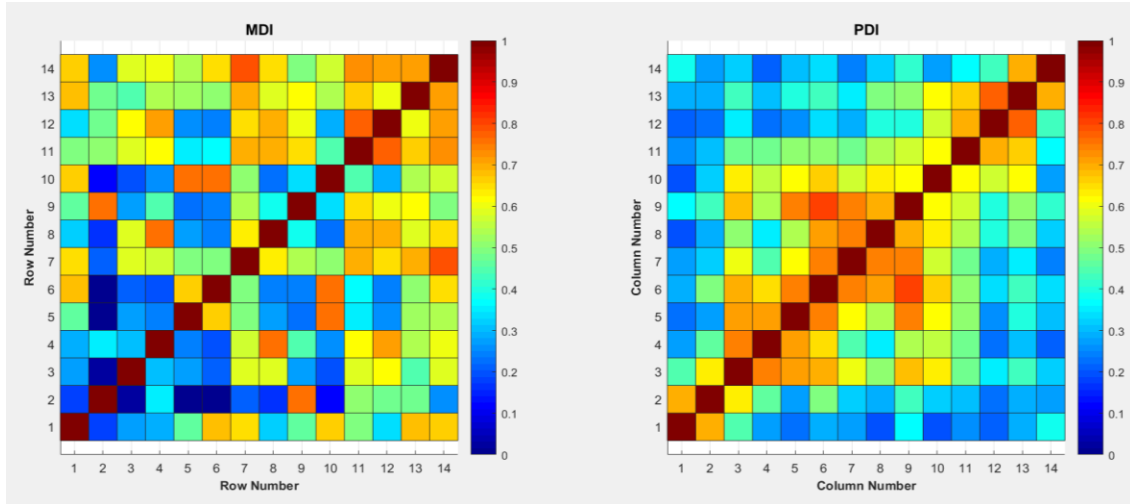


Figure 30. Single Pin, Spring, Point Mass Composite Matrix
MDI and PDI

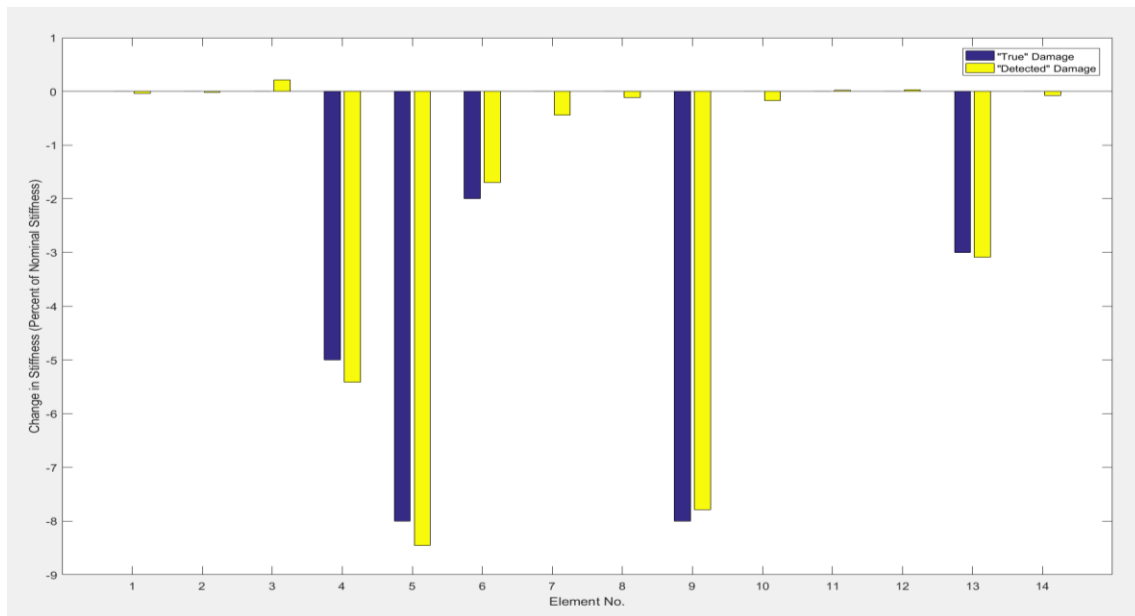


Figure 31. Simulated Damage Results with Single Pin, Spring,
Point Mass Composite Matrix

D. CONCLUDING REMARKS

In total five different composite sensitivity matrices were constructed and evaluated (including the baseline sensitivity matrix). The specific rows used in their construction are listed in Appendix C. A quantitative comparison is shown in

Table 5. Maximum false damage error is the value of the largest damage detection return for a non-damaged element. Maximum damaged element error is the largest difference between the “true” damage value and the “detected” value for a damaged element. Total stiffness error is simply the sum of all differences between “true” and “detected” damage across all elements.

Table 5. Composite Sensitivity Matrix Comparison

Available ABCs	Library Size (rows)	Condition Number	Max false damage error (%)	Max damaged element error (%)	Total stiffness error (%)
None	14	13786	119.00	113.11	852.49
1 Pin	224	11.204	0.17028	0.50788	1.6279
1 Pin, 2 Pins	1694	6.9989	0.14012	0.33576	1.2594
1 Pin, 2 Pins, 3 Pins	8064	5.7334	0.14128	0.22850	1.0642
1 Pin, 1 Spring, 1 Pt. Mass	3164	9.3595	0.43835	0.45066	2.5892

It is obvious that the use of ABCs to improve matrix conditioning is required. It is also clear that increasing the number of pins further improves condition number and reduces overall error. However, there is a diminishing return on increasing the pin count. As more pins are added, the accuracy improves by smaller magnitudes. On another note, the implementation of spring-ABCs was deemed worthwhile, per orthogonal projection selection. Compared to a single pin composite matrix, the pin-spring composite matrix featured a lower condition number. While, the total stiffness error was slightly higher for the pin-spring composite, it did have a lower maximum damaged element error.

THIS PAGE INTENTIONALLY LEFT BLANK

VI. FEM UPDATING

With several viable composite sensitivity matrices available, all prerequisites for model updating are met. The FEM to be updated is the same as the Simple FEM described in Chapter IV, minus the dedicated element for damage insertion. This model provides fourteen interior elements representing the sections of the beam encompassed by the mounted accelerometers. These are the elements that will be updated during the model update process. The remaining part of the beam (the space between the beam's edges and the outboard accelerometers) are represented by two additional elements that will remain constant.

In an effort to bring FEM natural frequencies into close alignment with the experimentally obtained values, the following multiple-iteration update process is used:

1. Let $\{\Delta p\} \triangleq \{\Delta p^{(i)}\}$, $[\bar{S}] \triangleq [\bar{S}^{(i)}]$, $\{\Delta \Lambda\} \triangleq \{\Delta \Lambda^{(i)}\}$ (first iteration $i=1$)
2. Update the FEM with $\{\Delta p^{(i)}\}$
3. Recalculate the sensitivity rows $[\bar{S}^{(i+1)}]$ and natural frequencies calculated in Step 2.
4. Construct $\{\Delta \Lambda^{(i+1)}\}$ using the newly calculated natural frequencies along with the frequencies already found from curve-fitting the synthesized FRF.
5. Solve for $\{\Delta p^{(i+1)}\}$
6. If $\{\Delta p^{(i+1)}\} \cong \{\Delta p^{(i)}\}$, End.

7. Otherwise, let $\{\Delta p^{(i)}\} \Leftarrow \{\Delta p^{(i+1)}\}$, $[\bar{S}^{(i)}] \Leftarrow [\bar{S}^{(i+1)}]$, $\{\Delta \Lambda^{(i)}\} \Leftarrow \{\Delta \Lambda^{(i+1)}\}$
and return to Step 1.

Four separate modal tests were conducted on the intact test article, using a variety of FRF frequency resolutions. The first test, using the single impact method, features a resolution of 0.3125 Hz. The second test, also using single impact, has a resolution of 0.08 Hz. However, the requisite response recording time for this resolution is twelve seconds. As this relatively long recording time makes this method increasingly susceptible to noise, an additional test at 0.08 Hz resolution was conducted using the random impact method. All utilized FRFs at this resolution were from the random impact test. A fourth test at a resolution of 0.02 Hz was performed with random impact. The measured FRFs are shown in Figure 32.

It is important to note that the peak frequencies are affected by damping and are, therefore, not the natural frequencies. Due to the free-free condition of the test article, damping is kept to a minimum. In order to obtain the most accurate results, a single-DOF curve fitter is applied to peaks of interest. This algorithm, developed A. M. Rinawi and R. W. Clough, analyzes the peak, estimates the damping ratio, and provides the natural frequency [14]. These values can then be compared to the associated FEM values. The differences between these frequencies can then be used to solve for the desired flexural rigidity adjustments in accordance with Equation (37).

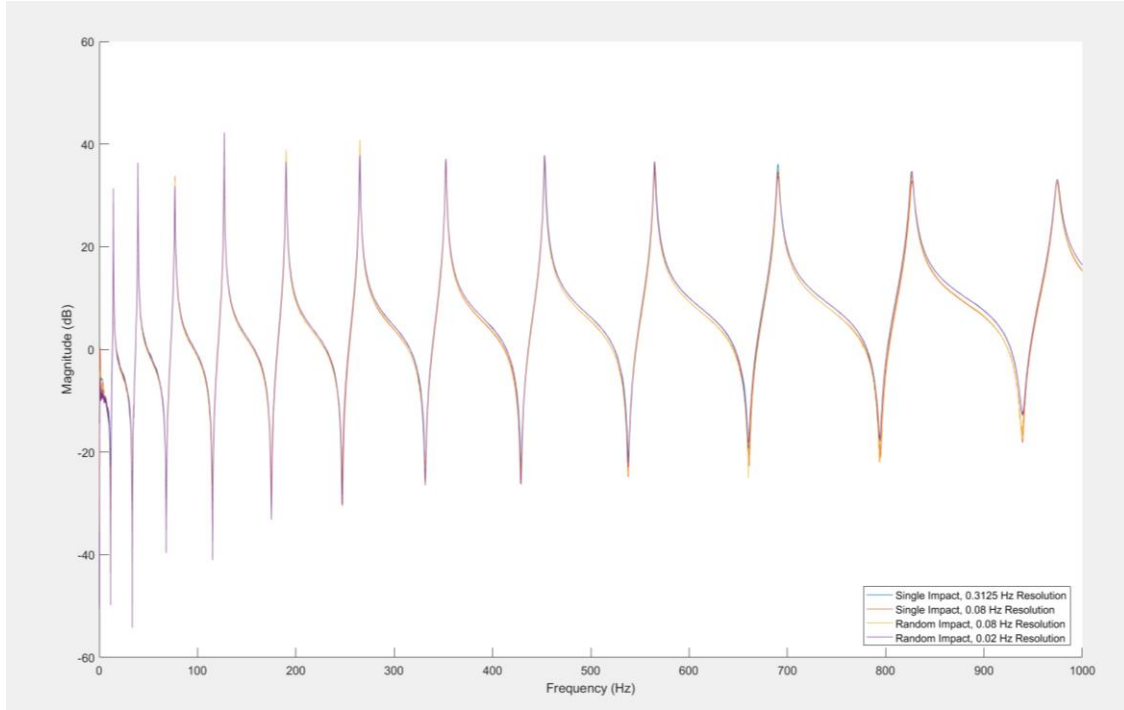


Figure 32. Experimentally Obtained FRFs from Each Modal Test

A. COMPLICATIONS REGARDING MODEL UPDATE

In an effort to obtain the best experimental results, a modal test using the random impact method with a high frequency resolution of 0.02 Hz was conducted. The experimentally obtained FRF is shown in Figure 33. With the H matrix obtained, the ABCs can be applied to the experimental data using synthesis. The first ABC sets to be applied are those used to construct the two-pin composite sensitivity matrix. As previously discussed in Chapter V, this matrix featured a very low condition number while still maintaining a reasonably sized sensitivity library (keeping computation times reasonable). Based on the merits of high FRF frequency resolution and ABCs associated with minimal sensitivity linear dependence, an exceptional model updating result is expected.

However, when artificial pins were applied at accelerometer locations 1 and 7, the resultant H^* matrix produced the accompanying FRF shown in Figure

33. This synthesized FRF is severely distorted compared to its baseline counterpart.

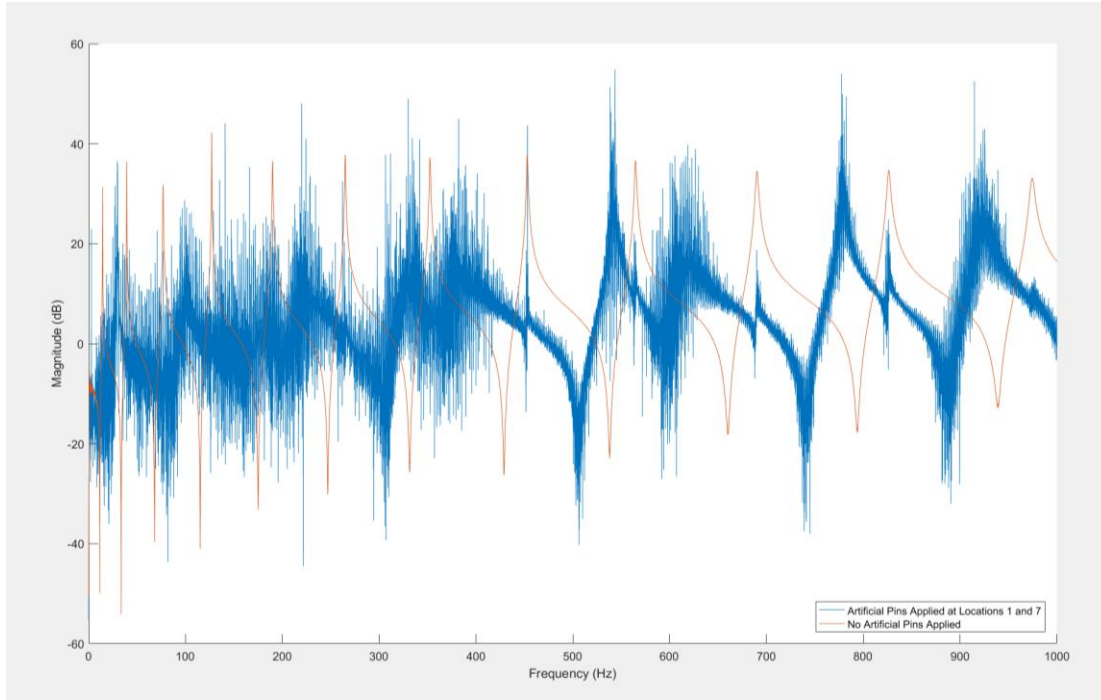


Figure 33. FRF Distortion with 0.02 Hz Resolution and Two Pin ABCs

Other ABC configurations required by the composite sensitivity matrix also produce varying degrees of distortion. Figure 34 shows the synthesized FRF from a different ABC set. This figure highlights the influence of artificial pin location on FRF synthesis.

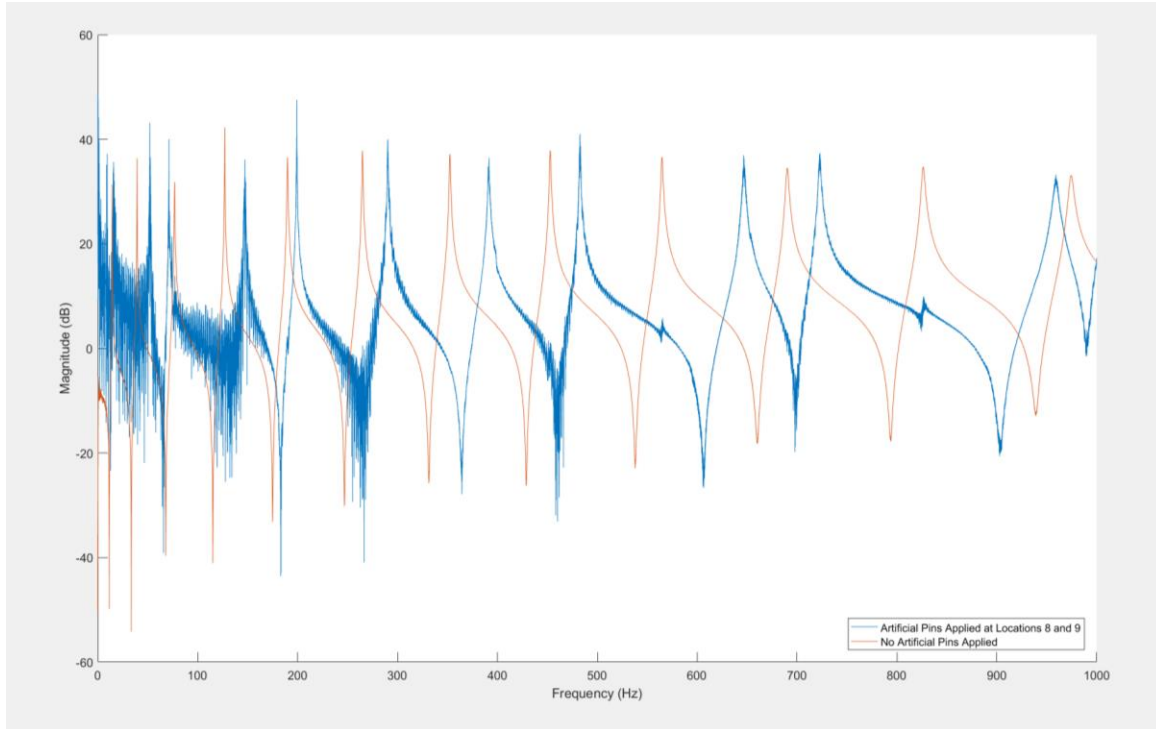


Figure 34. FRF Distortion with 0.02 Hz Resolution and Two Pin ABCs

While Figure 34 shows a less severe distortion case, in general, the extent of distortion makes peak identification impossible. This precludes the identification of their respective frequencies. Without the peak frequencies, the experimental natural frequencies remain unattainable, flexural rigidity adjustments remain unsolved, and FEM updating becomes an impossible task.

Additional attempts at FRF synthesis are made using lower resolutions in an effort to avoid this debilitating distortion. Figures 35 through 37 show samples of FRFs synthesized from a variety of ABCs and resolutions.

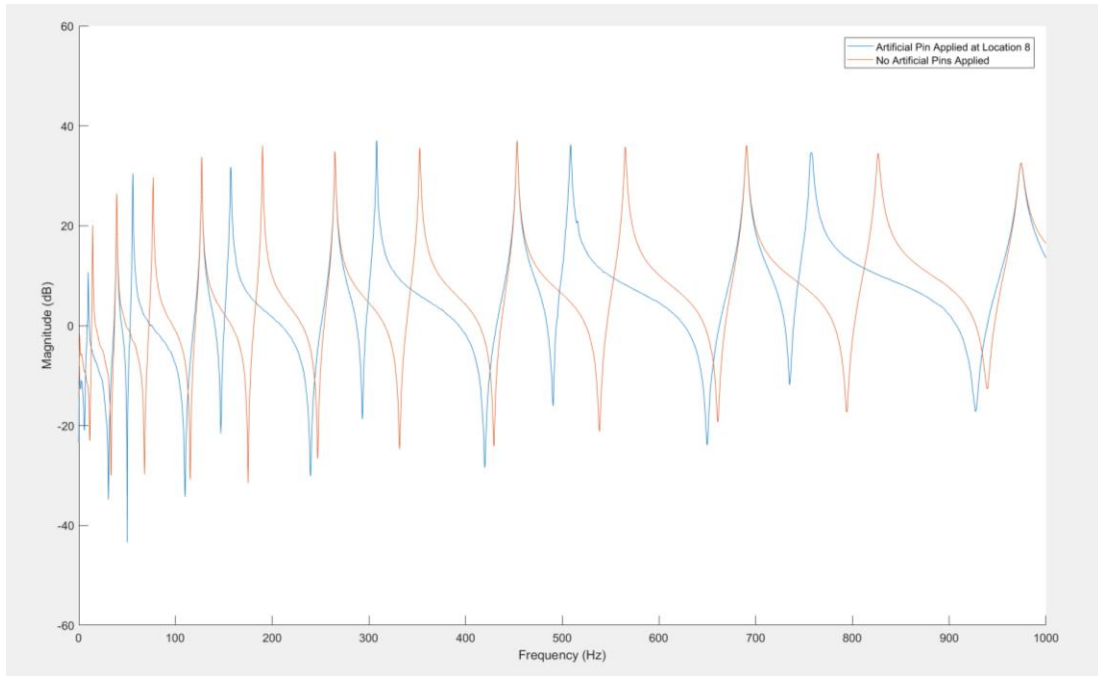


Figure 35. Synthesized FRF with One Pin at 0.3125 Hz Resolution

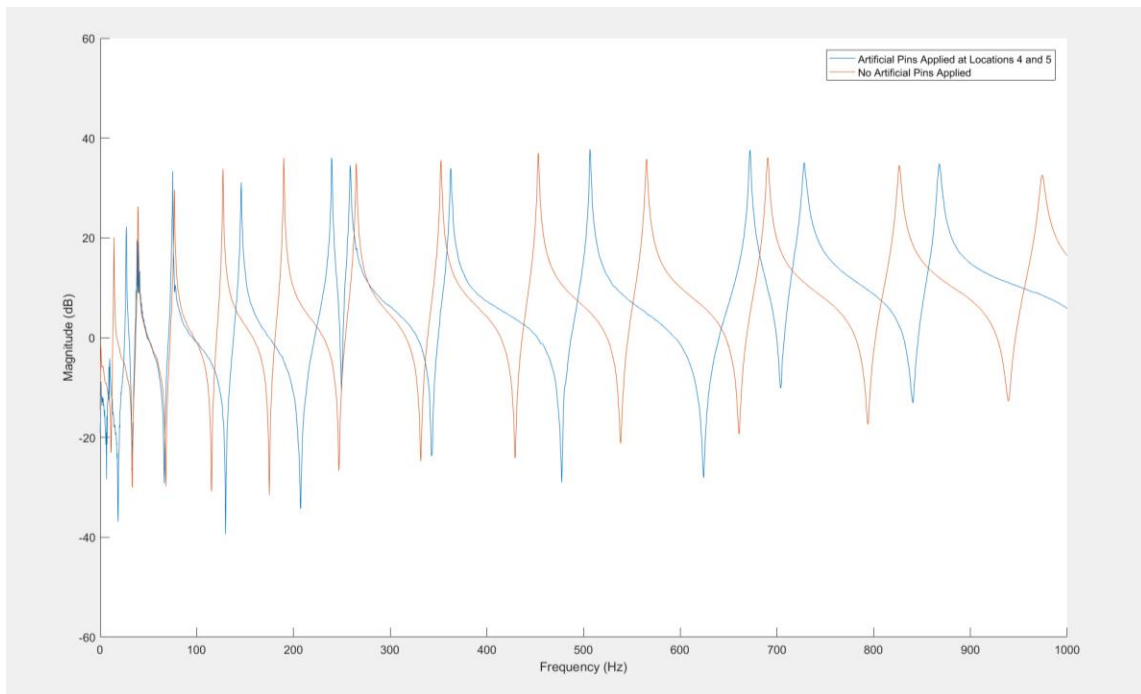


Figure 36. Synthesized FRF with Two Pins at 0.3125 Hz Resolution

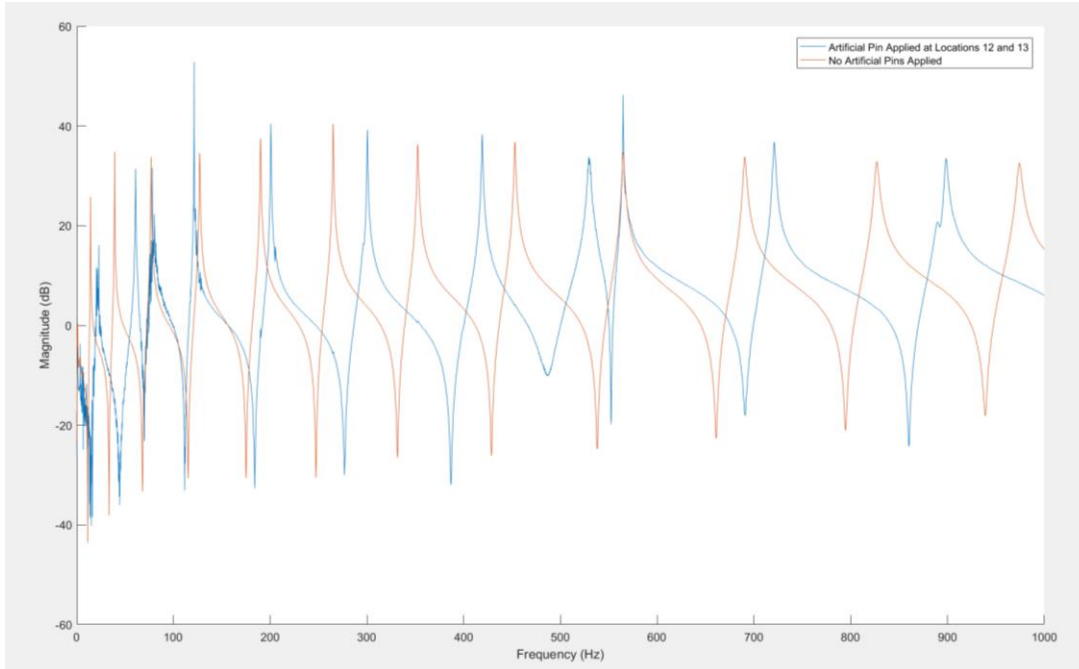


Figure 37. Synthesized FRF with Two Pins at 0.08 Hz Resolution

Based on these FRFs, it is clear that distortion is a function of both ABC count and resolution. Figures 35 and 36 show increased distortion due to using two pins instead of one. Figures 36 and 37 show increased distortion due to higher resolution.

With viable synthesized FRFs obtained, model update is first attempted using single pin ABCs and a resolution of 0.3125 Hz. Due to its minimal distortion, peaks and their frequencies are readily identified. Due to the minimal damping of the test article, these peak frequencies are extremely close to the actual natural frequencies. With the experimentally obtained natural frequency inputs, the flexural rigidity adjustments are computed. Each adjustment can then be individually applied to its respective interior element.

It is important to note that E. Damanakis's research on model updating advocated averaging all flexural rigidity adjustments and uniformly applying the average to the FEM [15]. While this research presents a successful case, there is a critical caveat. This approach requires average values that are positive be

completely disregarded. Uniformly applying a positive flexural rigidity adjustment would result in higher FEM natural frequencies, thus producing larger eigenvalue differences between the model and the test article [15]. The fact that positive flexural rigidity adjustment averages prevent any form of model update makes this approach far from ideal. Figure 38 highlights this deficiency. It is for this reason that individual element adjustments are utilized here.

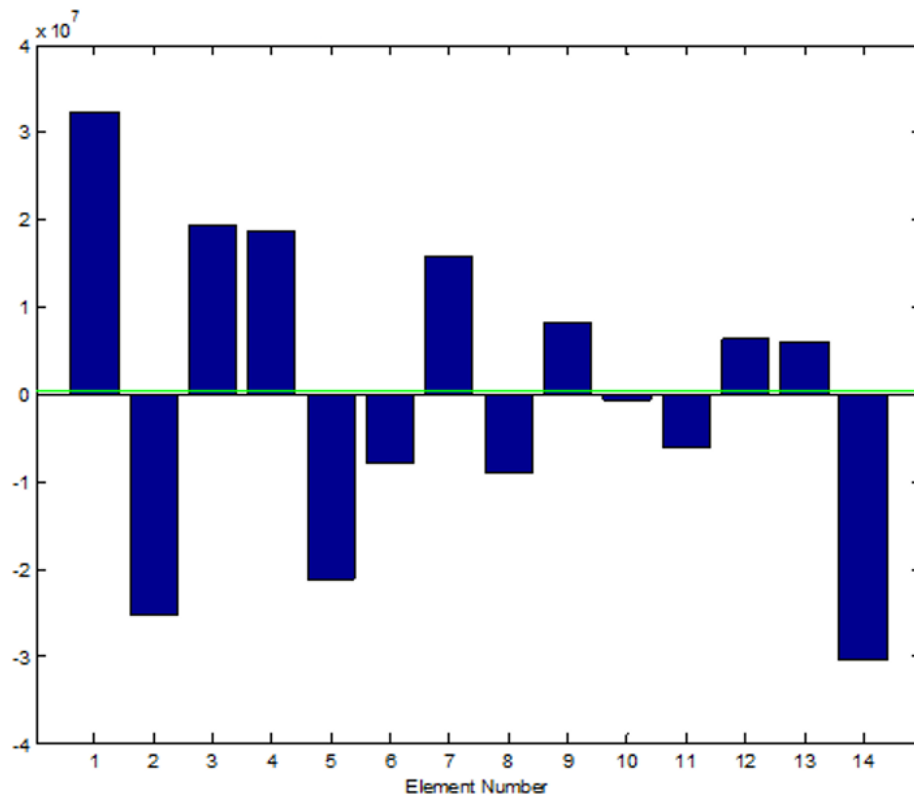


Figure 38. Example of Disregarded Flexural Rigidity Adjustments. Source: [15]. Their positive average (green line) precluded their consideration.

As previously discussed, this model updating process employs a multiple iteration procedure. With every iteration, as the FEM frequencies converge on the experimental values, the required adjustments should decrease. Figure 39

exhibits the calculated adjustments over the course of two model update iterations.

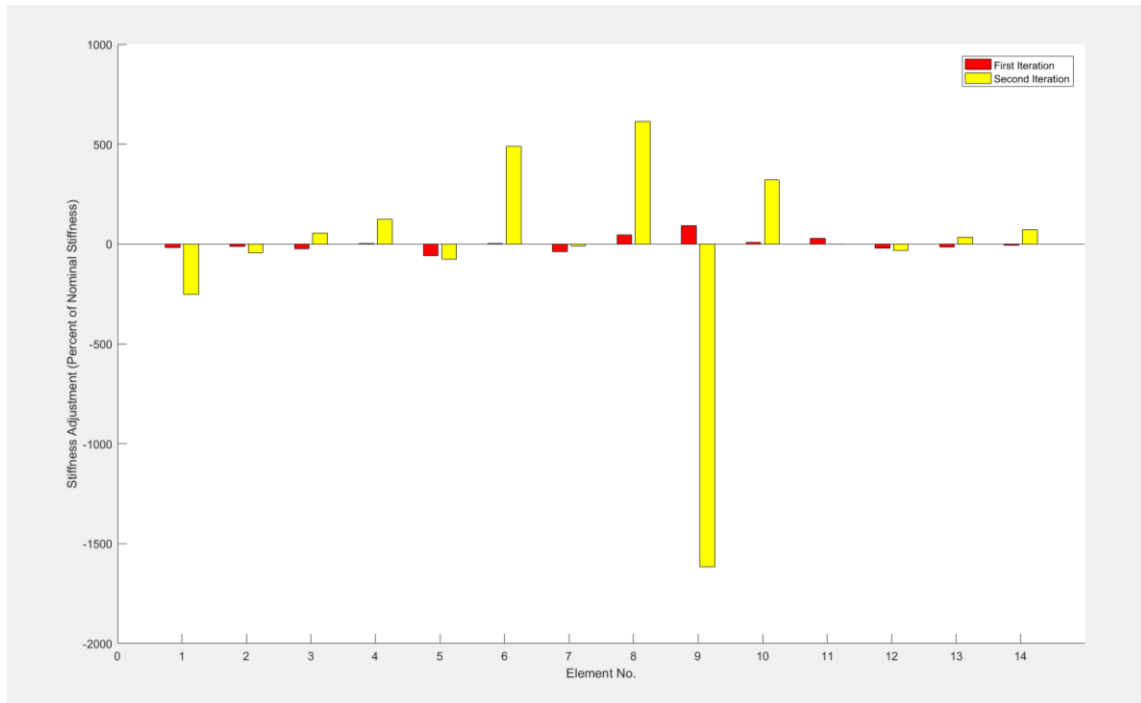


Figure 39. Model Update with Single Pin ABC at 0.3125 Hz Resolution. All modes were available from sensitivity library.

This figure clearly shows the flexural rigidity adjustments growing in magnitude, indicating divergence. This unfortunate result is another example of a failed model update.

The cause of this phenomenon is found in the lower modes of the synthesized FRF. The percent eigenvalue differences between the FEM and the experimental data are noticeably larger in several instances where a low mode frequency is used. Appendix C features tables containing all the initial eigenvalue differences. The consequence of these larger differences is that they exceed eigenvalue sensitivity linearity, thus resulting in a failure to converge. These abnormally large percent differences can be attributed to one of three separate

causes, depending on the scenario. The first source of error is increased peak distortion at the lower modes of the synthesized FRF. This trend is visible in Figure 37 and an extreme case shown in detail in Figure 40.

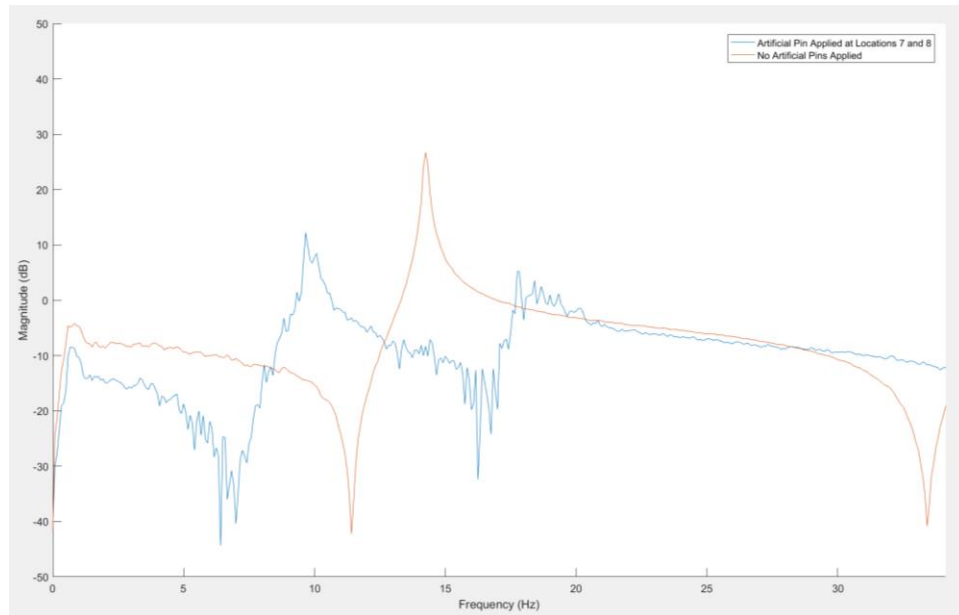


Figure 40. Distortion of an FRF Peak at Mode 2. Based on FEM predictions, the peak should be in the vicinity of 19.572 Hz.

Due to this distortion, peak selection is skewed, resulting in large eigenvalue differences. Another cause of error is the shifting of modes into extremely low frequencies. At frequencies of six Hz or less, the impact testing can fail to produce an FRF peak in its entirety. An example is shown in Figure 41.

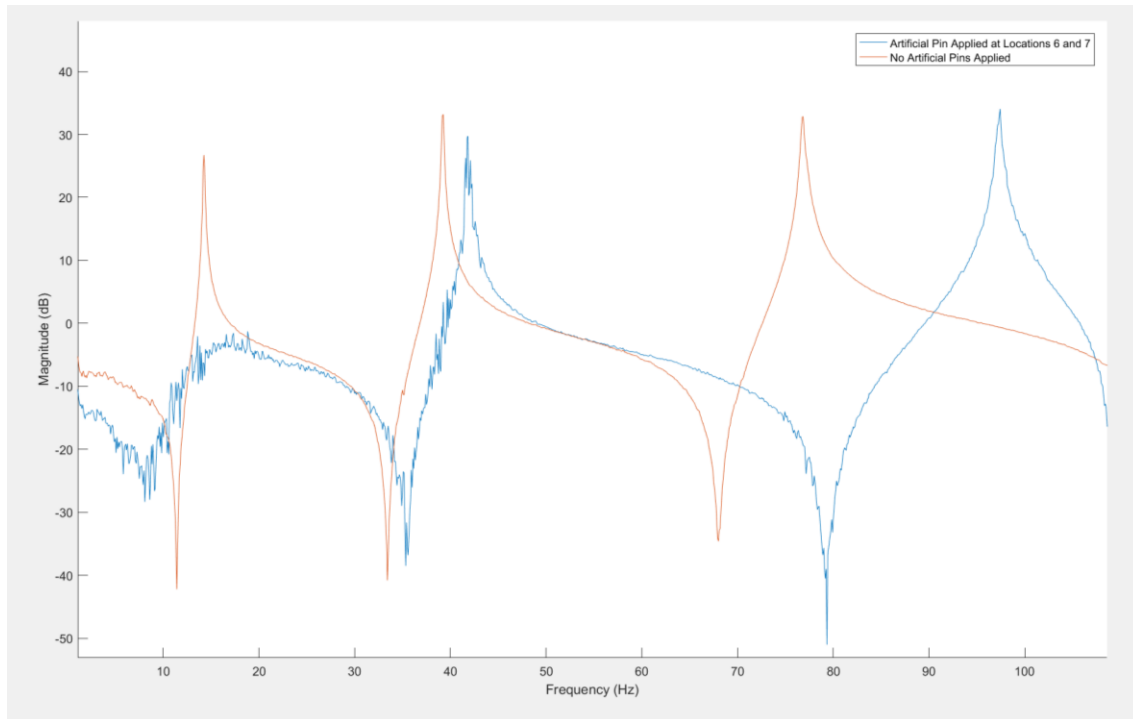


Figure 41. Example of Shifting Mode Frequencies.
The first mode shifts to such a low frequency that a peak is not generated. A peak should exist in the vicinity of 0.6445 Hz (per initial FEM).

A third source of error is more subtle. There are instances where a peak is produced with minimal distortion, yet still produces large eigenvalue differences. One such case is shown in Figure 42.

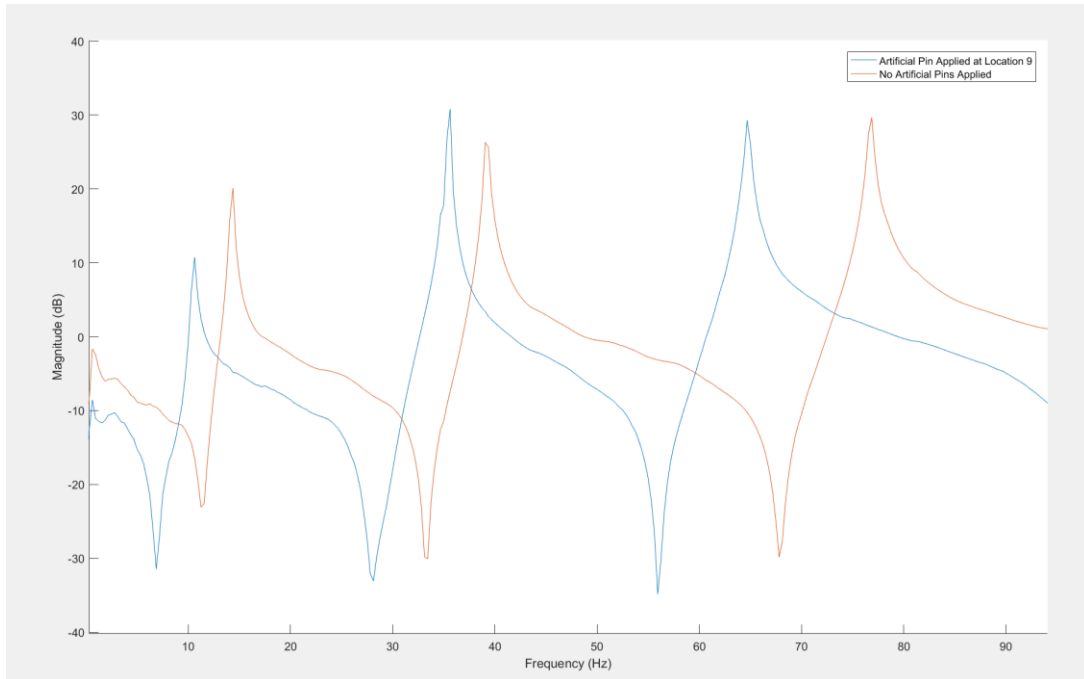


Figure 42. Clean Peak at Mode 1 at 10.625 Hz. Associated FEM frequency is 9.552 Hz. Resultant eigenvalue percent difference is 22.362%.

Such large percent eigenvalue differences, like the example in Figure 42, stand out from the rest of eigenvector. All of the initial percent differences are tabularized in Table 11 in Appendix C. Referring to Table 10 in conjunction with Table 11, it is clear that the larger differences are found in the lowest modes. This eigenvalue difference can be further exacerbated by the frequency resolution, which has a larger effect on low frequency modes as opposed to high modes. Differences of such magnitude can easily exceed sensitivity linearity.

It is clear that low modes introduce potential error sources in both modal testing and ABC synthesis. These errors can lead to high percent eigenvalue differences exceeding sensitivity linearity, and, in turn, divergence during model update. However, the lowest modes are not the only potential source of divergence. As previously shown in Table 3, FEM generated natural frequencies begin to deviate from theoretical values, especially when the FEM has a relatively low element count. This is highlighted in Figure 43.

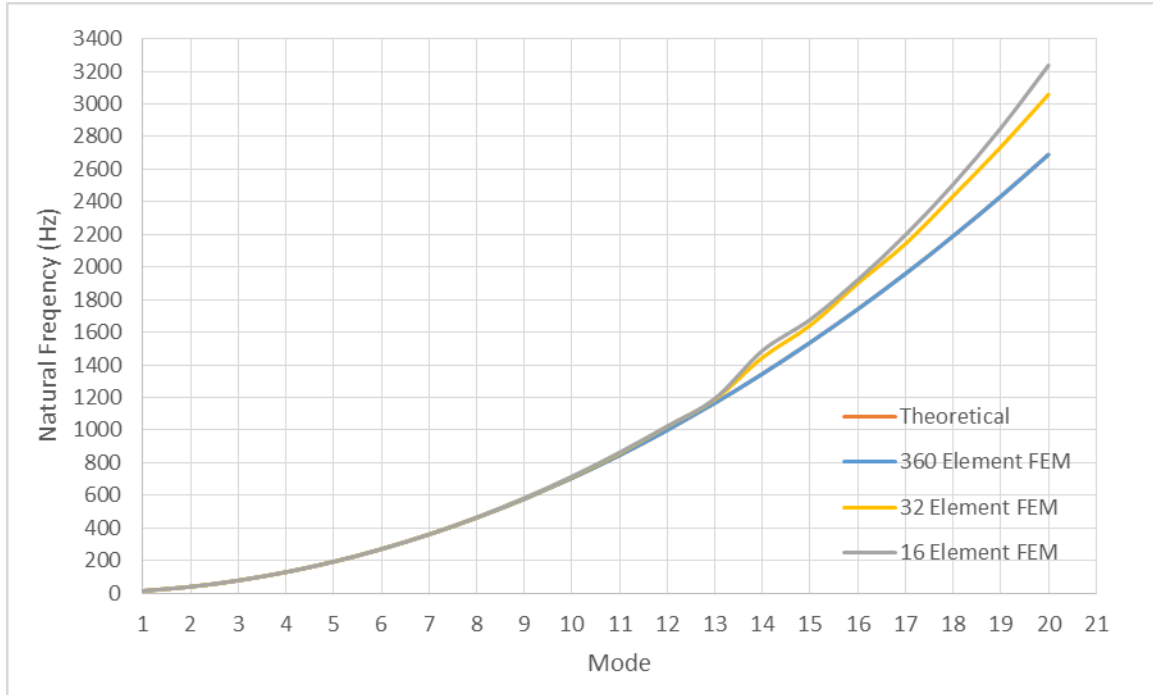


Figure 43. Deviation of FEM Natural Frequencies from Theoretical Values at Higher Modes

Fortunately, none of the composite sensitivity matrices used in model updating utilize modes higher than 10. This mode does not feature significant natural frequency deviation. However, this phenomenon should be taken into consideration.

B. MODEL UPDATE RESULTS

Based on these potential error sources, a conservative approach is taken, and the sensitivity library is limited to rows utilizing modes 4 through 8 only for future model update attempts. Since the natural frequency deviation at higher modes is not extreme, as shown by Figure 43, an additional model update scenario using a library with modes 4–14 is also tried for the sake of comparison. Scenarios where multiple pins are synthesized into high resolution FRFs are avoided entirely.

These new model update attempts result in remarkable success. These successful model updating cases and, and their conditions, are summarized in Table 6.

Table 6. Updated FEM Case Comparison

Updated FEM Case	Resolution (Hz)	ABCs	Available Modes	Test Method
A	0.3125	1 Pin	4-14	Single Impact
B	0.3125	1 Pin	4-8	Single Impact
C	0.3125	2 Pins	4-8	Single Impact
D	0.08	1 Pin	4-8	Random Impact
E	0.08	2 Pins	4-8	Random Impact
F	0.02	1 Pin	4-8	Random Impact

The first encouraging indication is the reduction in flexural rigidity adjustments with each successive update iteration. Figures 44 through 49 exhibit this trend.

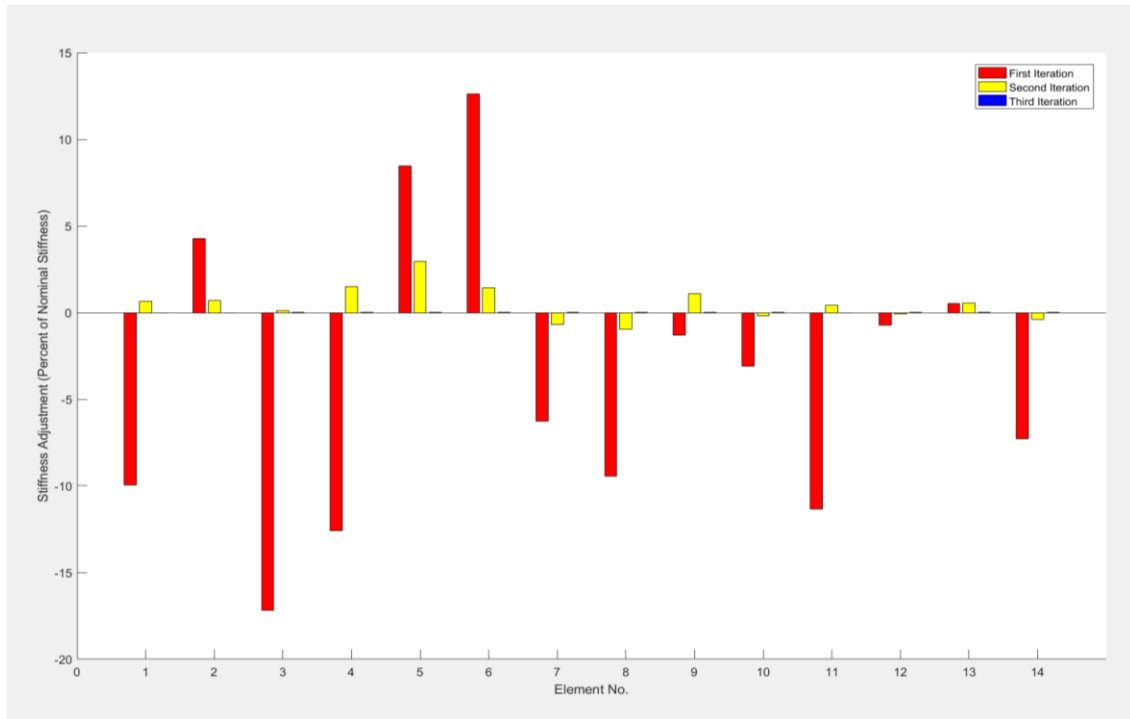


Figure 44. FEM Case A Flexural Rigidity Updates Over Three Iterations

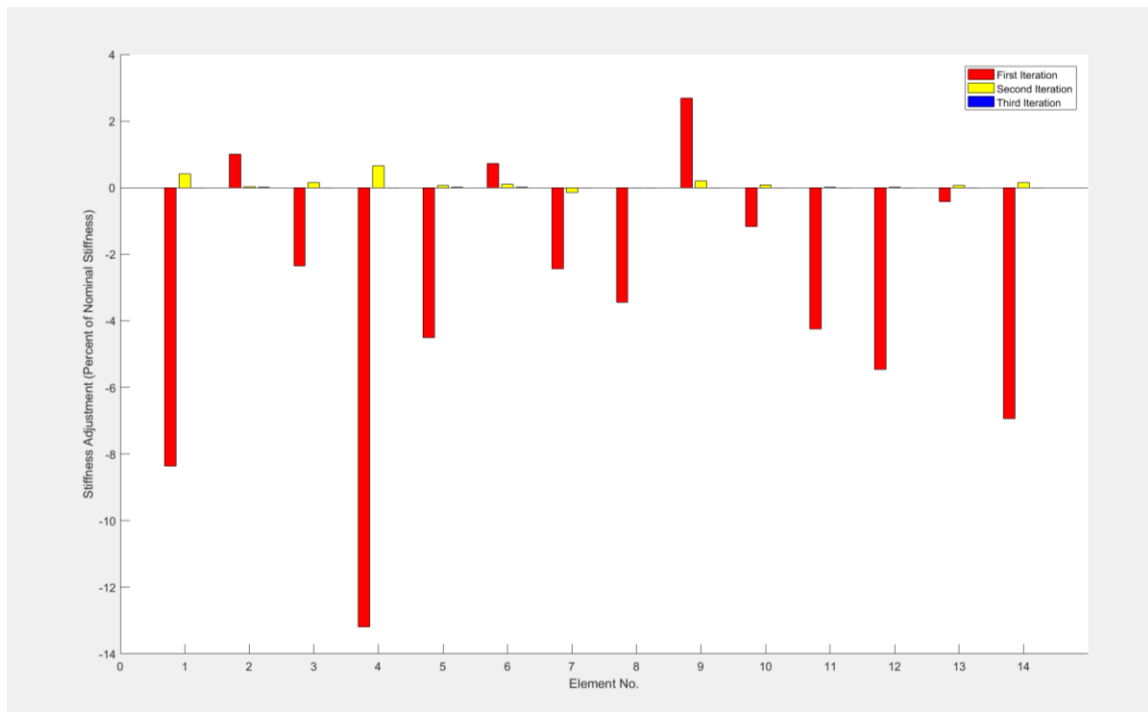


Figure 45. FEM Case B Flexural Rigidity Updates Over Three Iterations

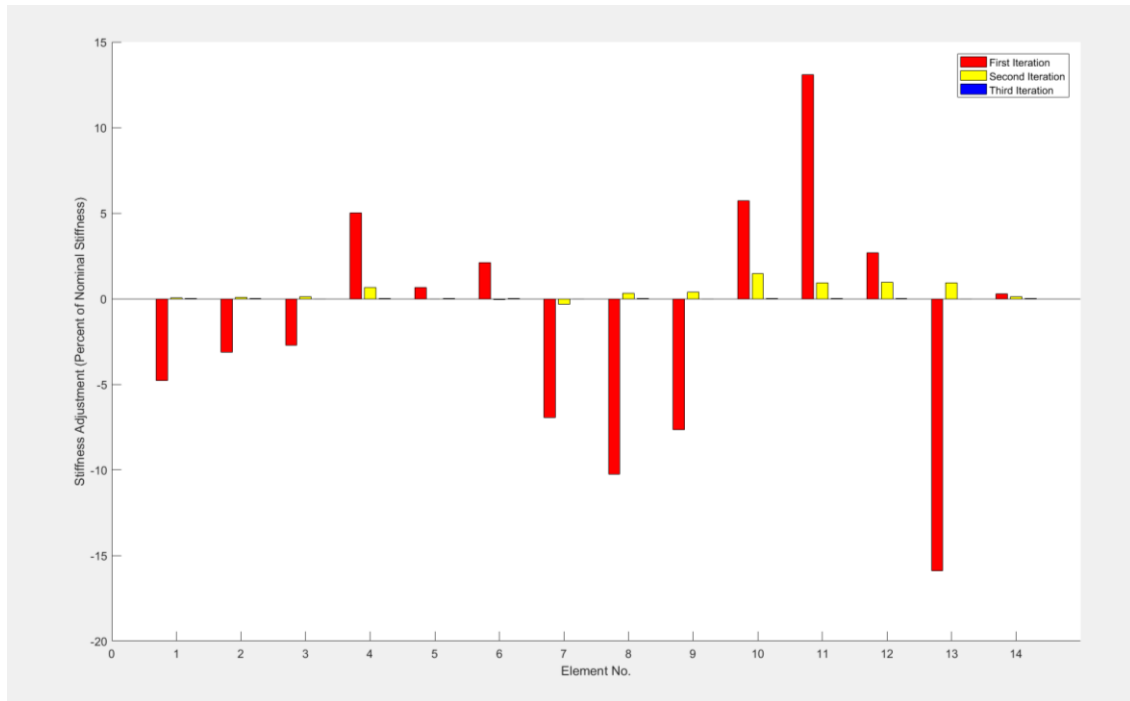


Figure 46. FEM Case C Flexural Rigidity Updates Over Three Iterations

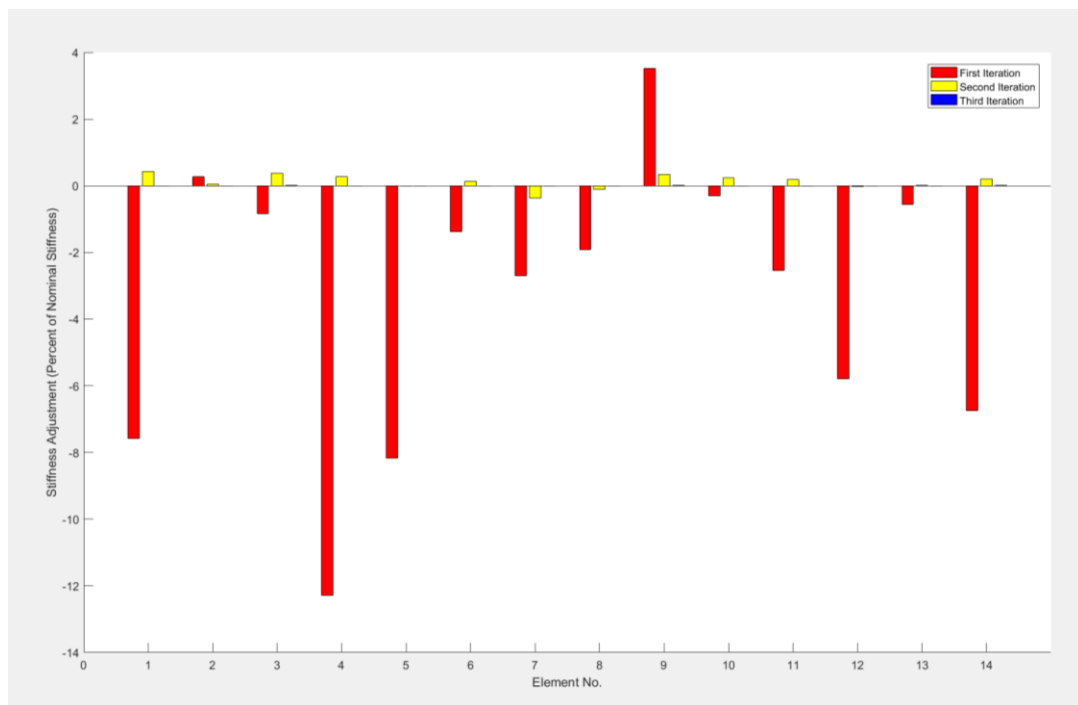


Figure 47. FEM Case D Flexural Rigidity Updates Over Three Iterations

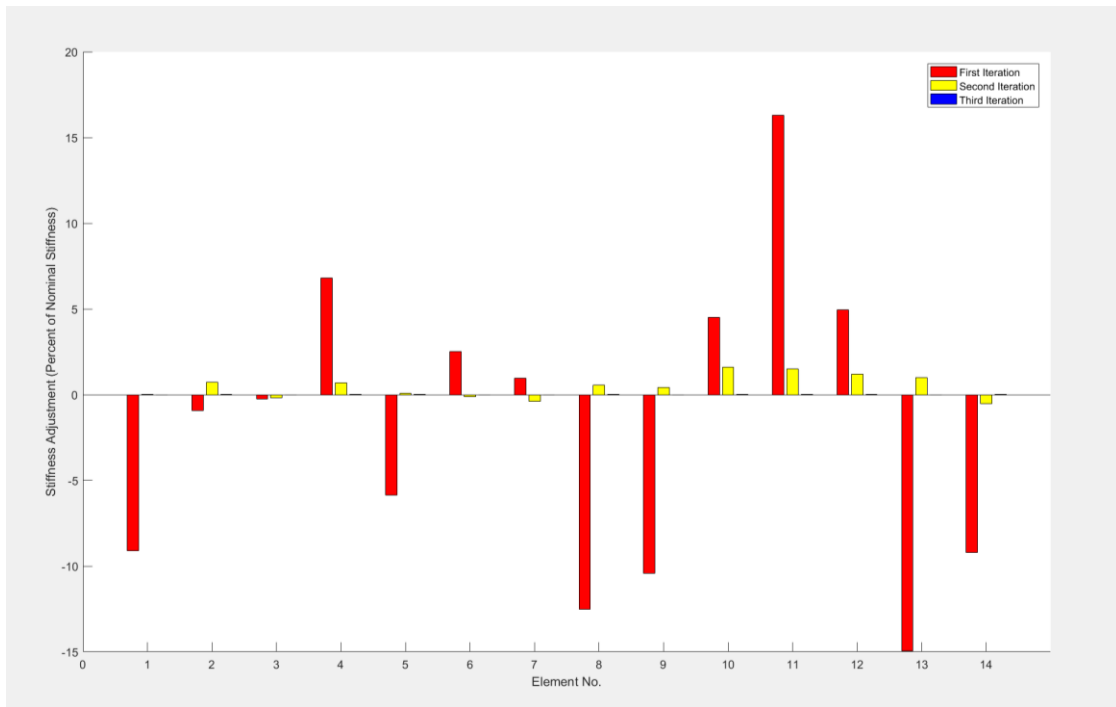


Figure 48. FEM Case E Flexural Rigidity Updates Over Three Iterations

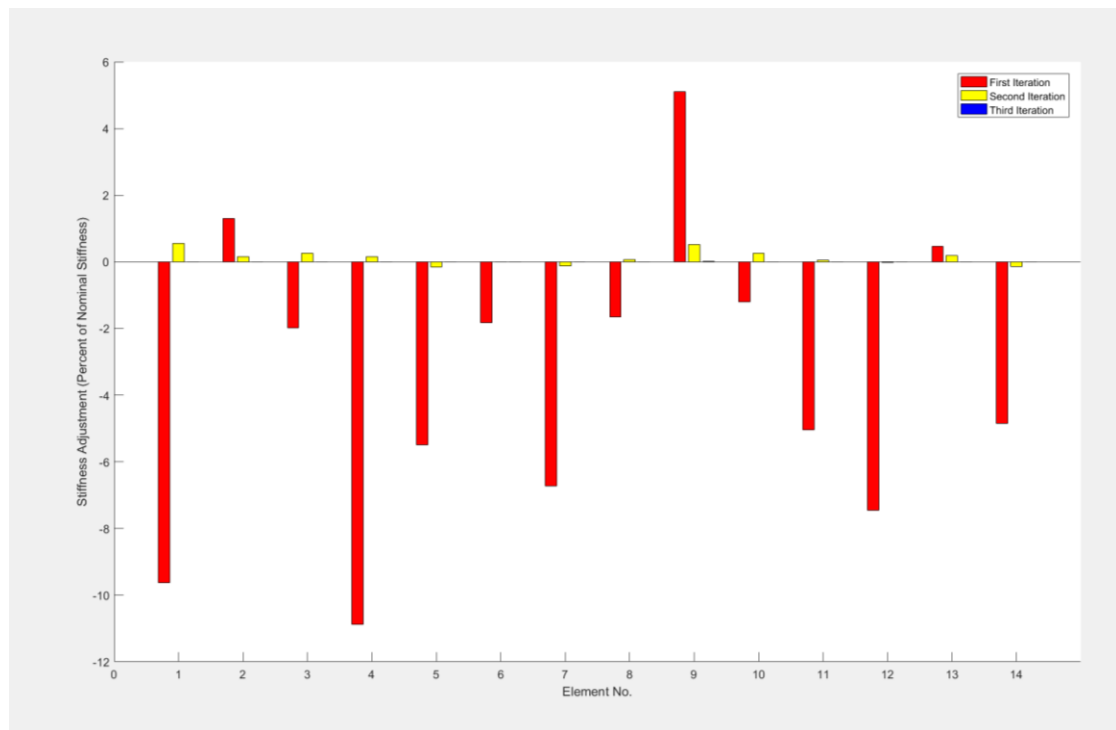


Figure 49. FEM Case F Flexural Rigidity Updates Over Three Iterations

With these updates applied individually to their respective interior elements, the percent differences between FEM natural frequencies and their experimental counterparts are significantly reduced. Figure 50 shows the extent of the model updating success. This plot features the initial FEM, all six updated FEM cases, and a manually adjusted FEM implemented by Damanakis in his research (“Adjusted FEM” in Figure 50).

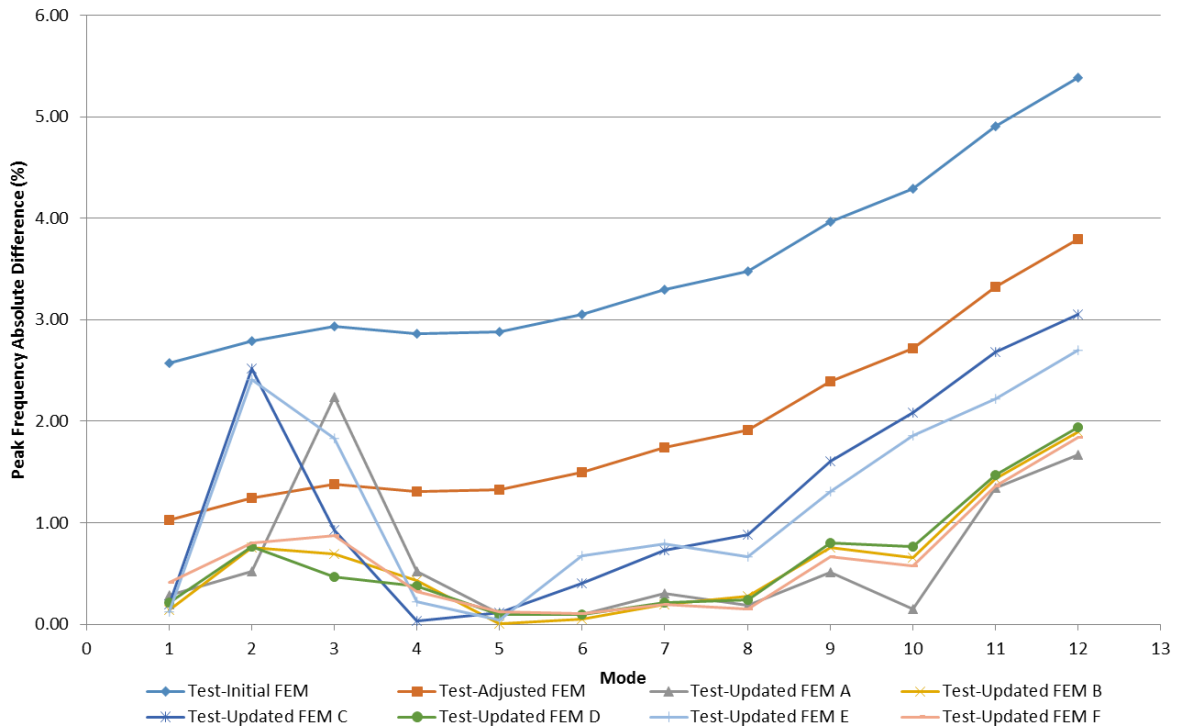


Figure 50. Reduction of Eigenvalue Percent Differences between FEMs and Experimental Values

C. CONCLUDING REMARKS

As seen in this chapter, combining multiple pin ABCs with high resolution FRFs produce severe distortion, and such combinations must be avoided. The lowest modes introduce multiple error sources that prevent converging model updates, and their use should also be avoided. While FEM natural frequencies

deviate from theoretical values at higher modes, these differences are not large enough to preclude successful model updating.

Per Figure 50, a three-iteration, individual element model updating approach is superior to a uniformly applied, manual FEM adjustment. It is important to note that updating cases utilizing two artificial pins resulted in less difference reduction than single pin cases. These relatively mediocre results might offset any advantage the two pins provide in terms of sensitivity condition number.

THIS PAGE INTENTIONALLY LEFT BLANK

VII. DAMAGE DETECTION

With multiple updated FEMs available, damage detection testing can be conducted. As previously discussed, this involves comparing the natural frequencies of the updated models to the experimentally obtained natural frequencies of the “damaged” test article. Of note, the damage detection case notation corresponds to the model updating cases.

A. DAMAGE DETECTION COMPLICATIONS

The first attempts at damage detection utilize updated FEMs C and E, which feature two pin ABCs. As mentioned in Chapter VI, two pin model updating was not as effective as the cases using single pins. However, as shown in Chapter V, two pin ABCs provided exceptional damage detection results in simulation. The resultant damage detection graphs for cases C and E are shown in Figures 51 and 52. The damage should be manifested as a distinct drop in flexural rigidity at the correct damage location element (interior Element 5).

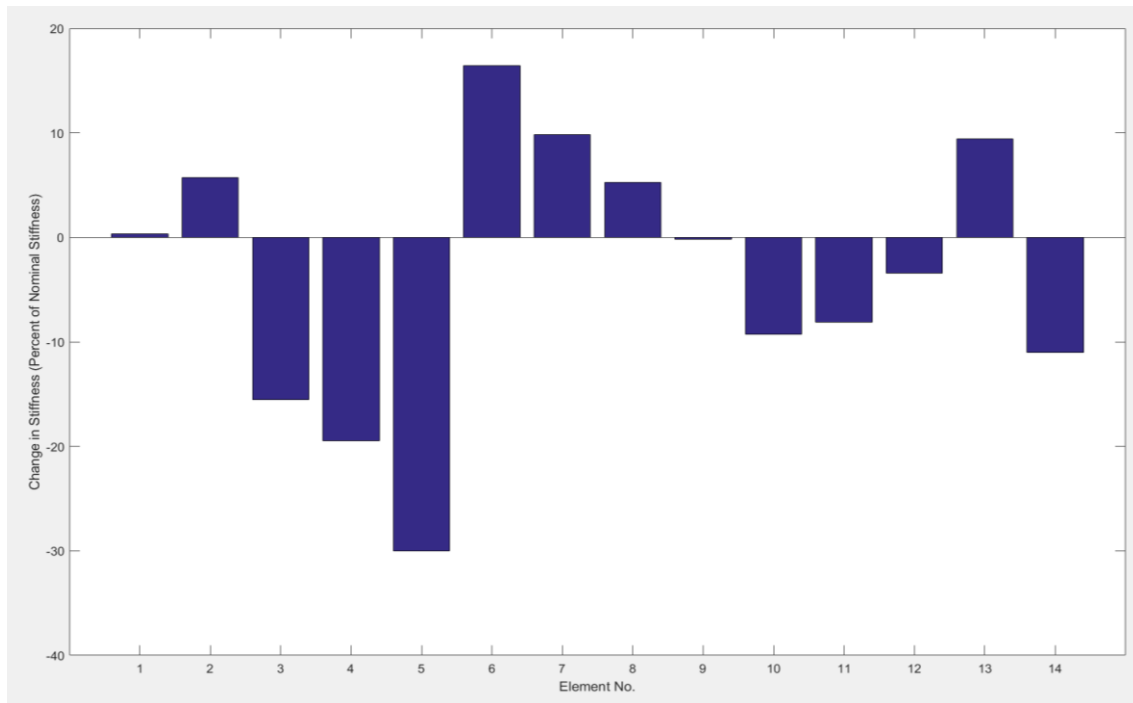


Figure 51. Case C Damage Detection Results. The correct damage location is shown at Element 5, but with significant false alarms.

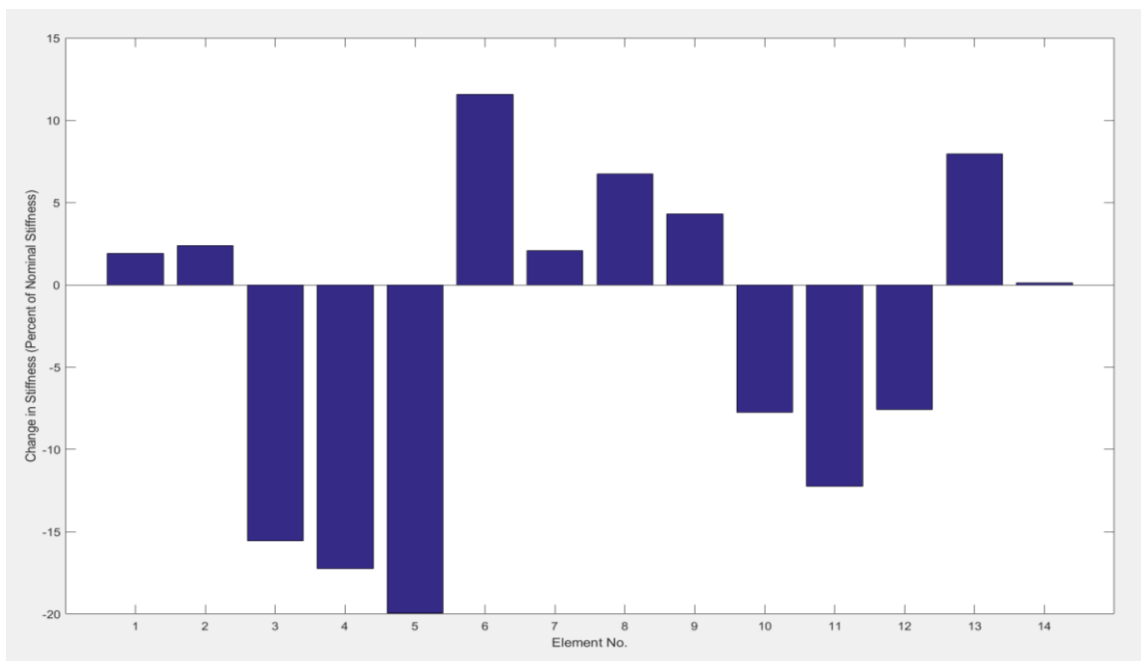


Figure 52. Case E Damage Detection Results. The correct damage location at is shown at Element 5, but with significant false alarms.

Both Cases C and E correctly locate the test article's installed "damage," as shown with the large reduction in flexural rigidity at Element 5. However, there are numerous false alarms with significant magnitudes. These false alarms are large enough to completely compromise the ability to distinguish damaged elements from undamaged ones. Table 7 summarizes the quantitative damage detection results.

An analysis of these disappointing results quickly reveals the limiting factor. As with model updating, even mild FRF peak distortion can have a negative impact on damage detection, even when modes 1 through 3 are excluded. Figure 53 shows the effect of two pin ABC configurations on the synthesized FRF.

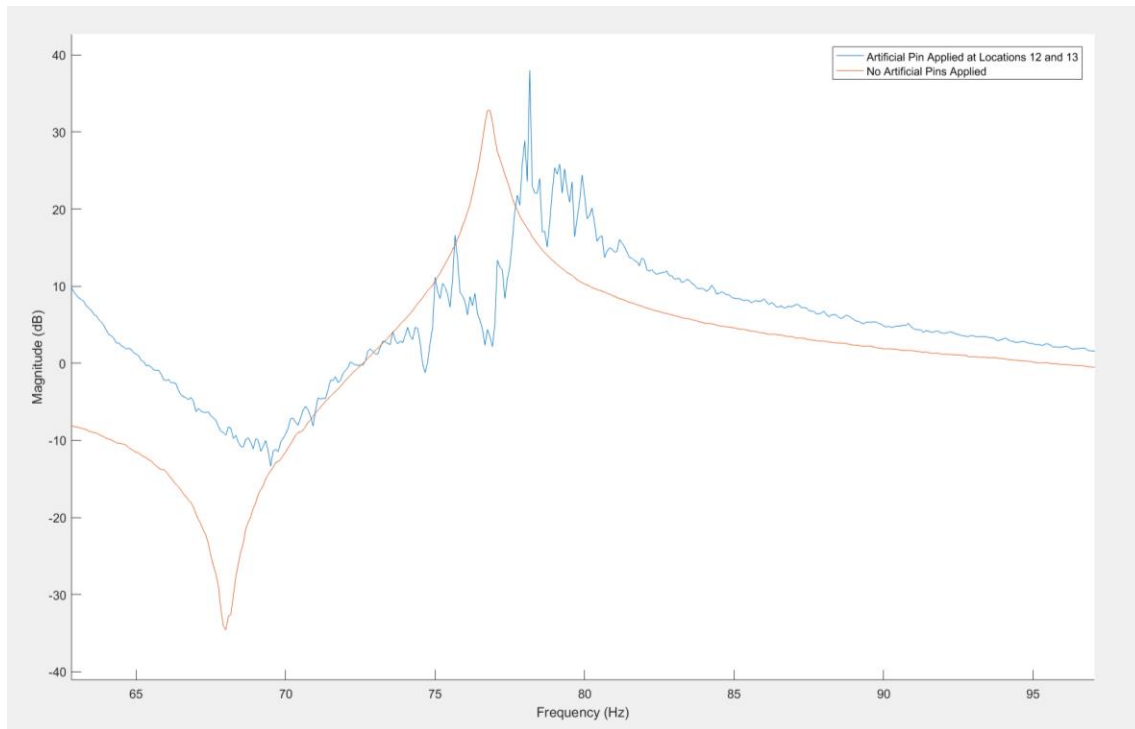


Figure 53. Detail of FRF Peak Distortion with Two Pin ABC Configuration

B. DAMAGE DETECTION RESULTS

Due to the negative impact of two pin ABC configurations on the synthesized FRF, further damage detection efforts are limited to single pin configurations. Damage detection results from Cases A, B, D, and E are exhibited in Figures 54 through 57.

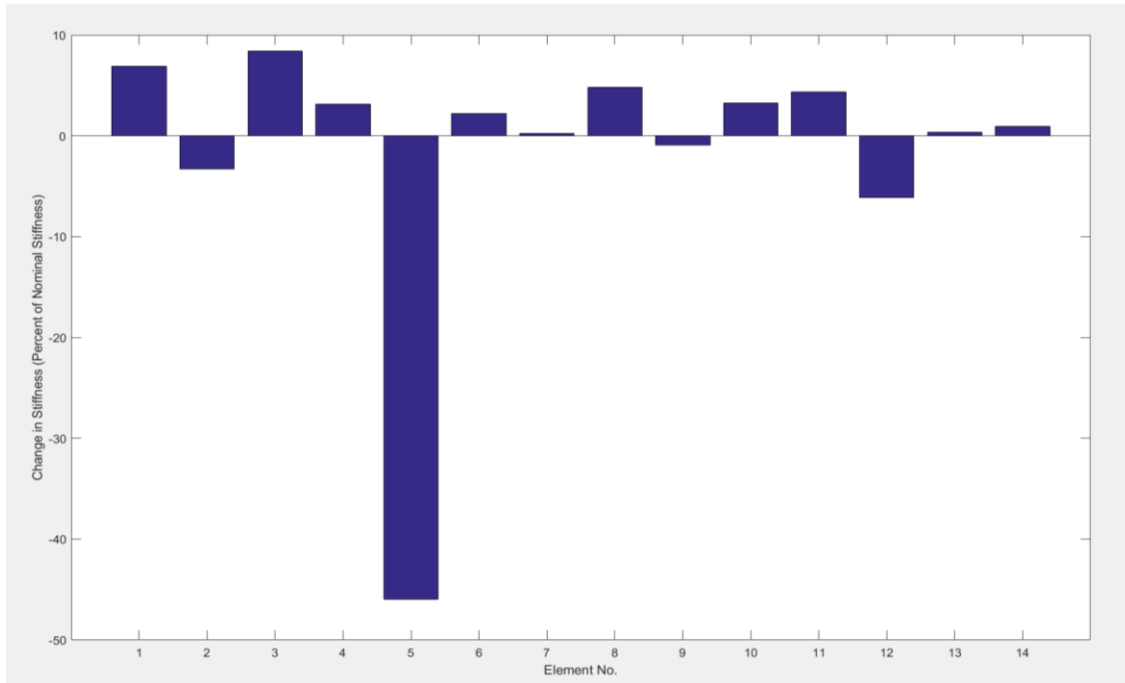


Figure 54. Case A Damage Detection Results with Clear Damage Location

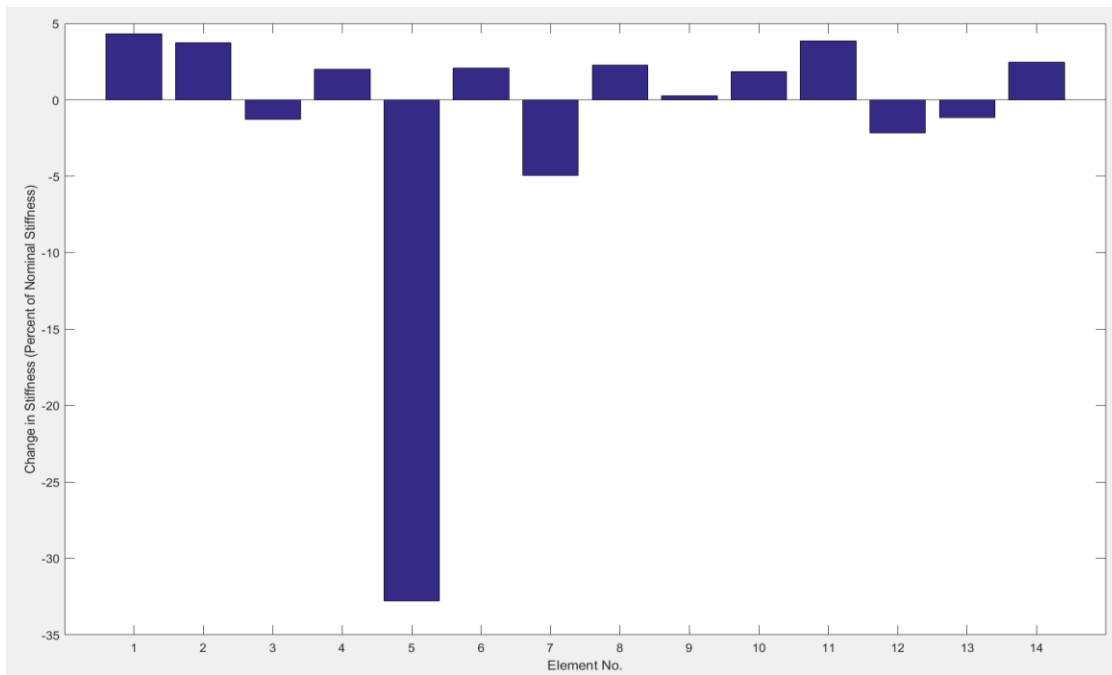


Figure 55. Case B Damage Detection Results with Clear Damage Location

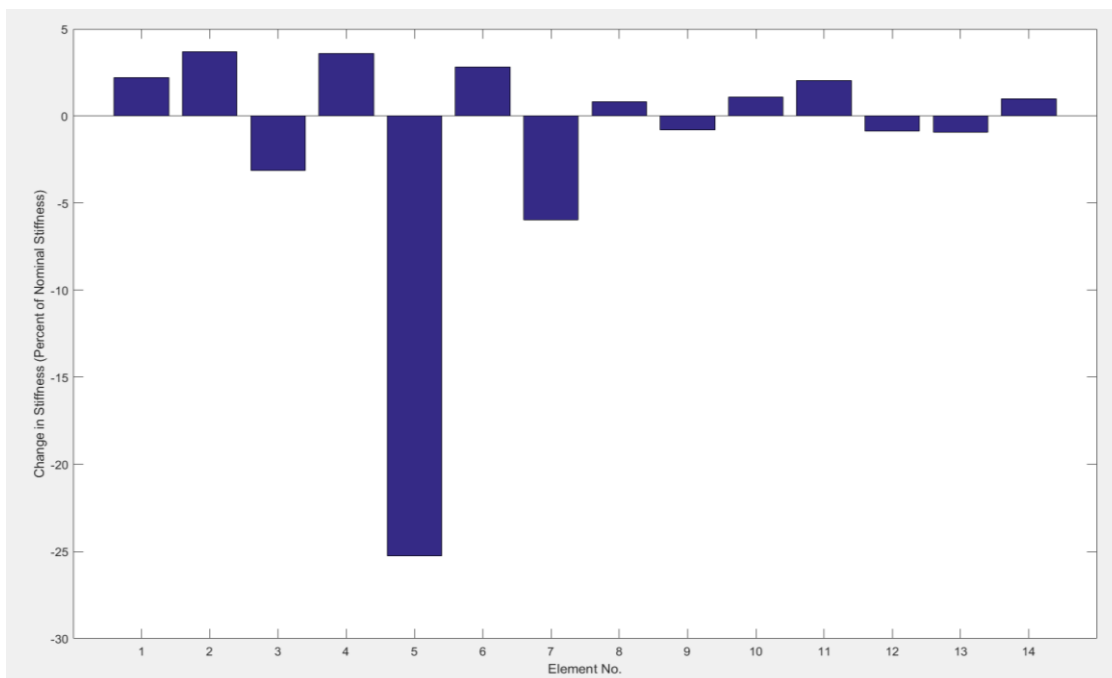


Figure 56. Case D Damage Detection Results with Clear Damage Location

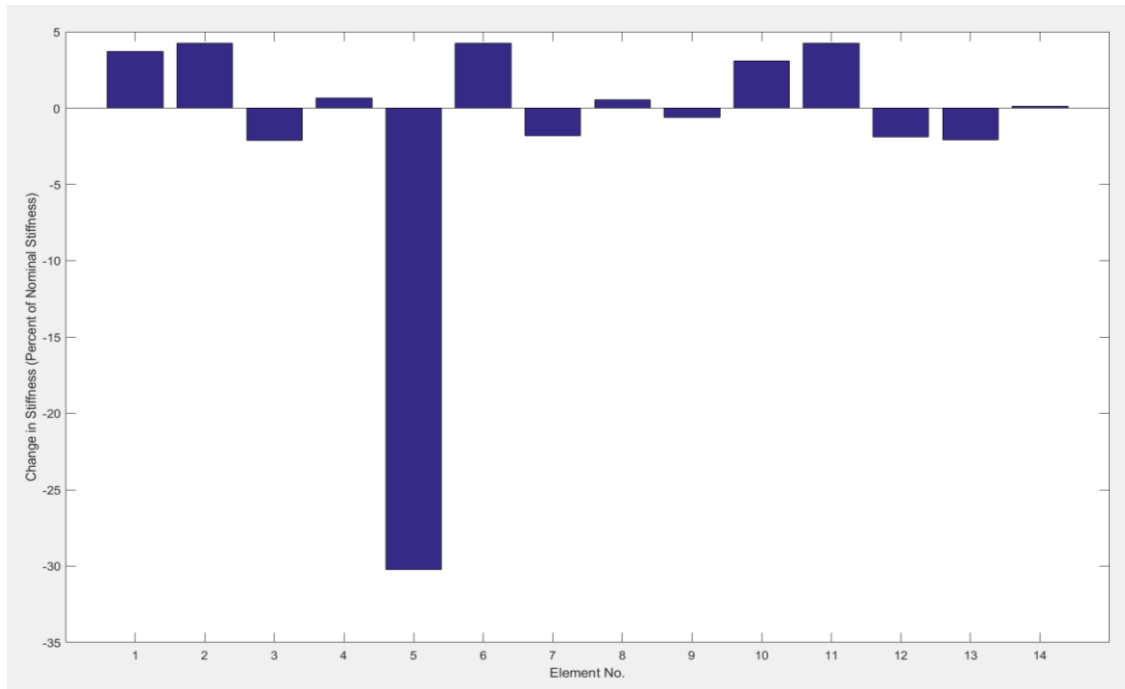


Figure 57. Case F Damage Detection Results with Clear Damage Location

Based on these figures, it is clear that the damaged element can be readily and consistently identified. The quantitative results are summarized in Table 7.

C. CONCLUDING REMARKS

With regard to damage detection, the advantages of single pin ABC configurations over two pin configurations is obvious. Table 7 compares the damage detection performance of each of the test cases. Total noise indicates the sum of all returns associated with an undamaged element. Maximum false detection is the largest single false damage return on an intact element.

Table 7. Damage Detection Performance Comparison

Damage Detection Case	Total Noise (%)	Maximum False Detection (%)
A	44.879	8.3842
B	32.425	4.9576
C	114.14	19.489
D	28.953	5.9607
E	97.431	17.234
F	29.357	4.2635

Table 7 emphasizes the superior results produced by single pin ABC configurations. It is also important to note that Case A has slightly higher error than the other single pin cases. However, the calculated flexural rigidity drop at the damage element has a higher magnitude than the other cases, and, therefore, maintains a similar prominence against the false returns.

THIS PAGE INTENTIONALLY LEFT BLANK

VIII. CONCLUSION

A. KEY OUTCOMES

The first key area of research involved the assessment of various FEM meshing schemes to simulate potential damage scenarios. The concept of a transitional mesh in which mesh size gradually expands with increased distance from installed damage offered a compromise of natural frequency accuracy and reasonable computation time. Additionally, it provides the flexibility required to assess damage of various dimensions. While the savings in computation time is not critical for a simple beam, it will become increasingly important as test articles of increasingly complex geometry are tested.

With regard to using ABCs to reduce linear dependency in the composite sensitivity matrix, it is obvious that there are many various combinations and configurations that can be employed. Using orthogonal projection to select the sensitivity rows, it is clear that multiple ABCs are ideal for driving condition number toward unity. When comparing single pin to double pin to triple pin configurations, orthogonal projection selects the rows generated from triple pin conditions. As shown with damage detection simulations, the sensitivity matrices with lower condition numbers have superior performance with regard to detection accuracy. However, using multi-pin combinations greatly increases the size of the sensitivity library and results in longer computation times. With every additional pin added, there is a diminishing return on performance improvement.

The comparison of pin-based ABCs to other types, such as spring and point masses, reveals interesting results. When provided with a library with single pin, single spring, and single point mass ABCs, orthogonal projection constructed a composite matrix made from mostly spring-based rows and several-pin based rows. While overall accuracy was not improved in comparison to the single-pin matrix, the mixed ABC matrix offered reduced maximum error in the damaged elements.

Turning to the experimental portion of the research, it quickly became clear that raw FRF data is susceptible to distortion. The magnitude of distortion is a function of FRF frequency resolution and the number of ABCs synthesized into the H matrix. Higher ABC counts and higher resolution lead to higher distortion. Lower modes are particularly vulnerable to this phenomenon, as well as sources of experimental error.

These complications can be avoided through the judicious use of select ABCs, FRF resolution, and modes. With the proper conditions employed, iterative model updating can be employed. This allows for flexural rigidity adjustments to be applied to every individual interior element. When compared to manual adjustments uniformly applied to the entire FEM (as performed in Damanakis's research), the iterative model update is shown to be superior.

The concerns regarding distortion and experimental error in model updating also apply for damage detection. Even mild FRF peak distortion can compromise damage detection. Even if damage is correctly located via indications of flexural rigidity reduction, false returns can compromise the process's effectiveness. However, as with model updating, prudent usage of ABCs, resolution, and modes can lead to clear, consistent damage detection.

B. RECOMMENDATIONS

Based on obtaining these promising results, the next stage of research should be optimization. Additional ABC combinations should be investigated in an effort to drive sensitivity matrix condition number toward unity. Since this will greatly expand the sensitivity library, high-power computers should be employed to avoid unreasonable computation times. On the experimental side, various curve fitters should be evaluated to generate an FRF that is less susceptible to distortion. Additionally, the existing MATLAB code should be optimized. Currently, existing code requires a large amount of user input. Any automation that can be integrated into the program would be a welcome improvement. This

improved model updating and damage detection ability should be evaluated with a beam featuring multiple damage locations of various dimensions.

With an optimized process, more realistic scenarios can be tested. Instead of milling notches into the beam, cracking should be induced in multiple locations. Another possible test would utilize a heavily corroded test article. Additional features can be evaluated such as welds and bolted connections. With these situations investigated, test articles with more complex geometry can be used. Instead of using a simple rectangular beam, I, T, and box beams can be utilized. Eventually, more sophisticated structures such as trusses and frames can be tested.



Figure 58. A Potential Future Test Article; an Available Frame

THIS PAGE INTENTIONALLY LEFT BLANK

<u>Customer Name</u>	<u>Customer PO#</u>	<u>Shipper No</u>	<u>Heat Number</u>
Naval Postgraduate School	KFS66964	856510	201620673

Service Center Metals
5850 Quality Way
Prince George, VA 23875

CERTIFIED INSPECTION REPORT AND TEST RESULTS FOR EXTRUDED PRODUCTS

OUR ORDER NUMBER	279948	ITEM	19
------------------	--------	------	----

ALL TO	SALES ORDER NUMBER	DATE OF SHIPMENT
Copper & Brass Sales, Western	316202	12/9/2016
SHIP TO	SHIP TO / COMPANY	SHIP TO / COMPANY
Copper & Brass Sales, Inc.	5403330488	David Schroeder (West)
Quantity Certified	1,143 lbs	108 pcs
	CUSTOMER PART NUMBER	DESCRIPTION
	ALRECO0133	SCRB .375 x 2.000

CERTIFICATION	ASTM-B221-14 StencilCont
SPECIFICATION	AMS-QQA-2008 Rev-A
PREPARATION	PERMUTATION
REHS	2011/ESU Compliant

We hereby certify that the material covered by this report has been inspected in accordance with the most recent certification revision, and has been found to meet the applicable requirements described herein, including any specifications forming a part of the description, and that samples representative of the material met the composition limits and had the mechanical properties shown. Items produced and certified as 6061-T6511 also meet the requirements of 6061-T6.

This product is REHS-2, REACH, and DPAK3 compliant.

Mechanical Properties	
Tests	Lot No.

Tests	Lot No.	Test Date	Ultimate Tensile Strength (KSI)	Yield Strength (KSI)	Percent Elongation
-------	---------	-----------	---------------------------------	----------------------	--------------------

4	201620673	11/23/16	min 45.10 max 46.30	min 41.40 max 43.20	min 14.50 max 15.50
---	-----------	----------	---------------------	---------------------	---------------------

Chemical Composition for Aluminum Alloy 6061

Cast #	Lot No.	Alloy	Si	Fe	Cu	Mn	Mg	Cr	Zn	Al	Others	Each	Total	Melt Source:
2K16117B	201620673	6061	0.05	0.18	0.19	0.07	0.86	0.07	<0.01	0.02	97.86	0.05	0.15	Unior States of America

PRISM property assessment only - extruded in the US-NA

CUSTOMER: ONLINE METALS LAX WILL CALL

Order: 69620

Date: 01/16/2017

Print Date: 12/21/2016

Calvin J. Wiggins, Director of Quality & Technical Services

the parts

James L. Wiggins

Figure 59. Test Beam Inspection Report

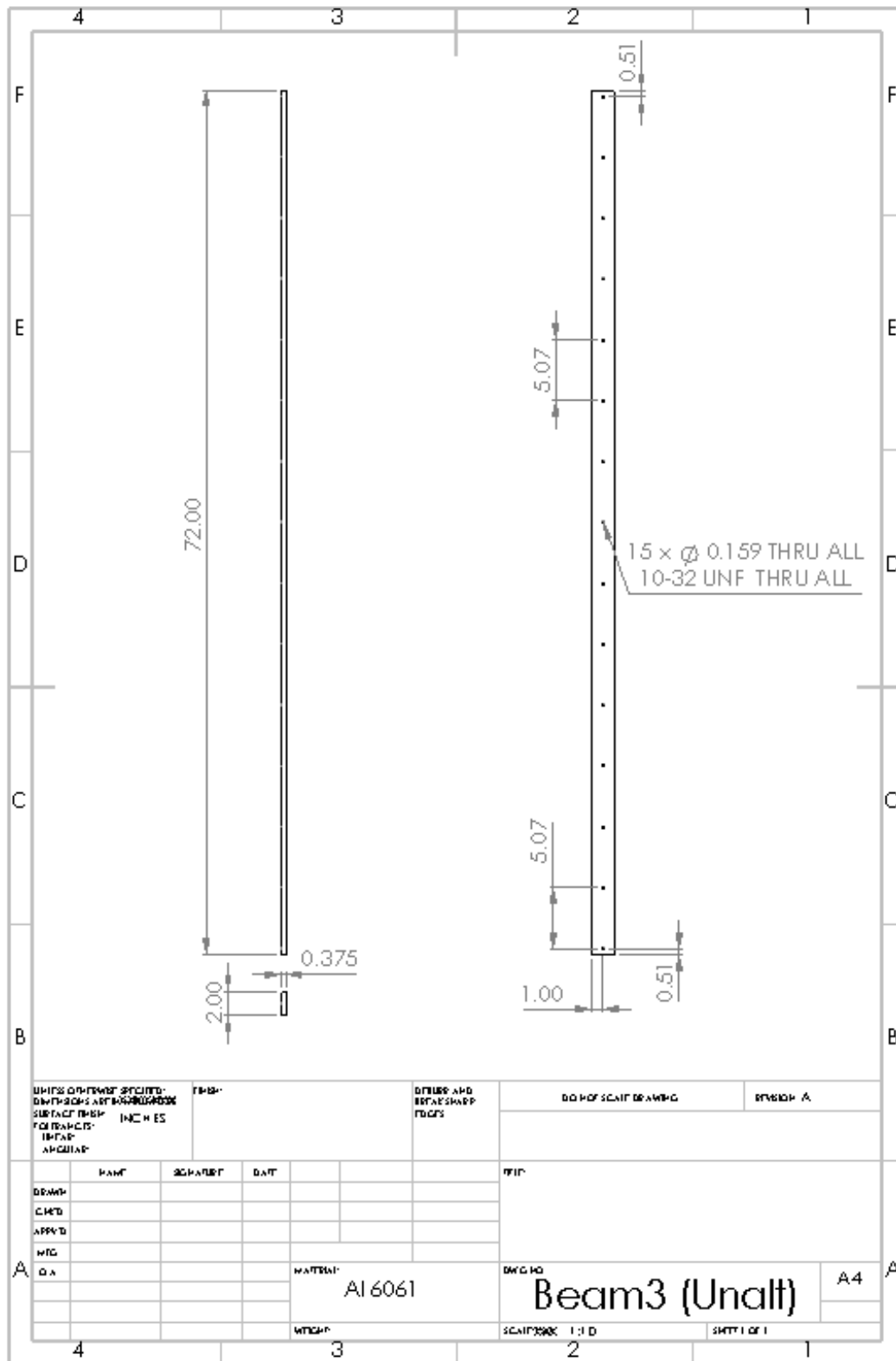


Figure 60. Drawing of "Intact" Test Article

THIS PAGE INTENTIONALLY LEFT BLANK

APPENDIX B. INSTRUMENTATION DETAILS

PCB
PIEZOTRONICS

PCB CALIBRATION CERTIFICATE

IMPULSE FORCE HAMMER

Model No. 086B03
Serial No. 2195

Customer: Supply NAVAL POSTGRADUATE SCHOOL

Range 0-500 lb
Linearity error <1.0 %
Discharge Time Constant 2000 s
Output Impedance 100 ohms
Output Bias 9.30 volts

Traceable to NBS through 737/236905 Calibration Specification MIL-STD 45662
Invoice No.: 35777

Initials: PJ Date: 5-22-86

Accelerometer: Model No. 302A07 Serial No. 7607 Sens. 9.91 mV/g
Pendulous Test Mass 1.05 lb (476 gram) including accelerometer

Hammer Sensitivity:

CONFIGURATION	Tip Extender	PLASTIC/VINYL NONE	PLASTIC/VINYL STEEL
SCALING FACTOR (SENSITIVITY RATIO)	lb/g	1.05 (SEE NOTE)	0.99
Accel/Force	(N/ms ⁻²)	0.47	0.45
HAMMER SENSITIVITY	mV/lb	9.48	9.99
	(mV/N)	2.13	2.25

NOTES:

- The sensitivity ratio (Sa/Sf) is the scaling factor for converting structural transfer measurements into engineering units. Divide results by this ratio.
- Each specific hammer configuration has a different sensitivity. The difference is a constant percentage, which depends on the mass of the cap and tip assembly relative to the total mass of the head. Calibrating the specific hammer structure being used automatically compensates for mass effects.

Effective mass 0.265 with 302A07 attached and vinyl capped plastic tip.

PCB PIEZOTRONICS, INC. 3425 WALDEN AVENUE DEPEW, NEW YORK 14043-2495 TELEPHONE 716-684-0001 TWX 710-263-1371

Figure 62. Force Hammer with Calibration Certificate

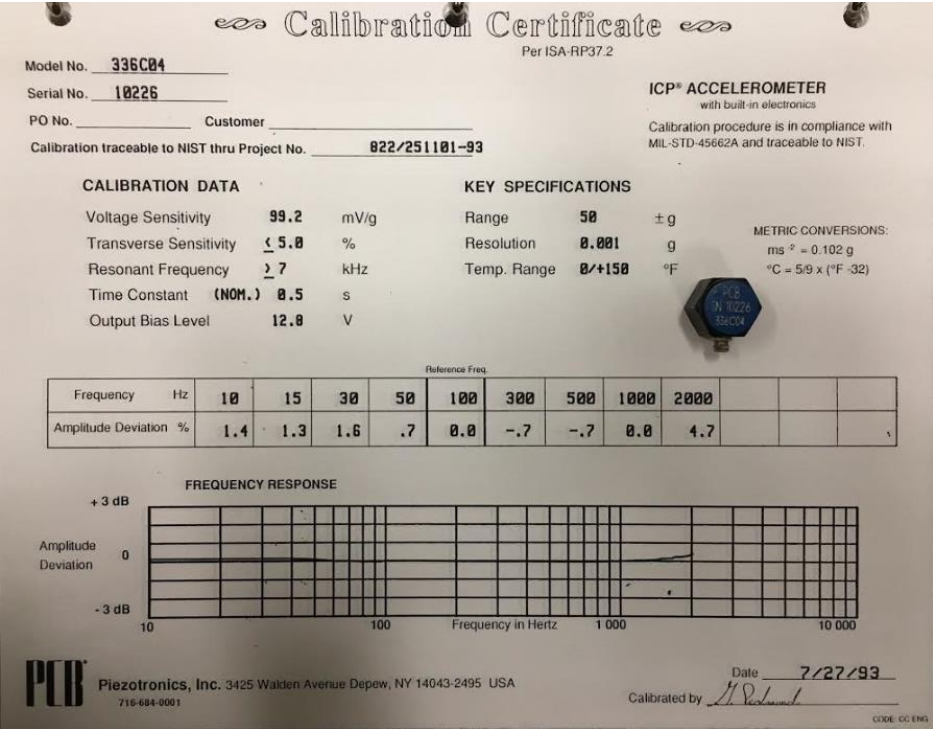


Figure 63. Accelerometer SN# 10226 with Calibration Sheet



Figure 64. Accelerometer SN# 10847 with Calibration Sheet

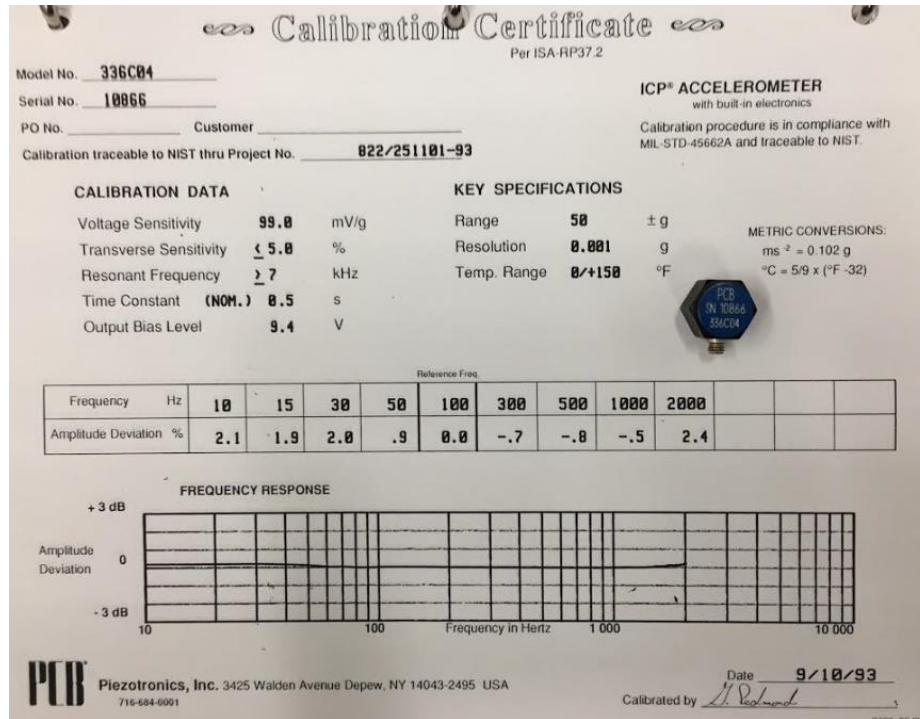


Figure 65. Accelerometer SN# 10866 with Calibration Sheet

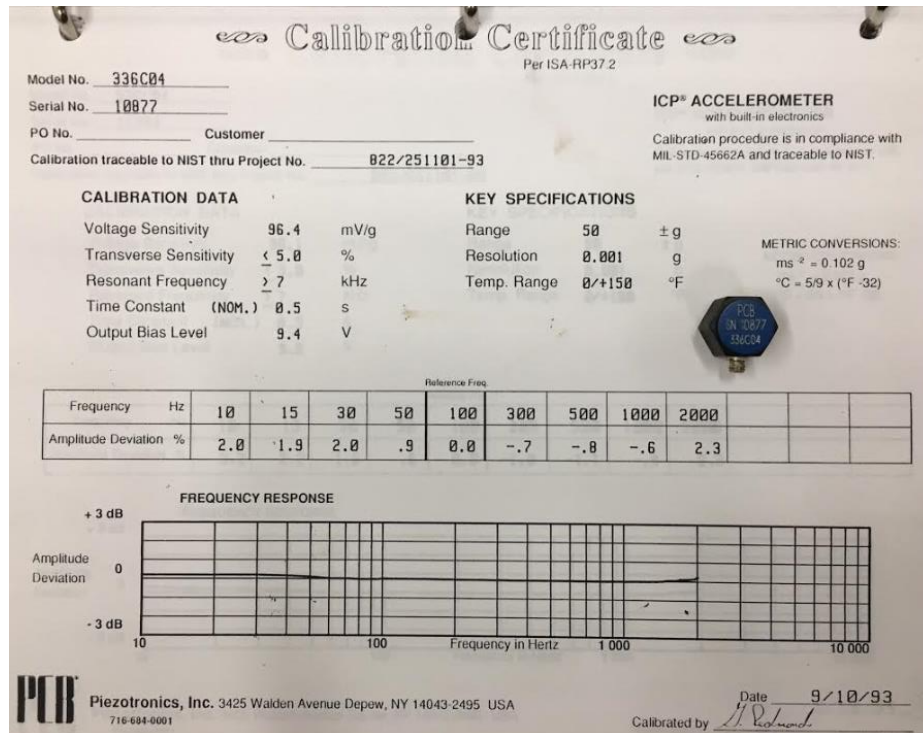


Figure 66. Accelerometer SN# 10877 with Calibration Sheet

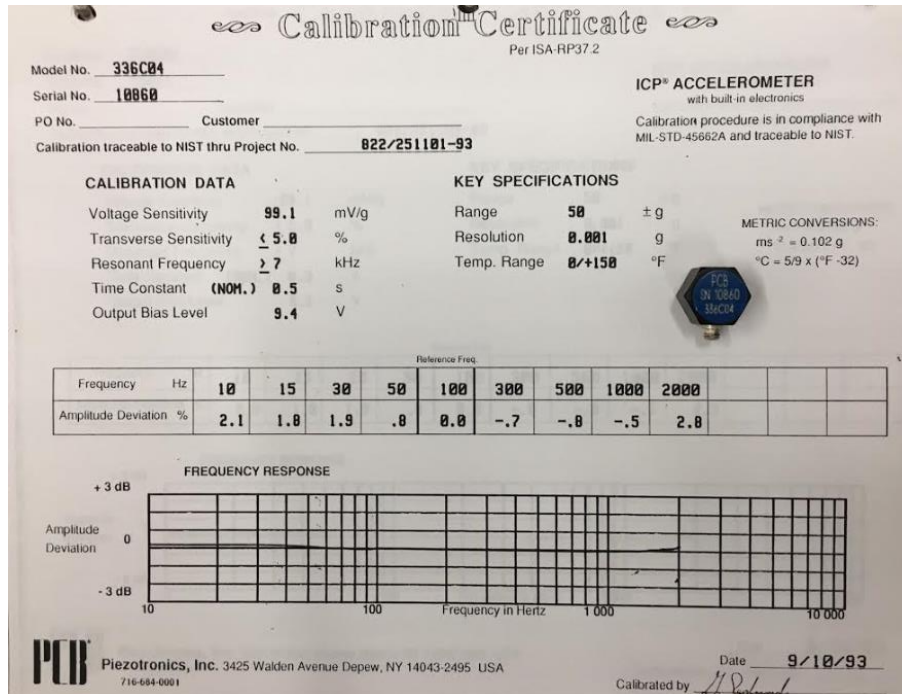


Figure 67. Accelerometer SN# 10860 with Calibration Sheet

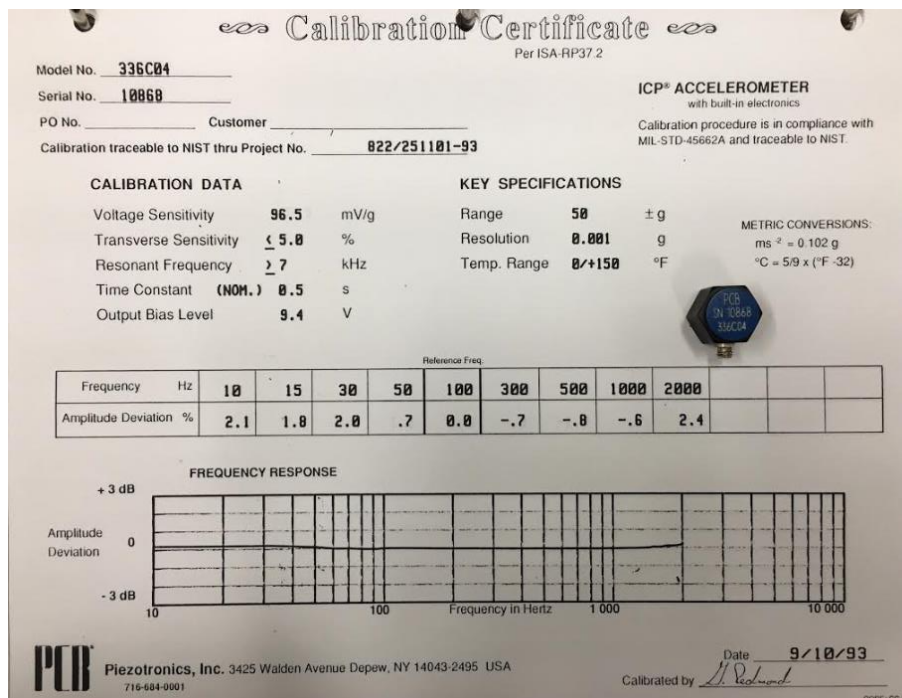


Figure 68. Accelerometer SN# 10868 with Calibration Sheet

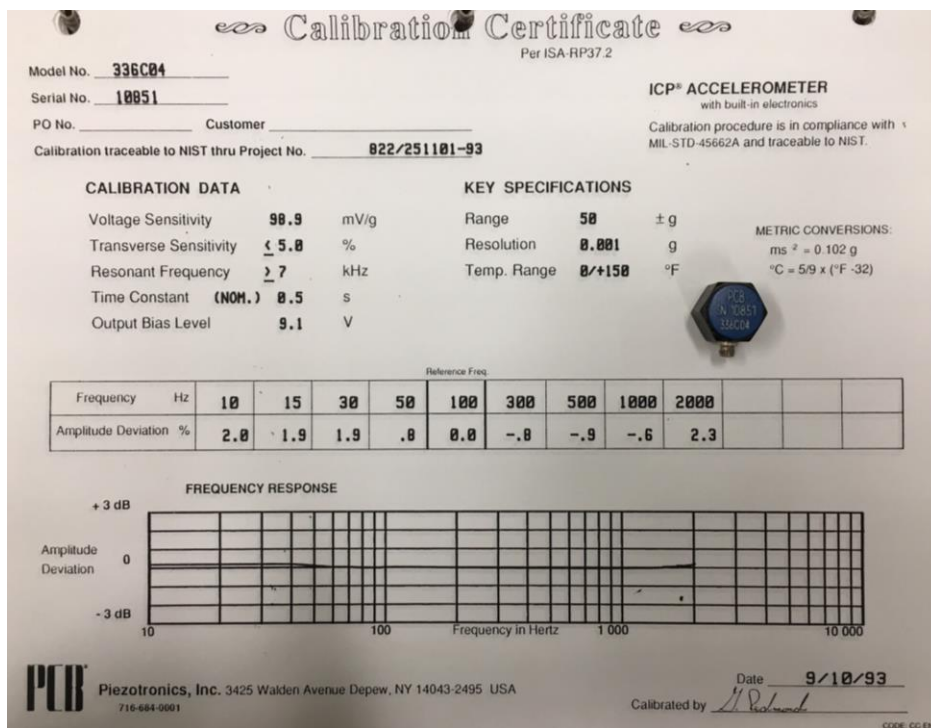


Figure 69. Accelerometer SN# 10851 with Calibration Sheet

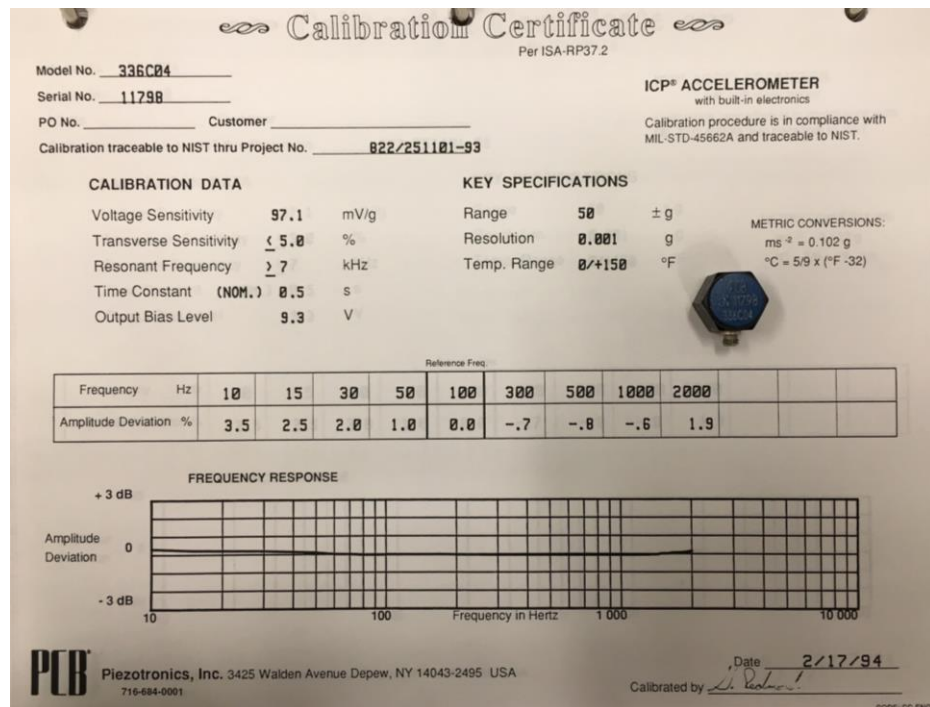


Figure 70. Accelerometer SN# 11798 with Calibration Sheet

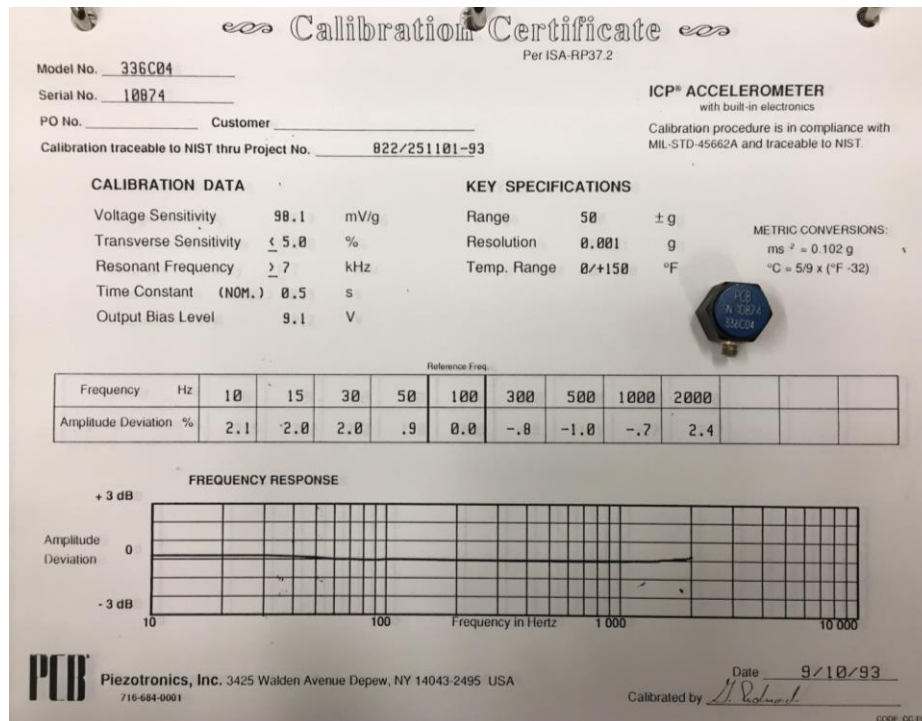


Figure 71. Accelerometer SN# 10874 with Calibration Sheet

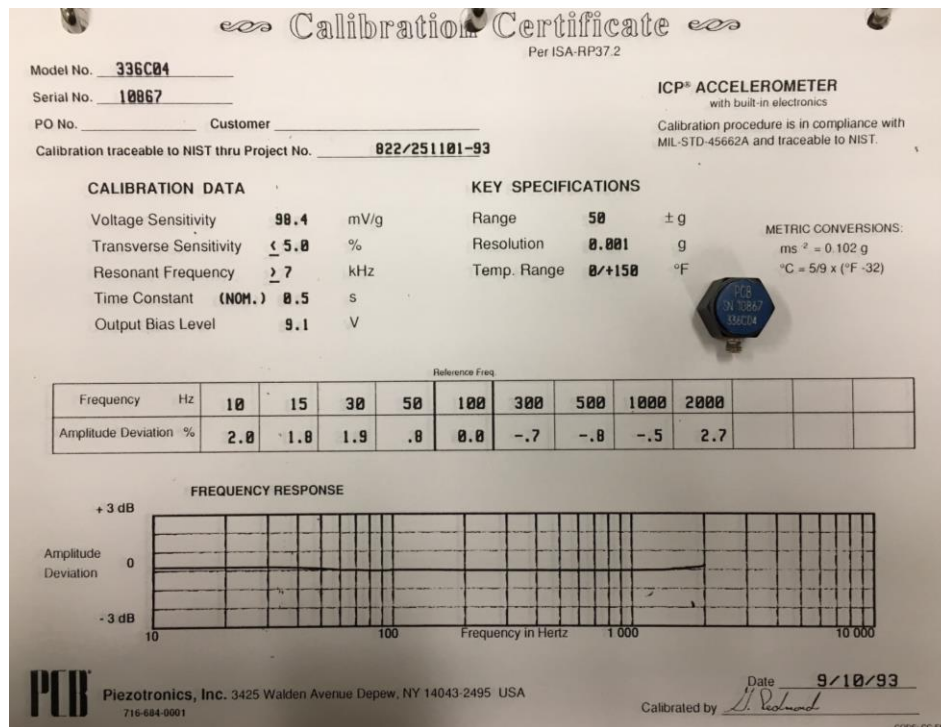


Figure 72. Accelerometer SN# 10867 with Calibration Sheet

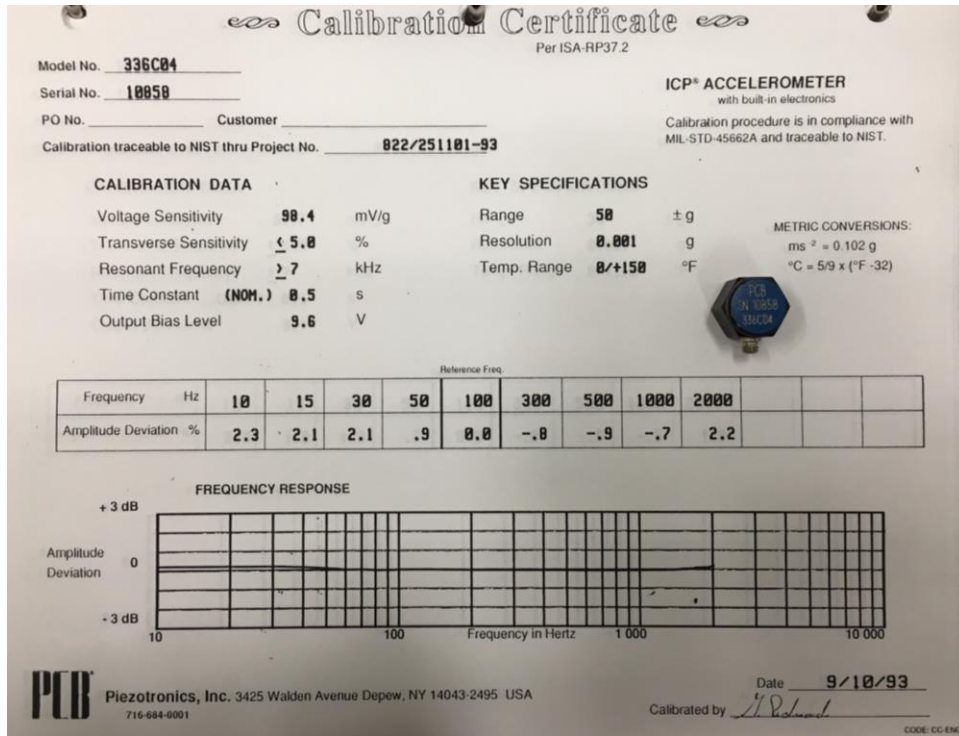


Figure 73. Accelerometer SN# 10858 with Calibration Sheet

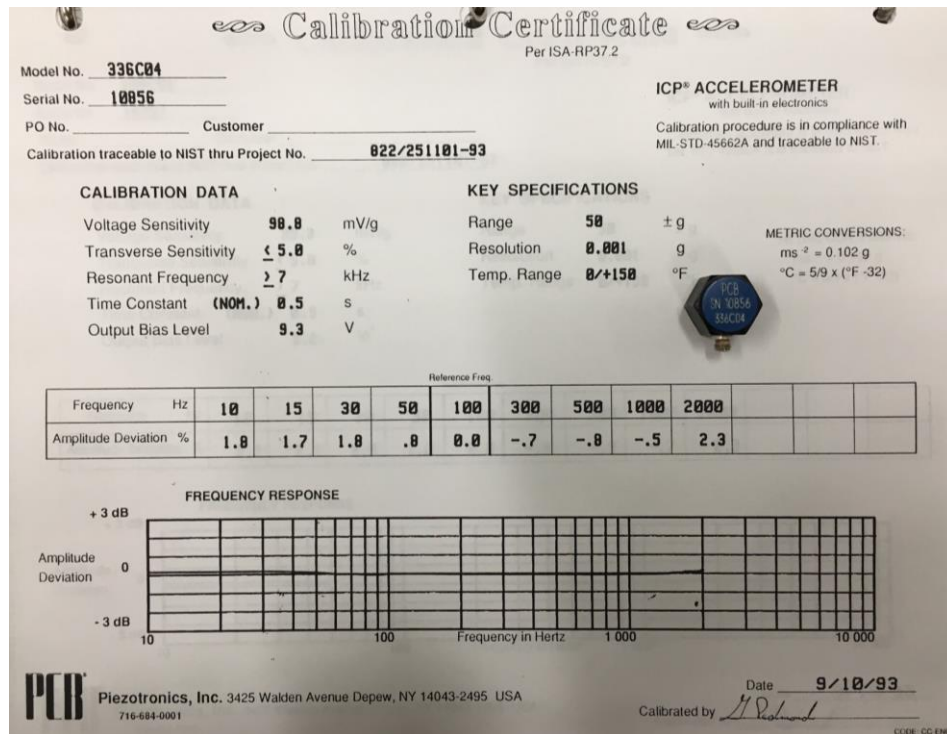


Figure 74. Accelerometer SN# 10856 with Calibration Sheet

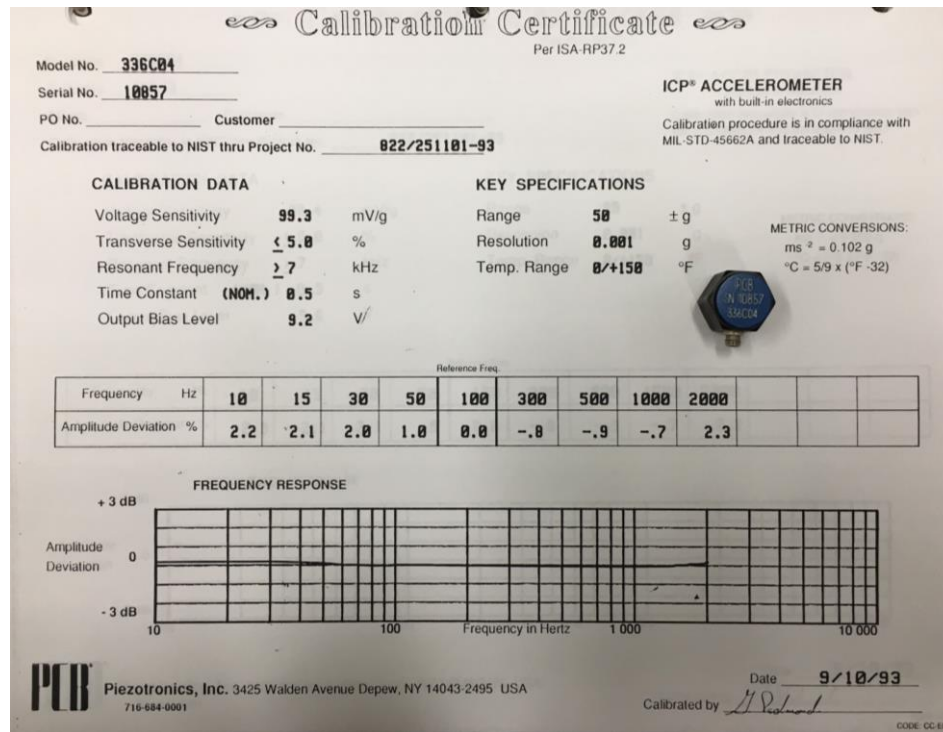


Figure 75. Accelerometer SN# 10857 with Calibration Sheet

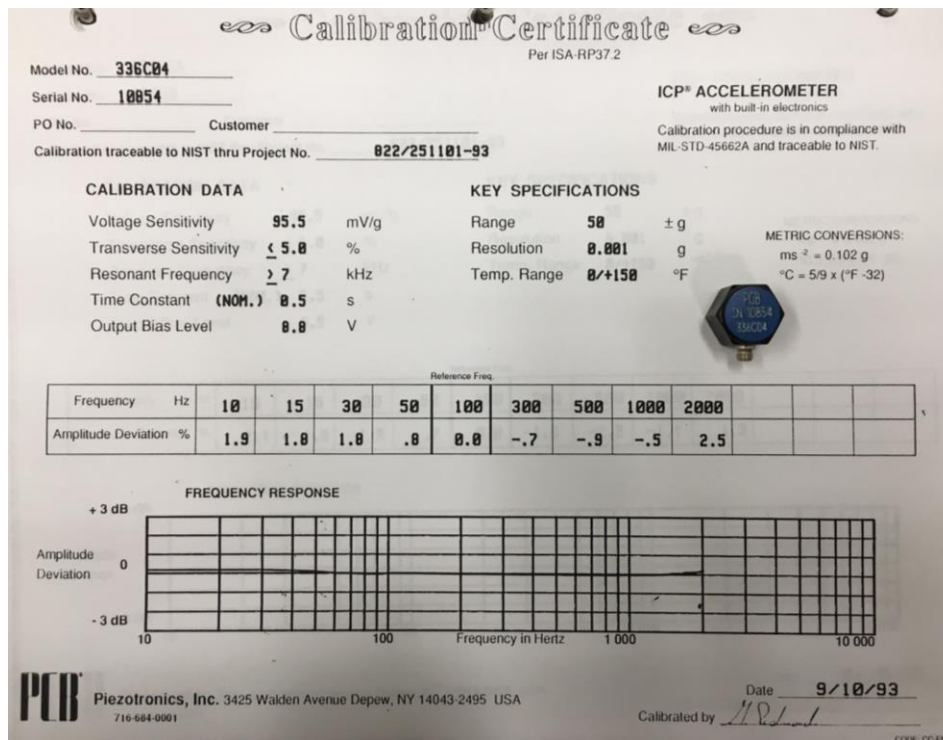


Figure 76. Accelerometer SN# 10854 with Calibration Sheet

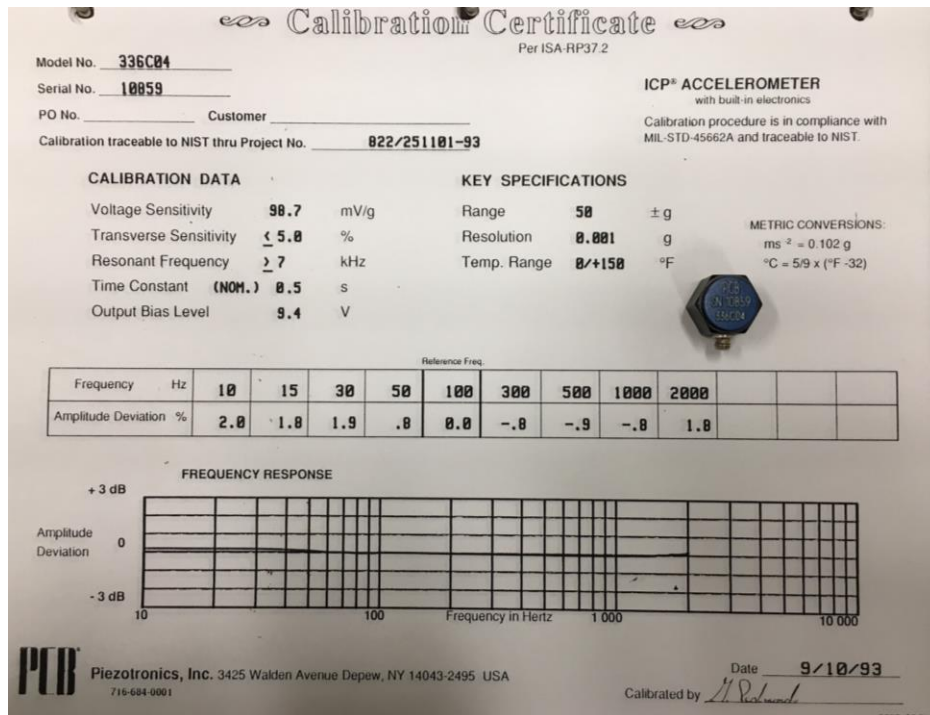



Figure 77. Accelerometer SN# 10859 with Calibration Sheet

Model Number 394C06		HAND HELD SHAKER		Revision: H ECN #: 40107	
Performance Operating Frequency(± 1 %) Acceleration Output(± 3 %) Velocity Output Displacement Output Transverse Output Distortion(0 to 99 grams load) Distortion(100 to 149 grams load) Distortion(150 to 210 grams load) Maximum Load Automatic Switch Off Time Calibration Cycles(2 gram load) Calibration Cycles(25 gram load) Calibration Cycles(50 gram load) Calibration Cycles(100 gram load) Calibration Cycles(150 gram load) Calibration Cycles(210 gram load) Environmental Temperature Range(Operating) Electrical Ramp-Up time Internal Battery(Quantity) Internal Battery(Type) DC Power Battery Life(2 gram load) Battery Life(25 gram load) Battery Life(50 gram load) Battery Life(100 gram load) Battery Life(150 gram load) Battery Life(210 gram load) Physical Size (Diameter x Height) Weight(with batteries) Mounting Thread Mounting Torque(Maximum)		ENGLISH 159.2 Hz 1.00 g rms 0.39 in/sec rms 0.39 mil rms ≤ 3 % ≤ 2 % ≤ 5 % ≤ 9 % 7.4 oz 1.0 to 2.5 minutes 320 cycles 600 cycles 1600 cycles 400 cycles 160 cycles 80 cycles +15 to +130 °F ≤ 3 sec 4 AA 10 VDC 2.4 amps 8 hours 15 hours 40 hours 10 hours 4 hours 2 hours 2.2 in x 7.8 in 31 oz 10-32 Female 10 in-lb		SI 159.2 Hz 9.81 m/s ² rms 9.81 mm/s rms 9.81 µm rms ≤ 3 % ≤ 2 % ≤ 5 % ≤ 9 % 210 gm 1.0 to 2.5 minutes 320 cycles 600 cycles 1600 cycles 400 cycles 160 cycles 80 cycles -10 to +55 °C ≤ 3 sec 4 AA 10 VDC 2.4 amps 8 hours 15 hours 40 hours 10 hours 4 hours 2 hours 56 mm x 200 mm 900 gm 10-32 Female 112 N-cm	OPTIONAL VERSIONS Optional versions have identical specifications and accessories as listed for the standard model except where noted below. More than one option may be used. M - Metric Mount Acceleration Output(± 3 %) 1.02 g rms 10.0 m/s ² rms NOTES: [1] Typical. [2] Alkaline type recommended for longest service life. [3] This specification for external DC power supply (optional). [4] Maximum. [5] Approximate values, based on automatic switch off time and dependent on type of batteries. [6] Unit supplied set to rms; see manual for peak selection. [7] Calculated values for reference only. [8] Maximum load includes sensor, connector and cabling. [9] Unit supplied set to auto shut off; see manual for continuous use selection. [10] Test sensor should be hand tightened (without tools). [11] Transducer to shaker table. [12] See PCB Declaration of Conformance PS022 for details. SUPPLIED ACCESSORIES: Model 073A15 Battery Pack (1) Model 080A109 Petro Wax (1) Model 080A84 Mounting Base (5-40 to 10-32) (1) Model 080A85 Mounting Base (M3 X 0.5 to 10-32) (1) Model 081A08 Mounting Stud (10-32 to 1/4-28) (1) Model 081B05 Mounting Stud (10-32 to 10-32) (2) Model M081B05 Mounting Stud 10-32 to M6 X 0.75 (1) Model M081B23 Metric mounting stud, 10-32 to M5 x 0.80 long (1) OPTIONAL ACCESSORIES: Model 073A16 DC switching power supply (for Model 394C06) (1) Model 080A150 Mounting Base (1/4-28) (1) Model 080B44 3-Pin Mounting Adapter (1)
Entered: AP		Engineer: AJP	Sales: WDC	Approved: JWH	Spec Number:
Date: 1/28/2013		Date: 1/28/2013	Date: 1/28/2013	Date: 1/28/2013	1345



PCB PIEZOTRONICS™
3425 Walden Avenue, Depew, NY 14043
Phone: 716-684-0001
Fax: 716-684-0987
E-Mail: info@pcb.com

All specifications are at room temperature unless otherwise specified.
In the interest of constant product improvement, we reserve the right to change specifications without notice.
ICP® is a registered trademark of PCB Group, Inc.

Figure 78. PCB Shaker Specifications Sheet. Source: [16]

APPENDIX C. SUPPLEMENTARY TABLES

Table 8. FEM-Generated Natural Frequency Comparison

Mode	Theoretical Natural Freq (Hz)	HIFI FEM Natural Freq (Hz)	Theory-HIFI FEM Difference (%)	Simple FEM Natural Freq (Hz)	HIFI-Simple FEM Difference (%)	Transition FEM Natural Freq (Hz)	HIFI-Transition FEM Difference (%)
RIGID	0.00	0.00	-	0.00	-	0.00	-
RIGID	0.00	0.00	-	0.00	-	0.00	-
1	14.51	14.51	0.0001	14.51	0.0008	14.51	0.0006
2	40.00	40.00	0.0000	40.00	0.0054	40.00	0.0044
3	78.41	78.41	0.0000	78.42	0.0201	78.42	0.0173
4	129.61	129.61	0.0000	129.69	0.0597	129.67	0.0489
5	193.62	193.62	0.0000	193.86	0.1283	193.81	0.1005
6	270.42	270.42	0.0000	271.01	0.2178	270.98	0.2076
7	360.03	360.03	0.0000	361.41	0.3821	361.29	0.3504
8	462.44	462.44	0.0000	465.59	0.6817	464.78	0.5064
9	577.65	577.65	0.0000	583.42	0.9993	582.25	0.7962
10	705.66	705.66	0.0000	714.57	1.2631	712.91	1.0278
11	846.47	846.47	0.0000	861.33	1.7552	858.11	1.3744
12	1000.08	1000.08	0.0000	1024.34	2.4256	1022.66	2.2570
13	1166.50	1166.50	0.0000	1191.95	2.1817	1188.16	1.8568
14	1345.71	1345.71	0.0000	1474.10	9.5406	1445.81	7.4384

Table 9. Natural Frequency Shift for Various Damage Scenarios

Interior Element	Damage Width (cm)	0.15875	0.3175	0.47625	0.635	0.79375	0.9525	1.11125	1.27	1.42875	1.5875	1.74625	1.905	2.06375	2.2225	2.38125	2.54	2.69875	2.8575	3.01625	3.175	3.33375	3.4925	3.65125	3.81	3.96875	4.1275	4.28625	4.445	4.60375	4.7625	4.92125	5.08	5.23875	5.3975	5.55625	5.715	5.87375	6.0325	6.19125	6.35	6.50975	6.66875	6.8275	6.98625	7.145	7.30375	7.4625	7.62125	7.78	7.93875	8.0975	8.25625	8.415	8.57375	8.7325	8.89125	9.05	9.20875	9.3675	9.52625	9.685	9.84375	10.0025	10.16125	10.32	10.47875	10.6375	10.79625	10.955	11.11375	11.2725	11.43125	11.59	11.74875	11.9075	12.06625	12.225	12.38375	12.5425	12.70125	12.86	13.01875	13.1775	13.33625	13.495	13.65375	13.8125	13.97125	14.13	14.28875	14.4475	14.60625	14.765	14.92375	15.0825	15.24125	15.4	15.55875	15.7175	15.87625	16.035	16.19375	16.3525	16.51125	16.67	16.82875	16.9875	17.14625	17.305	17.46375	17.6225	17.78125	17.94	18.09875	18.2575	18.41625	18.575	18.73375	18.8925	19.05125	19.21	19.36875	19.5275	19.68625	19.845	20.00375	20.1625	20.32125	20.48	20.63875	20.7975	20.95625	21.115	21.27375	21.4325	21.59125	21.75	21.90875	22.0675	22.22625	22.385	22.54375	22.7025	22.86125	23.02	23.17875	23.3375	23.49625	23.655	23.81375	23.9725	24.13125	24.29	24.44875	24.6075	24.76625	24.925	25.08375	25.2425	25.40125	25.56	25.71875	25.8775	26.03625	26.195	26.35375	26.5125	26.67125	26.83	26.98875	27.1475	27.30625	27.465	27.62375	27.7825	27.94125	28.1	28.25875	28.4175	28.57625	28.735	28.89375	29.0525	29.21125	29.37	29.52875	29.6875	29.84625	30.005	30.16375	30.3225	30.48125	30.64	30.79875	30.9575	31.11625	31.275	31.43375	31.5925	31.75125	31.91	32.06875	32.2275	32.38625	32.545	32.70375	32.8625	33.02125	33.18	33.33875	33.4975	33.65625	33.815	33.97375	34.1325	34.29125	34.45	34.60875	34.7675	34.92625	35.085	35.24375	35.4025	35.56125	35.72	35.87875	36.0375	36.19625	36.355	36.51375	36.6725	36.83125	36.99	37.14875	37.3075	37.46625	37.625	37.78375	37.9425	38.10125	38.26	38.41875	38.5775	38.73625	38.895	39.05375	39.2125	39.37125	39.53	39.68875	39.8475	40.00625	40.165	40.32375	40.4825	40.64125	40.8	40.95875	41.1175	41.27625	41.435	41.59375	41.7525	41.91125	42.07	42.22875	42.3875	42.54625	42.705	42.86375	43.0225	43.18125	43.34	43.49875	43.6575	43.81625	43.975	44.13375	44.2925	44.45125	44.61	44.76875	44.9275	45.08625	45.245	45.40375	45.5625	45.72125	45.88	46.03875	46.1975	46.35625	46.515	46.67375	46.8325	46.99125	47.15	47.30875	47.4675	47.62625	47.785	47.94375	48.1025	48.26125	48.42	48.57875	48.7375	48.89625	49.055	49.21375	49.3725	49.53125	49.69	49.84875	50.0075	50.16625	50.325	50.48375	50.6425	50.80125	50.96	51.11875	51.2775	51.43625	51.595	51.75375	51.9125	52.07125	52.23	52.38875	52.5475	52.70625	52.865	53.02375	53.1825	53.34125	53.5	53.65875	53.8175	53.97625	54.135	54.29375	54.4525	54.61125	54.77	54.92875	55.0875	55.24625	55.405	55.56375	55.7225	55.88125	56.04	56.19875	56.3575	56.51625	56.675	56.83375	56.9925	57.15125	57.31	57.46875	57.6275	57.78625	57.945	58.10375	58.2625	58.42125	58.58	58.73875	58.8975	59.05625	59.215	59.37375	59.5325	59.69125	59.85	60.00875	60.1675	60.32625	60.485	60.64375	60.8025	60.96125	61.12	61.27875	61.4375	61.59625	61.755	61.91375	62.0725	62.23125	62.39	62.54875	62.7075	62.86625	63.025	63.18375	63.3425	63.50125	63.66	63.81875	63.9775	64.13625	64.295	64.45375	64.6125	64.77125	64.93	65.08875	65.2475	65.40625	65.565	65.72375	65.8825	66.04125	66.2	66.35875	66.5175	66.67625	66.835	66.99375	67.1525	67.31125	67.47	67.62875	67.7875	67.94625	68.105	68.26375	68.4225	68.58125	68.74	68.89875	69.0575	69.21625	69.375	69.53375	69.6925	69.85125	70.01	70.16875	70.3275	70.48625	70.645	70.80375	70.9625	71.12125	71.28	71.43875	71.5975	71.75625	71.915	72.07375	72.2325	72.39125	72.55	72.70875	72.8675	73.02625	73.185	73.34375	73.5025	73.66125	73.82	73.97875	74.1375	74.29625	74.455	74.61375	74.7725	74.93125	75.09	75.24875	75.4075	75.56625	75.725	75.88375	76.0425	76.20125	76.36	76.51875	76.6775	76.83625	76.995	77.15375	77.3125	77.47125	77.63	77.78875	77.9475	78.10625	78.265	78.42375	78.5825	78.74125	78.9	79.05875	79.2175	79.37625	79.535	79.69375	79.8525	80.01125	80.17	80.32875	80.4875	80.64625	80.805	80.96375	81.1225	81.28125	81.44	81.59875	81.7575	81.91625	82.075	82.23375	82.3925	82.55125	82.71	82.86875	83.0275	83.18625	83.345	83.50375	83.6625	83.82125	83.98	84.13875	84.2975	84.45625	84.615	84.77375	84.9325	85.09125	85.25	85.40875	85.5675	85.72625	85.885	86.04375	86.2025	86.36125	86.52	86.67875	86.8375	86.99625	87.155	87.31375	87.4725	87.63125	87.79	87.94875	88.1075	88.26625	88.425	88.58375	88.7425	88.90125	89.06	89.21875	89.3775	89.53625	89.695	89.85375	90.0125	90.17125	90.33	90.48875	90.6475	90.80625	90.965	91.12375	91.2825	91.44125	91.6	91.75875	91.9175	92.07625	92.235	92.39375	92.5525	92.71125	92.87	93.02875	93.1875	93.34625	93.505	93.66375	93.8225	93.98125	94.14	94.29875	94.4575	94.61625	94.775	94.93375	95.0925	95.25125	95.41	95.56875	95.7275	95.88625	96.045	96.20375	96.3625	96.52125	96.68	96.83875	97.0	97.15875	97.3175	97.47625	97.635	97.79375	97.9525	98.11125	98.27	98.42875	98.5875	98.74625	98.905	99.06375	99.2225	99.38125	99.54	99.69875	99.8575	100.01625	100.175	100.33375	100.4925	100.65125	100.81	100.96875	101.1275	101.28625	101.445	101.60375	101.7625	101.92125	102.08	102.23875	102.3975	102.55625	102.715	102.87375	103.0325	103.19125	103.35	103.50875	103.6675	103.82625	103.985	104.14375	104.3025	104.46125	104.62	104.77875	104.9375	105.09625	105.255	105.41375	105.5725	105.73125	105.89	106.04875	106.2075	106.36625	106.525	106.68375	106.8425	107.00125	107.16	107.31875	107.4775	107.63625	107.795	107.95375	108.1125	108.27125	108.43	108.58875	108.7475	108.90625	109.065	109.22375	109.3825	109.54125	109.7	109.85875	110.0175	110.17625	110.335	110.49375	110.6525	110.81125	110.97	111.12875	111.2875	111.44625	111.605	111.76375	111.9225	112.08125	112.24	112.39875	112.5575	112.71625	112.875	113.03375	113.1925	113.35125	113.51	113.66875	113.8275	113.98625	114.145	114.30375	114.4625	114.62125	114.78	114.93875	115.0975	115.25625	115.415	115.57375	115.7325	115.89125	116.05	116.20875	116.3675	116.52625	116.685	116.84375	117.0025	117.16125	117.32	117.47875	117.6375	117.79625	117.955	118.11375	118.2725	118.43125	118.59	118.74875	118.9075	119.06625	119.225	119.38375	119.5425	119.70125	119.86	120.01875	120.1775	120.33625	120.495	120.65375	120.8125	120.97125	121.13	121.28875	121.4475	121.60625	121.765	121.92375	122.0825	122.24125	122.4	122.55875	122.7175	122.87625	123.035	123.19375	123.3525	123.51125	123.67	123.82875	123.9875	124.14625	124.305	124.46375	124.6225	124.78125	124.94	125.09875	125.2575	125.41625	125.575	125.73375	125.8925	126.05125	126.21	126.36875	126.5275	126.68625	126.845	127.00375	127.1625	127.32125	127.48	127.63875	127.7975	127.95625	128.115	128.27375	128.4325	128.59125	128.75	128.90875	129.0675	129.22625	129.385	129.54375	129.7025	129.86125	130.02	130.17875	130.3375	130.49625	130.655	130.81375	130.9725	131.13125	131.29	131.44875	131.6075	131.76625	131.925	132.08375	132.2425	132.40125	132.56	132.71875	132.8775	133.03625	133.195	133.35375	133.5125	133.67125	133.83	133.98875	134.1475	134.30625	134.465	134.62375	134.7825	134.94125	135.1	135.25875	135.4175	135.57625	135.735	135.89375	136.0525	136.21125	136.37	136.52875	136.6875	136.84625	137.005	137.16375	137.3225	137.48125	137.64	137.79875	137.9575	138.11625	138.275	138.43375	138.5925	138.75125	138.91	139.06875	139.2275	139.38625	139.545	139.70375	139.8625	140.02125	140.18	140.33875	140.4975	140.65625	140.815	140.97375	141.1325	141.29125	141.45	141.60875	141.7675	141.92625	142.085	142.24375	142.4025	142.56125	142.72	142.87875	143.0375	143.19625	143.355	143.51375	143.6725	143.83125	143.99	144.14875	144.3075	144.46625	144.625	144.78375	144.9425	145.10125	145.26	145.41875	145.5775	145.73625	145.895	146.05375	146.2125	146.37125	146.53	146.68875	146.8475	147.00625	147.165	147.32375	147.4825	147.64125	147.8	147.95875	148.1175	148.27625	148.435	148.59375	148.7525	148.91125	149.07	149.22875	149.3875	149.54625	149.705	149.86375	150.0225	150.18125	150.34	150.49875	150.6575	150.81625	150.975	151.13375	151.2925	151.45125	151.61	151.76875	151.9275	152.08625	152.245	152.40375	152.5625	152.72125	152.88	153.03875	153.1975	153.35625	153.515	153.67375	153.8325	153.99125	154.15	154.30875	154.4675	154.62625	154.785	154.94375	155.1025	155.26125	155.42	155.57875	155.7375	155.89625	156.055	156.21375	156.3725	156.53125	156.69	156.84875	157.0075	157.166
------------------	-------------------	---------	--------	---------	-------	---------	--------	---------	------	---------	--------	---------	-------	---------	--------	---------	------	---------	--------	---------	-------	---------	--------	---------	------	---------	--------	---------	-------	---------	--------	---------	------	---------	--------	---------	-------	---------	--------	---------	------	---------	---------	--------	---------	-------	---------	--------	---------	------	---------	--------	---------	-------	---------	--------	---------	------	---------	--------	---------	-------	---------	---------	----------	-------	----------	---------	----------	--------	----------	---------	----------	-------	----------	---------	----------	--------	----------	---------	----------	-------	----------	---------	----------	--------	----------	---------	----------	-------	----------	---------	----------	--------	----------	---------	----------	------	----------	---------	----------	--------	----------	---------	----------	-------	----------	---------	----------	--------	----------	---------	----------	-------	----------	---------	----------	--------	----------	---------	----------	-------	----------	---------	----------	--------	----------	---------	----------	-------	----------	---------	----------	--------	----------	---------	----------	-------	----------	---------	----------	--------	----------	---------	----------	-------	----------	---------	----------	--------	----------	---------	----------	-------	----------	---------	----------	--------	----------	---------	----------	-------	----------	---------	----------	--------	----------	---------	----------	-------	----------	---------	----------	--------	----------	---------	----------	------	----------	---------	----------	--------	----------	---------	----------	-------	----------	---------	----------	--------	----------	---------	----------	-------	----------	---------	----------	--------	----------	---------	----------	-------	----------	---------	----------	--------	----------	---------	----------	-------	----------	---------	----------	--------	----------	---------	----------	-------	----------	---------	----------	--------	----------	---------	----------	-------	----------	---------	----------	--------	----------	---------	----------	-------	----------	---------	----------	--------	----------	---------	----------	-------	----------	---------	----------	--------	----------	---------	----------	-------	----------	---------	----------	--------	----------	---------	----------	------	----------	---------	----------	--------	----------	---------	----------	-------	----------	---------	----------	--------	----------	---------	----------	-------	----------	---------	----------	--------	----------	---------	----------	-------	----------	---------	----------	--------	----------	---------	----------	-------	----------	---------	----------	--------	----------	---------	----------	-------	----------	---------	----------	--------	----------	---------	----------	-------	----------	---------	----------	--------	----------	---------	----------	-------	----------	---------	----------	--------	----------	---------	----------	-------	----------	---------	----------	--------	----------	---------	----------	-------	----------	---------	----------	--------	----------	---------	----------	------	----------	---------	----------	--------	----------	---------	----------	-------	----------	---------	----------	--------	----------	---------	----------	-------	----------	---------	----------	--------	----------	---------	----------	-------	----------	---------	----------	--------	----------	---------	----------	-------	----------	---------	----------	--------	----------	---------	----------	-------	----------	---------	----------	--------	----------	---------	----------	-------	----------	---------	----------	--------	----------	---------	----------	-------	----------	---------	----------	--------	----------	---------	----------	-------	----------	---------	----------	--------	----------	---------	----------	-------	----------	---------	----------	--------	----------	---------	----------	------	----------	---------	----------	--------	----------	---------	----------	-------	----------	---------	----------	--------	----------	---------	----------	-------	----------	---------	----------	--------	----------	---------	----------	-------	----------	---------	----------	--------	----------	---------	----------	-------	----------	---------	----------	--------	----------	---------	----------	-------	----------	---------	----------	--------	----------	---------	----------	-------	----------	---------	----------	--------	----------	---------	----------	-------	----------	---------	----------	--------	----------	---------	----------	-------	----------	---------	----------	--------	----------	---------	----------	-------	----------	---------	----------	--------	----------	---------	----------	------	----------	---------	----------	--------	----------	---------	----------	-------	----------	---------	----------	--------	----------	---------	----------	-------	----------	---------	----------	--------	----------	---------	----------	-------	----------	---------	----------	--------	----------	---------	----------	-------	----------	---------	----------	--------	----------	---------	----------	-------	----------	---------	----------	--------	----------	---------	----------	-------	----------	---------	----------	--------	----------	---------	----------	-------	----------	---------	----------	--------	----------	---------	----------	-------	----------	---------	----------	--------	----------	---------	----------	-------	----------	---------	----------	--------	----------	---------	----------	------	----------	---------	----------	--------	----------	---------	----------	-------	----------	---------	----------	--------	----------	---------	----------	-------	----------	---------	----------	--------	----------	---------	----------	-------	----------	---------	----------	--------	----------	---------	----------	-------	----------	------	----------	---------	----------	--------	----------	---------	----------	-------	----------	---------	----------	--------	----------	---------	----------	-------	----------	---------	-----------	---------	-----------	----------	-----------	--------	-----------	----------	-----------	---------	-----------	----------	-----------	--------	-----------	----------	-----------	---------	-----------	----------	-----------	--------	-----------	----------	-----------	---------	-----------	----------	-----------	--------	-----------	----------	-----------	---------	-----------	----------	-----------	--------	-----------	----------	-----------	---------	-----------	----------	-----------	--------	-----------	----------	-----------	---------	-----------	----------	-----------	--------	-----------	----------	-----------	---------	-----------	----------	-----------	-------	-----------	----------	-----------	---------	-----------	----------	-----------	--------	-----------	----------	-----------	---------	-----------	----------	-----------	--------	-----------	----------	-----------	---------	-----------	----------	-----------	--------	-----------	----------	-----------	---------	-----------	----------	-----------	--------	-----------	----------	-----------	---------	-----------	----------	-----------	--------	-----------	----------	-----------	---------	-----------	----------	-----------	--------	-----------	----------	-----------	---------	-----------	----------	-----------	--------	-----------	----------	-----------	---------	-----------	----------	-----------	--------	-----------	----------	-----------	---------	-----------	----------	-----------	--------	-----------	----------	-----------	---------	-----------	----------	-----------	-------	-----------	----------	-----------	---------	-----------	----------	-----------	--------	-----------	----------	-----------	---------	-----------	----------	-----------	--------	-----------	----------	-----------	---------	-----------	----------	-----------	--------	-----------	----------	-----------	---------	-----------	----------	-----------	--------	-----------	----------	-----------	---------	-----------	----------	-----------	--------	-----------	----------	-----------	---------	-----------	----------	-----------	--------	-----------	----------	-----------	---------	-----------	----------	-----------	--------	-----------	----------	-----------	---------	-----------	----------	-----------	--------	-----------	----------	-----------	---------	-----------	----------	-----------	--------	-----------	----------	-----------	---------	-----------	----------	-----------	-------	-----------	----------	-----------	---------	-----------	----------	-----------	--------	-----------	----------	-----------	---------	-----------	----------	-----------	--------	-----------	----------	-----------	---------	-----------	----------	-----------	--------	-----------	----------	-----------	---------	-----------	----------	-----------	--------	-----------	----------	-----------	---------	-----------	----------	-----------	--------	-----------	----------	-----------	---------	-----------	----------	-----------	--------	-----------	----------	-----------	---------	-----------	----------	-----------	--------	-----------	----------	-----------	---------	-----------	----------	-----------	--------	-----------	----------	-----------	---------	-----------	----------	-----------	--------	-----------	----------	-----------	---------	-----------	----------	-----------	-------	-----------	----------	-----------	---------	-----------	----------	-----------	--------	-----------	----------	-----------	---------	-----------	----------	-----------	--------	-----------	----------	-----------	---------	-----------	----------	-----------	--------	-----------	----------	-----------	---------	-----------	----------	-----------	--------	-----------	----------	-----------	---------	-----------	----------	-----------	--------	-----------	----------	-----------	---------	-----------	----------	-----------	--------	-----------	----------	-----------	---------	-----------	----------	-----------	--------	-----------	----------	---------

97

Table 10. Orthogonal Projection Sensitivity Library Selections

ABCs Available: No Pins, 1 Pin			
Modes Available: 1-14			
Composite [S] Row	ABC Configuration	ABC Location (Node)	Mode
1	1 Pin	12	8
2	1 Pin	12	6
3	1 Pin	12	2
4	1 Pin	9	1
5	1 Pin	4	2
6	1 Pin	4	6
7	1 Pin	13	9
8	1 Pin	9	4
9	1 Pin	13	3
10	1 Pin	6	1
11	1 Pin	9	5
12	1 Pin	4	11
13	1 Pin	13	5
14	1 Pin	8	3

ABCs Available: No Pins, 1 Pin, 2 Pins			
Modes Available: 1-14			
Composite [S] Row	ABC Configuration	ABC Location (Node)	Mode
1	2 Pins	6, 12	3
2	2 Pins	3, 4	4
3	2 Pins	7, 8	2
4	2 Pins	12, 13	9
5	2 Pins	9, 10	2
6	2 Pins	5, 6	2
7	2 Pins	4, 5	11
8	2 Pins	10, 11	1
9	2 Pins	12, 13	4
10	2 Pins	4, 5	3
11	2 Pins	3, 4	7
12	2 Pins	4, 10	5
13	2 Pins	6, 7	1
14	2 Pins	1, 5	6

ABCs Available: Clean, 1 Pin, 2 Pins, 3 Pins		Modes Available: 1-14	
Composite [S] Row	ABC Configuration	ABC Location (Node)	Mode
1	3 Pins	10, 11, 12	6
2	3 Pins	6, 7, 8	2
3	3 Pins	2, 3, 4	6
4	3 Pins	1, 7, 8	1
5	3 Pins	4, 5, 11	2
6	3 Pins	2, 10, 11	1
7	3 Pins	8, 9, 10	1
8	3 Pins	10, 11, 12	3
9	3 Pins	10, 13, 15	7
10	3 Pins	4, 12, 15	3
11	3 Pins	3, 6, 8	5
12	3 Pins	8, 11, 13	5
13	3 Pins	3, 4, 5	4
14	3 Pins	3, 6, 12	4

ABCs Available: Clean, 1 Pin, 1 Point Mass, 1 Spring		Modes Available: 1-14	
Composite [S] Row	ABC Configuration (m ⁴ *Pa)	ABC Location (Node)	Mode
1	1 Pin	13	9
2	1 Spring (0.014349)	3	6
3	1 Spring (0.0028698)	8	1
4	1 Spring (0.0028698)	4	2
5	1 Spring (0.0028698)	9	3
6	1 Spring (0.011479)	9	5
7	1 Spring (0.0086094)	1	7
8	1 Spring (0.0028698)	10	2
9	1 Pin	3	9
10	1 Spring (0.0028698)	11	4
11	1 Spring (0.0057396)	14	5
12	1 Spring (0.0028698)	12	4
13	1 Spring (0.011479)	9	7
14	1 Spring (0.0028698)	1	6

ABCs Available: No Pins, 1 Pin			
Modes Available: 4-14			
Composite [S] Row	ABC Configuration	ABC Location (Node)	Mode
1	1 Pin	14	6
2	1 Pin	6	9
3	1 Pin	7	4
4	1 Pin	4	6
5	1 Pin	9	5
6	1 Pin	10	5
7	1 Pin	12	4
8	1 Pin	5	6
9	1 Pin	9	10
10	1 Pin	11	10
11	1 Pin	14	7
12	1 Pin	3	9
13	1 Pin	11	6
14	1 Pin	11	8

ABCs Available: No Pins, 1 Pin			
Modes Available: 4-8			
Composite [S] Row	ABC Configuration	ABC Location (Node)	Mode
1	1 Pin	2	5
2	1 Pin	7	4
3	1 Pin	9	4
4	1 Pin	12	6
5	1 Pin	4	8
6	1 Pin	13	6
7	1 Pin	2	6
8	1 Pin	2	7
9	1 Pin	13	5
10	1 Pin	5	8
11	1 Pin	1	4
12	1 Pin	11	8
13	1 Pin	9	5
14	1 Pin	14	6

ABCs Available: No Pins, 1 Pin, 2 Pins			
Modes Available: 4-8			
Composite [S] Row	ABC Configuration	ABC Location (Node)	Mode
1	2 Pins	8, 9	5
2	2 Pins	12, 13	4
3	2 Pins	8, 11	6
4	2 Pins	2, 3	6
5	2 Pins	5, 8	6
6	2 Pins	13, 15	8
7	2 Pins	4, 5	4
8	2 Pins	7, 8	4
9	2 Pins	9, 12	5
10	2 Pins	9, 10	7
11	2 Pins	1, 7	5
12	2 Pins	1, 10	8
13	2 Pins	4, 12	4
14	2 Pins	1, 3	4

Table 11. Initial FEM-Experimental Eigenvalue Percent Differences

Resolution (Hz)	0.3125	0.3125	0.3125	0.08	0.02	0.3125	0.08
ABC	1 Pin	1 Pin	1 Pin	1 Pin	1 Pin	2 Pins	2 Pins
Modes	1-14	4-14	4-8	4-8	4-8	4-8	4-8
Eigenvector Row 1	3.4637	2.9473	2.6898	2.8634	2.9555	2.3973	2.0436
Eigenvector Row 2	2.6867	4.8052	2.0781	1.9283	2.2504	8.5608	7.3151
Eigenvector Row 3	-0.7587	2.0781	2.0669	2.0799	2.4567	2.4638	1.9281
Eigenvector Row 4	-22.3621	3.1215	2.6975	2.6097	2.5103	3.0618	3.3268
Eigenvector Row 5	1.7494	2.4109	3.2100	3.2178	3.3033	1.4703	1.2834
Eigenvector Row 6	3.1224	2.2428	2.8386	2.8172	2.9656	2.7247	4.5891
Eigenvector Row 7	5.7367	2.4394	3.0714	2.9541	3.0365	0.2300	1.0581
Eigenvector Row 8	2.0632	2.3877	2.8435	2.8428	3.1403	0.4634	1.5534
Eigenvector Row 9	4.3355	4.8020	2.4715	2.5591	2.5908	2.2149	2.2450
Eigenvector Row 10	-1.5346	5.2326	3.9911	3.9735	3.9072	2.4571	2.4083
Eigenvector Row 11	2.4109	2.8098	2.0361	2.3619	2.2059	1.9038	1.8402
Eigenvector Row 12	6.0172	4.6801	3.4372	3.3107	3.4674	2.9499	3.3735
Eigenvector Row 13	2.4691	2.5715	2.4109	2.2858	2.4475	1.2182	1.4020
Eigenvector Row 14	4.5403	3.4372	2.9473	2.9634	2.6871	2.1961	2.4763

Table 12. Updated FEM Comparison

Mode No.	1	2	3	4	5	6	7	8	9	10	11	12
Test Freqs (Hz)	14.26	39.22	76.78	127.04	189.84	264.96	352.46	452.94	564.78	690.26	826.40	974.70
Initial FEM (Hz)	14.63	40.32	79.04	130.68	195.31	273.06	364.09	468.68	587.17	719.89	866.95	1027.19
Test-Initial FEM Delta (%)	2.57	2.79	2.94	2.86	2.88	3.06	3.30	3.48	3.96	4.29	4.91	5.39
Adjusted FEM (Hz)	14.41	39.71	77.84	128.70	192.36	268.93	358.59	461.60	578.29	709.01	853.85	1011.66
Test-Adjusted FEM Delta (%)	1.02	1.24	1.38	1.31	1.33	1.50	1.74	1.91	2.39	2.72	3.32	3.79
Updated FEM A (Hz)	14.22	39.01	75.06	127.70	190.03	265.21	353.54	453.77	567.69	691.29	837.49	990.96
Test-Updated FEM A Delta (%)	0.28	0.52	2.24	0.52	0.10	0.09	0.31	0.18	0.52	0.15	1.34	1.67
Updated FEM B (Hz)	14.24	38.92	76.25	127.58	189.85	265.10	353.15	454.18	569.03	694.80	838.2804	993.19
Test-Updated FEM B Delta (%)	0.14	0.76	0.70	0.43	0.00	0.05	0.19	0.27	0.75	0.66	1.44	1.90
Updated FEM C (Hz)	14.23	40.21	77.49	127.00	189.63	266.02	355.04	456.92	573.84	704.65	848.59	1004.48
Test-Updated FEM C Delta (%)	0.20	2.52	0.93	0.04	0.11	0.40	0.73	0.88	1.60	2.08	2.69	3.06
Updated FEM D (Hz)	14.23	38.92	76.42	127.52	189.66	265.20	353.20	454.02	569.32	695.52	838.53	993.62
Test-Updated FEM D Delta (%)	0.21	0.76	0.47	0.37	0.09	0.09	0.21	0.24	0.80	0.76	1.47	1.94
Updated FEM E (Hz)	14.24	40.16	78.19	127.32	189.76	266.76	355.25	455.96	572.14	703.12	844.78	1000.98
Test-Updated FEM E Delta (%)	0.12	2.41	1.84	0.22	0.04	0.68	0.79	0.67	1.30	1.86	2.22	2.70
Updated FEM F (Hz)	14.20	38.90	76.11	127.44	189.602	265.23	353.14	453.64	568.55	694.22	837.68	992.61
Test-Updated FEM F Delta (%)	0.42	0.81	0.87	0.32	0.13	0.10	0.19	0.15	0.67	0.57	1.36	1.84

Table 13. Averages of Eigenvalue Absolute Percent Differences

Modes	1-3	4-8	9-12	1-12
Initial FEM	2.769	3.116	4.637	3.536
Adjusted FEM	1.216	1.558	3.055	1.971
Updated FEM A	1.014	0.241	0.919	0.660
Updated FEM B	0.529	0.190	1.186	0.607
Updated FEM C	1.214	0.432	2.357	1.269
Updated FEM D	0.482	0.201	1.243	0.619
Updated FEM E	1.455	0.481	2.022	1.238
Updated FEM F	0.698	0.179	1.111	0.619

THIS PAGE INTENTIONALLY LEFT BLANK

LIST OF REFERENCES

- [1] COMSOL. The finite element method (FEM) [Online]. Available: <https://www.comsol.com/multiphysics/finite-element-method>. Accessed July 15, 2017.
- [2] T. J. Teo et al. (2015, June 29). Compliant manipulators [Online]. Available: https://www.researchgate.net/publication/279264596_Compliant_Manipulators. Accessed July 16, 2017.
- [3] O. A. Bauchau and J. I. Craig. (2009). *Structural Analysis* [Online]. Available: https://link.springer.com/chapter/10.1007/978-90-481-2516-6_5
- [4] J. H. Gordis. "Artificial boundary conditions for model updating and damage detection," *Mechanical Systems and Signal Processing*, vol. 13, no. 3, pp. 437–448, 1999.
- [5] J. H. Gordis and K. Papagiannakis. "Optimal selection of artificial boundary conditions for model update and damage detection," *Mechanical Systems and Signal Processing*, vol. 25, pp. 1451–1468, 2011.
- [6] J. Shin and J. H. Gordis. "Improved Selection of artificial boundary conditions for finite element model updating and structural damage detection," unpublished.
- [7] The MathWorks, Inc., Natick, MA, USA. 2017. MATLAB.
- [8] Brüel & Kjær Sound & Vibration Measurement A/S, Nærum, Denmark. 2003. Pulse Reflex.
- [9] W. T. Thomson and M.D. Dahleh. *Theory of Vibration with Applications*, 5th ed. Upper Saddle River, NJ: Prentice Hall, 1993.
- [10] R. R. Craig, Jr., *Structural Dynamics: An Introduction to Computer Methods*. New York, NY: John Wiley & Sons, 1981.
- [11] J. H. Gordis. "Eigenvalue sensitivities," unpublished.
- [12] R. J. C. Konze. "Synthetic modification in the frequency domain for finite element model update and damage detection," M.S. thesis, Mechanical and Aerospace Engineering Department, Naval Postgraduate School, Monterey, CA, 2017.
- [13] W. D. Pilkey. *Formulas for Stress, Strain, and Structural Matrices*. New York, NY: Wiley, 1994, pp. 564.

- [14] A. M. Rinawi and R. W. Clough, "Improved amplitude fitting for frequency and damping," in *Int. Modal Analysis Conf.*, San Diego, CA, 1992, p. 25.
- [15] E. Damanakis. "Artificial boundary conditions for finite element model update and damage detection," M.S. thesis, Mechanical and Aerospace Engineering Department, Naval Postgraduate School, Monterey, CA, 2017.
- [16] *Model 394C06 Handheld shaker, 1g at 159.2 Hz (for up to 210 grams total weight of Installation and Operating Manual*, PCB Piezotronics, Inc., Depew, NY, pp. 11.

INITIAL DISTRIBUTION LIST

1. Defense Technical Information Center
Ft. Belvoir, Virginia
2. Dudley Knox Library
Naval Postgraduate School
Monterey, California